![Chalmers University of Technology logo]

Dynamic response of railway bridges subjected to high speed trains
Parametrical case studies

Master's Thesis in the Master's Programme Structural Engineering and Building Technology

MARCUS HJELM
NICLAS KARLSSON

Dynamic response of railway bridges subjected to high speed trains

Parametrical case studies

Master's Thesis in the Master's Programme Structural Engineering and Building Technology

MARCUS HJELM

NICLAS KARLSSON

Department of Civil and Environmental Engineering
Division of Structural Engineering
Concrete structures
CHALMERS UNIVERSITY OF TECHNOLOGY
Göteborg, Sweden 2016

Dynamic response of railway bridges subjected to high speed trains
Parametrical case studies

Master's Thesis in the Master's Programme Structural Engineering and Building Technology

MARCUS HJELM

NICLAS KARLSSON

Department of Civil and Environmental Engineering
Division of Structural Engineering
Concrete structures
Chalmers University of Technology
SE-412 96 Göteborg
Sweden
Telephone: + 46 (0)31-772 1000

Cover:
A vertical bending mode shape of the 24 meter reinforced concrete slab bridge with end shields.

Dynamic response of railway bridges subjected to high speed trains

Parametrical case studies

Master's thesis in the Master's Programme Structural Engineering and Building Technology

MARCUS HJELM
NICLAS KARLSSON
Department of Civil and Environmental Engineering
Division of Structural Engineering
Concrete structures
Chalmers University of Technology

ABSTRACT

The interest in high-speed trains is increasing around the world and it provides a sustainable and effective way of travelling. A high-speed railway line is currently being planned in Sweden with an intended line speed of 320 km/h. High train speeds induce more critical dynamic effects on railway bridges and the purpose of this Master's thesis is to enhance the basic understanding of how different parameters influence the bridge response. A literature survey of the dynamic behaviour of railway bridges was carried out and numerical analyses were performed for different reinforced concrete bridges in Brigade/Plus. The outcome of the study was limited to assess vertical accelerations and vertical deflections of the bridge deck.

The FE-modelling of the bridges started with a simply supported case and different parameters were altered in order to assess their effect on the dynamic response. Influence of mass, stiffness, damping and span length were included. In addition, the bridges were provided with end shields in order to study their impact on the response. Moreover, a two- and three span continuous case with simply supported boundary conditions were analysed together with a situation with fixed columns as mid-support.

The results from numerical analyses have shown that the mass, stiffness and damping have a great influence on the dynamic response of the bridges. Greater mass lowered the critical train speed and reduced the deck accelerations whereas the maximum deflection values were unchanged. Higher stiffness increased the critical train speed and reduced the deflections instead and left the maximum deck accelerations unchanged. A higher damping value reduced both the accelerations and deflections.

Longer spans were found to enhance the dynamic performance while short span bridges with low natural frequencies resulted in excessive vibration levels. Increased stiffness of a short span bridge resulted in a satisfying dynamic behaviour since the critical resonance peaks were moved outside of the considered speed range. The continuous bridges indicated high accelerations for the short span cases due to the low natural frequencies. End shields were found to reduce the accelerations, especially for the shorter spans due to its mass contribution and transverse stiffening at the bridge ends. Finally, the dynamic behaviour was highly influenced by the span to coach length ratio, which effectively suppressed the resonance response in the vicinity of certain ratios.

Key words: Dynamic response, high-speed train, deck acceleration, natural frequency, railway bridge, resonance, vibrations

Dynamisk respons för järnvägsbroar belastade av höghastighetståg
Parametriska fallstudier

Examensarbete inom masterprogrammet Structural Engineering and Building
Technology

MARCUS HJELM
NICLAS KARLSSON
Institutionen för bygg- och miljöteknik
Avdelningen för Konstruktionsteknik
Betongbyggnad
Chalmers tekniska högskola

SAMMANFATTNING

Intresset för höghastighetståg ökar runtom i världen då det är ett hållbart och effektivt sätt att resa. En höghastighetsjärnväg planeras för tillfället i Sverige där hastigheten skall vara 320 km/h. Höga hastigheter innebär en ökning av de dynamiska effekterna på järnvägsbroar och syftet med denna uppsats är att öka förståelsen för hur olika parametrar påverkar broars dynamiska respons. En litteraturstudie genomfördes med avseende på järnvägsbroars dynamiska egenskaper och numeriska analyser utfördes på slakarmerade betongbroar i Brigade/Plus. De resultat som utvärderats var begränsade till vertikala accelerationer och vertikala nedböjningar.

FE-modelleringen av broarna utgick från fritt upplagda fall där olika parametrar modifierades för att utvärdera deras inverkan på den dynamiska responsen. Massa, styvhet, dämpning och spannlängd utvärderades i parameterstudien. Därefter kompletterades broarna med ändskärmar för att studera dess påverkan. Slutligen studeras även fritt upplagda kontinuerliga två- och trespannsbroar samt med fast inspända upplag.

Resultaten från de numeriska analyserna visade att massa, styvhet och dämpning hade stor inverkan på resultaten. Ökad massa sänkte resonanshastigheterna och reducerade accelerationerna i brodäcket men påverkade inte den dynamiska nedböjningen. Ökad styvhet medförde höjda resonanshastigheter, oförändrad acceleration och sänkt dynamisk nedböjning. Ökad dämpning sänkte både dynamisk nedböjning och acceleration.

Broar med långa spann visade sig ha bättre dynamiska egenskaper än korta broar med låg egenfrekvens. Genom att öka styvheten för en kort bro kunde resonanshastigheterna flyttas utanför analysernas hastighetsspektrum. Kontinuerliga broar uppvisade höga accelerationer för korta spännvidder på grund av låga egenfrekvenser. Accelerationerna reducerades när ändskärmar lades till i analyserna, speciellt för de korta broarna då dess massa och transversella styvhet hade stor påverkan. Slutligen visade analyserna att kvoten mellan spann- och vagnlängd hade stor inverkan på resultaten, och responsen vid resonans minskade avsevärt vid särskilda kvoter.

Nyckelord: Dynamisk respons, höghastighetståg, brodäcksacceleration, egenfrekvens, järnvägsbro, resonans, vibrationer

Contents

Preface

COWI is currently involved in the planning of constructing a high-speed railway line in Sweden. The purpose of this Master's Thesis is to increase the basic understanding of the dynamic response of railway bridges subjected to high-speed trains. The thesis was carried out at COWI AB in Gothenburg during the spring of 2016 in collaboration with the Department of Civil and Environmental Engineering and the Department of Applied Mechanics at Chalmers University of Technology.

Joosef Leppänen, PhD, at Concrete Structures at Chalmers University of Technology was examiner. Peter Möller, PhD, at the Department of Applied Mechanics at Chalmers University of Technology, Magnus Bäckström, PhD, at COWI AB and Isak Svensson, MSc, at COWI AB has been supervisors.

We would like to thank our supervisors and examiner for their remarks and positive guidance throughout the project. We would also like to thank COWI for providing us with a stimulating working place and with the right tools in order to complete this thesis work. Lastly, we would like to thank the opposition group, Carl Hoff and Isak Näslund, for their inputs and comments.

Göteborg June 2016

Marcus Hjelm and Niclas Karlsson

Notations

The following notations are used throughout the report. Time derivatives are notated with a dot e.g. $\dot{u} = \frac{\partial u}{\partial t}$ and space derivatives are denoted with a prime e.g. $u' = \frac{\partial u}{\partial x}$.

Transposed vectors and matrices are denoted with a T e.g. $\begin{bmatrix} a & b \end{bmatrix}^{\mathrm{T}} = \begin{bmatrix} a \\ b \end{bmatrix}$

Roman upper case letters

A	Cross-section area [m²]
$\mathbf{C}$	Damping matrix [Ns/m]
$\boldsymbol{C}$	Modal damping matrix [Ns/m]
$\overline{C}$	Mathematical variable
D	Coach length [m]
D_s	Steady-state amplification factor
DOF	Degrees of freedom
E	Young's modulus [Pa]
ERRI	European Rail Research Institute
FE	Finite element
FEM	Finite element method
FVD	Fluid viscous damper
HSLM	High-speed load model
I	Moment of inertia [m⁴]
$\mathbf{K}$	Stiffness matrix [N/m]
$\boldsymbol{K}$	Modal stiffness matrix
L	Length of span [m]
L_Φ	Determinant length [m]
$\mathbf{M}$	Mass matrix
$\boldsymbol{M}$	Modal mass matrix
MDOF	Multi degree of freedom
ORE	Office for Research and Experiments
SDOF	Single degree of freedom
S_n	Non-dimensional speed parameter
TMD	Tuned mass damper
U	Steady-state amplitude [m]
$\mathbf{U}$	Amplitude vector [m]
U_0	Static displacement [m]

Roman lower case letters

c	Damping coefficient [Ns/m]
c_{cr}	Critical damping coeffiecient [Ns/m]
f	Frequency [Hz]
k	Spring stiffness [N/m]
m	Mass [kg]
n_0	First natural frequency
n_T	First natural torsional frequency
p	Force [N]
q	Generalised coordinates

r	Loading frequency ratio
$\bar{s}$	Mathematical variable
u	Displacement or deflection [m]
$\boldsymbol{u}$	Displacement vector [m, rad]

Greek upper case letters

Φ	Dynamic factor
$\boldsymbol{\Phi}$	Eigenvector matrix
Ω	Loading frequency [rad/s]

Greek lower case letters

α	Phase angle [m]
$\boldsymbol{\phi_n}$	Mode shape
φ''	Factor for track irregularities
ρ	Density [kg/m³]
ζ	Viscous damping factor [%]
ω_d	Damped circular natural frequency [rad/s]
ω_n	Undamped circular natural frequency [rad/s]

1 Introduction

1.1 Background

High-speed trains are getting more common around the world and are soon to be introduced in Sweden. The construction of a double track railway line for high-speed trains between Gothenburg and Stockholm is currently being planned with an intended line speed of 320 km/h. By introducing new high-speed routes, travelling times for passengers can be reduced and existing lines can be utilized by additional freight traffic. High-speed railway lines offer a sustainable and comfortable way of travel. The high-speed trains are very energy efficient with a low environmental impact and it promotes economic growth by connecting larger regions (Europakorridoren AB, 2016).

Bridges are an important asset in order to utilize the landscape and avoid interruption of existing infrastructure. Increased train speeds induce higher dynamic effects on railway bridges and these effects must be considered in design. The dynamic response is important in order to ensure traffic safety and comfort for the passengers. High accelerations in the bridge deck may cause destabilization of the ballast and high accelerations in the train cabin may cause an unpleasant journey for the passengers.

For railway bridges with an intended train speed below 200 km/h it is generally sufficient to design for static loads. The dynamic effects may be accounted for by increasing the static loads with a dynamic amplification factor. According to Eurocode 1, SS-EN 1991-2 (CEN, 2003), a dynamic analysis is typically required for railway bridges subjected to train speeds exceeding 200 km/h, or for bridges with a fundamental frequency outside specified limits. A finite element analysis is required for complex systems to simulate the response, and account for the dynamic effects of the bridge. There are specifications in Eurocode on what a dynamic analysis should include and there are also limitations that needs to be fulfilled. Vertical accelerations of the bridge deck are generally the decisive factor in dynamic analyses (Andersson, et al., 2011).

When designing a railway bridge for high-speed traffic, it is important to understand how different parameters influence the dynamic response. Even though a bridge is satisfactory for static load effects, it might be inadequate in terms of dynamic behaviour. Different structural choices may have a great impact on the dynamic response and by having some basic dynamic knowledge behind the most influential parameters, a better bridge design can be obtained early in the design phase.

1.2 Purpose

The purpose of this Master's Thesis was to increase the understanding of structural dynamics of railway bridges subjected to high-speed trains. The aim was also to be able to describe for engineers and non-specialists what parameters are the most influential when designing railway bridges subjected to high-speed trains.

1.3   Limitations

This thesis was limited to describe the structural response of railway bridges and the FE-analyses were focused on comparing the following bridge types:

- Simply supported reinforced concrete slab bridge (with and without end shields)

- Simply supported reinforced concrete trough bridge (with and without end shields)

- Continuous reinforced concrete slab bridge with end shields (two-span and three-span)

Dynamics in vertical direction was primarily considered and emphasis was put on vertical accelerations and deflections. Only bridges with ballasted single tracks were considered in the numerical analyses.

1.4   Method

To augment the understanding of theoretical models, a literature study was carried out. The studied subjects were structural dynamics for railway bridges, implementation of Eurocode and TRVK Bro 11 as well as how the dynamic response could be modelled in BRIGADE/Plus.

The dynamic analyses were performed in BRIGADE/Plus using Eurocode and TRVK Bro 11 specifications and it included several different types of reinforced concrete bridges as described above. In the initial part of the analyses, the simply supported bridges without end shields were subjected to a single moving point load. The response was then compared to the same case of an analytical beam model for verification and in order to comprehend the dynamic behaviour. The complexity of the analyses was then successively increased by introducing train load models and providing the bridges with end shields as well as continuity.

Static deflection from deadweight and natural frequencies of the less complex models were compared to hand calculations for verification. Hand calculations were carried out using Mathcad and MATLAB.

This master thesis was a co-operation between COWI and Chalmers University of Technology. The thesis was carried out at COWI, Division of Civil Structures in Gothenburg.

2   Introduction to structural dynamics

Structural dynamics is an important topic when it comes to designing different structures subjected to dynamic loading such as bridges, vehicles, offshore oil platforms etc. The dynamic response of a structure differs from the static one since inertial effects are induced, arising from accelerations of the structure. Furthermore, it is a more complicated problem than the static one due to its time dependency. A dynamic load can vary in time with respect to magnitude, direction, or point of application and a solution has to be established for each time step of interest. If the inertial forces from dynamic loading have a considerable effect on the response of a structure, a dynamic analysis is necessary (Craig Jr & Kurdila, 2006).

In the following chapter, the basics of structural dynamics will be presented in order to establish a basic understanding of the dynamic phenomenon.

2.1   Vibration of SDOF systems

In order to understand the basics of structural dynamics it is convenient to start with a single-degree-of-freedom (SDOF) spring-mass system as presented in Figure 2.1. The system can be complemented with a damping model. The simplest analytical damping model is the linear viscous dashpot model, where the damping force is a linear function of the relative velocity. The equation of motion can be established by adopting Newton´s second law and include all forces acting on the system (Craig Jr & Kurdila, 2006).
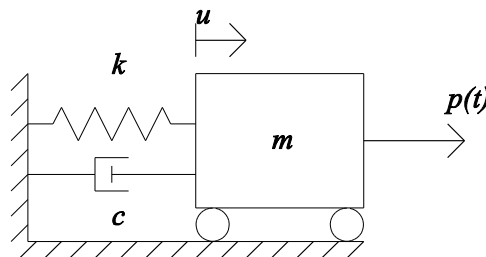
Figure 2.1   Simple spring-mass-dashpot model.

$$m\ddot{u} + c\dot{u} + ku = p(t) \tag{2.1}$$

where m is the mass, c is the damping coefficient and k is the spring stiffness. Equation (2.1) can be solved analytically according to eq (2.2) with a particular solution $u_p(t)$, related to forced motion, and a complementary solution $u_c(t)$, related to natural motion.

$$u(t) = u_p(t) + u_c(t) \tag{2.2}$$

Equation (2.1) can be rewritten as

$$\ddot{u} + 2\zeta\omega_n\dot{u} + \omega_n^2 u = \omega_n^2 \frac{p(t)}{k} \tag{2.3}$$

where $\omega_n = \sqrt{k/m}$ is the undamped circular natural frequency, $\zeta = c/c_{cr}$ is the viscous damping factor and $c_{cr} = 2\sqrt{km}$ is the critical damping coefficient.

The complementary solution is assumed to be on the form

$$u(t) = \overline{C}e^{\overline{s}t} \tag{2.4}$$

Inserting eqs (2.3) and (2.4) gives the following characteristic equation

$$\overline{s}^2 + 2\zeta\omega_n\overline{s} + \omega_n^2 = 0 \tag{2.5}$$

whose roots are given by

$$\overline{s}_{1,2} = -\zeta\omega_n \pm \omega_n\sqrt{\zeta^2 - 1} \tag{2.6}$$

The solution of the characteristic equation will be different depending on the value of the viscous damping factor ζ. Three different cases can be studied: underdamped (0 < ζ < 1), critically damped (ζ = 1) and overdamped (ζ > 1). The underdamped case can be characterised by an oscillating motion with decreasing amplitude. For the overdamped system, the amplitude will decay slowly and no oscillation will occur. The last case with critical damping is also characterised by no oscillation but the amplitude will decay faster than for the two other cases (Craig Jr & Kurdila, 2006). Figure 2.2 illustrates the behaviour of these three cases for a SDOF system.
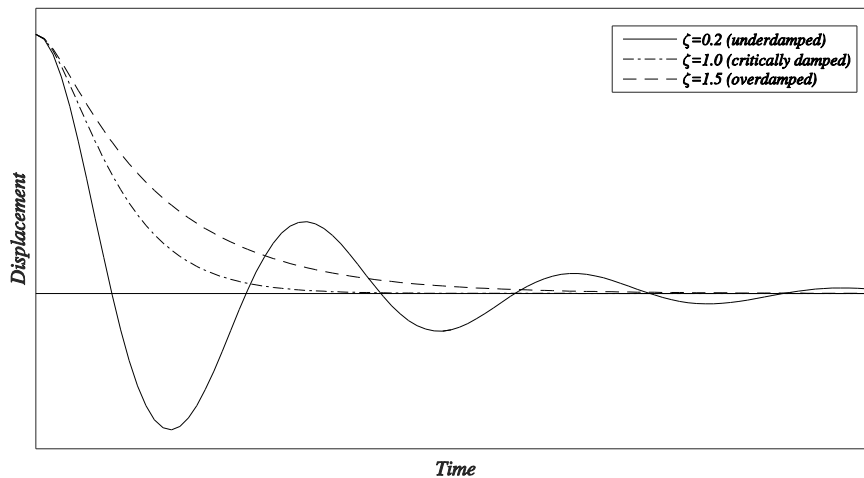
Figure 2.2   Comparison between underdamped, critically damped and overdamped SDOF system.

For structural dynamics applications, the underdamped case is most relevant since the viscous damping factor is usually well below the critical damping for real structures and this case will therefore be studied further.

For an underdamped system, the characteristic equation will have complex roots and Eq (2.6) can then be rewritten as

$$\overline{s}_{1,2} = -\zeta\omega_n \pm i\omega_d \tag{2.7}$$

where ω_d is the damped circular natural frequency, given by

$$\omega_d = \omega_n \sqrt{1 - \zeta^2} \qquad (2.8)$$

By adopting Euler´s formula, the general solution for a free vibrating case can be expressed in terms of trigonometric functions

$$u_c(t) = e^{-\zeta \omega_n t} \left(A_1 \cos(\omega_d t) + A_2 \sin(\omega_d t) \right) \qquad (2.9)$$

Now consider the particular solution of eq (2.1), assuming a harmonic excitation of the force *p(t)*.

$$p(t) = p_0 \cos(\Omega t) \qquad (2.10)$$

where Ω is the exciting frequency given in radians per second. The particular solution will be given by

$$u_p = U \cos(\Omega t - \alpha) \qquad (2.11)$$

where U is the steady-state amplitude and α is the phase angle, arising from the fact that the steady-state response will be out of phase with the excitation due to the damping. The velocity and acceleration will then be expressed as

$$\dot{u}_p = -\Omega U \sin(\Omega t - \alpha) \qquad (2.12)$$

$$\ddot{u}_p = -\Omega^2 U \cos(\Omega t - \alpha) \qquad (2.13)$$

By inserting eqs (2.10), (2.11), (2.12) and (2.13) into (2.1) the following expression is obtained

$$-m\Omega^2 U \cos(\Omega t - \alpha) - cU \sin(\Omega t - \alpha) + kU \cos(\Omega t - \alpha) = p_0 \cos(\Omega t) \qquad (2.14)$$

which can be used to obtain an expression for the steady-state amplitude *U*,

$$U = \frac{p_0}{\sqrt{(k - m\Omega)^2 + (c\Omega)^2}} \qquad (2.15)$$

Eq (2.15) can be rewritten as

$$U = \frac{U_0}{\sqrt{(1 - r)^2 + (2\zeta r)^2}} \qquad (2.16)$$

where the static displacement is defined as

$$U_0 = \frac{p_0}{k} \qquad (2.17)$$

and the frequency ratio is defined as the ratio between the loading frequency and the natural frequency of the system given by

$$r = \frac{\Omega}{\omega_n} \tag{2.18}$$

The phase angle is given by

$$\tan(\alpha) = \frac{2\zeta r}{1 - r^2} \tag{2.19}$$

By combining the particular solution and the complementary solution, the total response of the damped SDOF system can be expressed as

$$u(t) = \frac{U_0}{\sqrt{(1 - r^2)^2 + (2\zeta r)^2}} \cos(\Omega t - \alpha) + e^{-\zeta \omega_n t} \left(A_1 \cos(\omega_d t) + A_2 \sin(\omega_d t) \right) \tag{2.20}$$

The constants A_1 and A_2 can be determined from the initial conditions of the system.

2.2   Resonance

Resonance is a very important phenomenon when it comes to structural dynamics and it can cause major damages of structures if it is not considered in the design. Resonance occurs when a frequency of an external excitation coincides with the natural frequency of a system, i.e. if r in eq (2.18) is close or equal to one. The dynamic response of the system will then increase rapidly.

One way to study the resonance effect is to introduce the steady-state amplification factor $D_s(r)$, defined as the ratio between the dynamic amplitude and the static displacement amplitude given by

$$D_s(r) = \frac{U(r)}{U_0} \tag{2.21}$$

Substituting eqs (2.16) and (2.17) into eq (2.21) yields

$$D_s(r) = \frac{1}{\sqrt{(1 - r^2)^2 + (2\zeta r)^2}} \tag{2.22}$$

By plotting the steady-state amplification factor $D_s(r)$ against the frequency ratio r, a very clear illustration of the resonance phenomenon is obtained, see Figure 2.3.
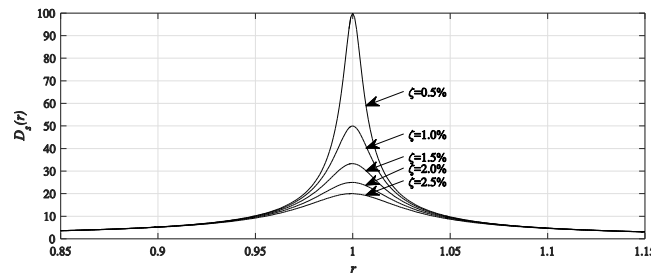
Figure 2.3   Resonance peaks for different amount of damping.

2.3   MDOF systems

In Section 2.1, a simple SDOF system was discussed and a solution for an underdamped system subjected to a harmonic excitation was derived. In order to model more complex structures, it is generally necessary to adopt a more complex model, such as the multi-degree-of-freedom (MDOF) system. MDOF models are the basis of finite element modelling and thus they are crucial when analysing complex dynamic problems.

The equation of motion for a MDOF system can be derived in the same manner as for SDOF systems, but including more degrees of freedom. Figure 2.4 illustrates a damped spring-mass system with two degrees of freedom.
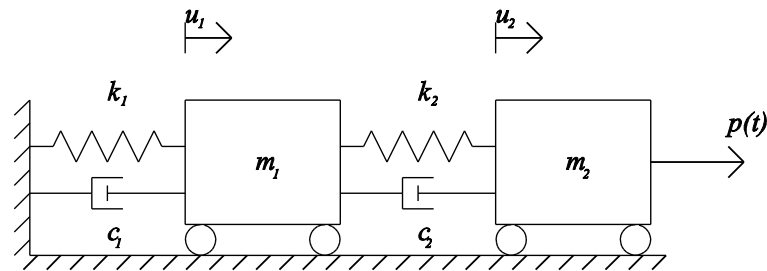
Figure 2.4   A MDOF system with two degree of freedom.

The equation of motion can be written on matrix form as

$$\mathbf{M\ddot{u}} + \mathbf{C\dot{u}} + \mathbf{Ku} = \mathbf{p}(t) \tag{2.23}$$

where $\mathbf{M}$, $\mathbf{C}$ and $\mathbf{K}$ are the mass, damping and stiffness matrices respectively. Equation (2.23) can be expressed explicitly as

$$\begin{bmatrix} m_1 & 0 \\ 0 & m_2 \end{bmatrix} \begin{bmatrix} \ddot{u}_1 \\ \ddot{u}_2 \end{bmatrix} + \begin{bmatrix} c_1 + c_2 & -c_2 \\ -c_2 & c_2 \end{bmatrix} \begin{bmatrix} \dot{u}_1 \\ \dot{u}_2 \end{bmatrix} + \begin{bmatrix} k_1 + k_2 & -k_2 \\ -k_2 & k_2 \end{bmatrix} \begin{bmatrix} u_1 \\ u_2 \end{bmatrix} = \begin{bmatrix} 0 \\ p(t) \end{bmatrix} \tag{2.24}$$

The same principal can be adopted for many degree of freedom systems and even for 3D-systems.

2.3.1   Solving the dynamic response of MDOF systems

The natural frequencies of a system are of great importance for the dynamic response and they are essential for the systems reaction to dynamic loading. In Section 2.1 it was presented how the eigenfrequencies of a SDOF system could be obtained analytically. Eigenfrequencies for simple MDOF system can also be derived analytically, however, a numerical solution is generally required for more complex systems. Different strategies can be employed for solving a MDOF system in order to obtain the dynamic response. The most commonly used methods for complex systems is the mode superposition and direct time integration (Craig Jr & Kurdila, 2006). In the following sections some of the methods for solving MDOF systems is presented.

2.3.1.1 Natural frequencies of undamped MDOF system

The simplest MDOF system to determine the natural frequencies from is an undamped free vibrating case, with an equation of motion defined as

$$\mathbf{M\ddot{u} + Ku = 0} \tag{2.25}$$

Assuming a harmonic solution of the form

$$\mathbf{u}(t) = \mathbf{U}\cos(\omega_n t - \alpha) \tag{2.26}$$

and substituting eq (2.26) into eq (2.25) yields the following eigenvalue problem

$$\left[\mathbf{K} - \omega_n^2 \mathbf{M}\right]\mathbf{U} = \mathbf{0} \tag{2.27}$$

For the nontrivial solution of this problem, the following characteristic equation should be satisfied

$$\det(\mathbf{K} - \omega_n^2 \mathbf{M}) = \mathbf{0} \tag{2.28}$$

The roots of eq (2.28) corresponds to the eigenvalues of the system. For a system of N degrees of freedom, there will be N eigenvalues and N eigenmodes. The eigenvalues corresponds to squared eigenfrequencies. The eigenmodes can be determined by substituting the eigenfrequencies back into eq (2.27).

2.3.1.2 Mode superposition

In general, the dynamic problem equations are coupled and hence, the computational effort may be very extensive for large systems. An effective way to evaluate a dynamic problem is to adopt the mode-superposition method. The advantages is that the coupled equations can be transformed into uncoupled equations and the system can be solved as a number of SDOF equations. The eigenmodes are generally evaluated from the undamped system and they can be used to transform the stiffness, mass and damping matrices into diagonal modal matrices using the following expressions (Craig Jr & Kurdila, 2006),

$$K = \mathbf{\Phi}^{\mathrm{T}}\mathbf{K}\mathbf{\Phi} \tag{2.29}$$

$$M = \mathbf{\Phi}^{\mathrm{T}}\mathbf{M}\mathbf{\Phi} \tag{2.30}$$

$$C = \mathbf{\Phi}^{\mathrm{T}}\mathbf{C}\mathbf{\Phi} \tag{2.31}$$

where $\mathbf{\Phi}$ is the eigenvector matrix including all eigenmodes. The fundamental step for mode superposition is to adopt a coordinate transformation of the displacement according to eq (2.32).

$$\mathbf{u}(t) = \mathbf{\Phi}\boldsymbol{\eta}(t) = \sum_{r=1}^{N} \boldsymbol{\phi}_r\, \eta_r(t) \tag{2.32}$$

where $\boldsymbol{\eta}(t)$ is the principal coordinate vector, $\boldsymbol{\phi}_r$ is the rth eigenvector and $\eta_r(t)$ is the rth principle coordinate.

Equation (2.32) can be substituted into eq (2.23) in order to obtain the equation of motion in principle coordinates:

$$M\ddot{\eta} + C\dot{\eta} + K\eta = f(t) \qquad (2.33)$$

where

$$f(\mathrm{t}) = \Phi^{\mathrm{T}} \mathbf{p}(t) \qquad (2.34)$$

Another advantage with the mode superposition method is that the system can be reduced by only include eigenvectors corresponding to the lowest eigenfrequencies. In structural dynamic application, higher frequencies have often a negligible effect on the structure and by only include the lowest frequencies, a very good approximation can be obtained. Hence, the dynamic analysis will be less extensive and less time consuming.

It should be noted that mode superposition can only be adopted when the damping matrix can be represented by diagonal terms only. There are some situations where this is not possible and one such modelling case may be a building and its surrounding soil, in which the damping matrix will have off-diagonal values. Furthermore, mode-superposition can only be used for linear systems and in order to include non-linearities, other methods need to be considered. In such cases it is convenient to use numerical integration methods instead (Craig Jr & Kurdila, 2006).

2.4 Continuous systems – Vibration of beams

In the previous sections, SDOF and MDOF systems have been presented in order to understand the dynamic behaviour of a structure. These models are discrete-parameter models with a finite number of degrees of freedom. However, a real structure constitutes of an infinite number of degrees of freedom and hence, an infinite number of eigenfrequencies. Such continuous system can be represented by partial differential equation models and are recognised as the exact analytical solution of a system (Craig Jr & Kurdila, 2006).

A railway bridge can generally be idealized as beam elements and therefore a continuous beam system will be presented in the following section.

2.4.1 Transverse vibration of beams

The simplest way to represent a beam member is to implement Bernoulli-Euler beam theory, which can be adopted for members with small transverse dimensions compared to the longitudinal length (Craig Jr & Kurdila, 2006). The differential equation of motion of such beam is

$$\frac{\partial^2}{\partial x^2}\left(EI\,\frac{\partial^2 u}{\partial x^2} \right) + c\,\frac{\partial u}{\partial t} + \rho A\,\frac{\partial^2 u}{\partial t^2} = p_y(x,t) \qquad (2.35)$$

where u is the vertical deflection, x is the length coordinate, EI is the flexural rigidity, c is the damping coefficient and ρA is the mass per unit length.

For free vibrations of an undamped uniform beam with constant flexural rigidity eq (2.35) can be reduced to

$$(EIu'')'' + \rho A \ddot{u} = 0 \qquad (2.36)$$

Assuming harmonic motion given by

$$U(x,t) = U(x)\cos(\omega t - \alpha) \qquad (2.37)$$

and inserting this into eq (2.36) will result in the eigenvalue equation

$$(EIU'')'' - \rho A \omega^2 U = 0 \qquad (2.38)$$

which can be rewritten as

$$\frac{d^4 U}{dx^4} - \lambda^4 U = 0 \qquad (2.39)$$

where

$$\lambda^4 = \omega^2 \frac{\rho A}{EI} \qquad (2.40)$$

The general solution of eq (2.39) can be expressed as

$$U(x) = C_1 \sinh(\lambda x) + C_2 \cosh(\lambda x) + C_3 \sinh(\lambda x) + C_4 \cosh(\lambda x) \qquad (2.41)$$

The constants may be determined in terms of boundary conditions. For a simply supported beam, there are zero deflection and zero moment at the supports, i.e. the boundary conditions are

$$u(0,t) = 0 \qquad (2.42)$$

$$u''(0,t) = 0 \qquad (2.43)$$

$$u(L,t) = 0 \qquad (2.44)$$

$$u''(L,t) = 0 \qquad (2.45)$$

By using these together with eq (2.41), the eigenfrequencies and mode shapes can be determined as

$$\omega_n = \left(\frac{n\pi}{L}\right)^2 \sqrt{\frac{EI}{\rho A}} \qquad (2.46)$$

$$\phi_n = \sin\left(\frac{n\pi x}{L}\right), \quad n = 1,2,3... \qquad (2.47)$$

The first three mode shapes are illustrated in Figure 2.5.
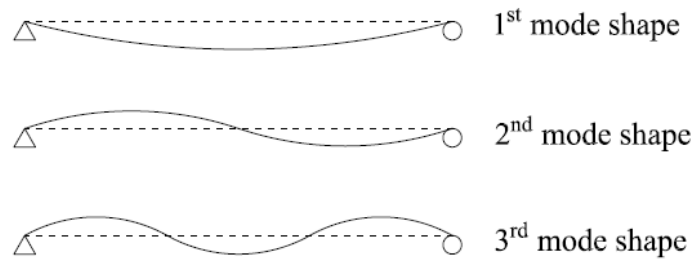
Figure 2.5   First three mode shapes of a simply supported beam.

2.4.2   Beam subjected to a moving point load

A beam subjected to a moving point load can be solved analytically by consider the beam in Figure 2.6 with a length L and a point load p_0 moving at constant speed v_0.
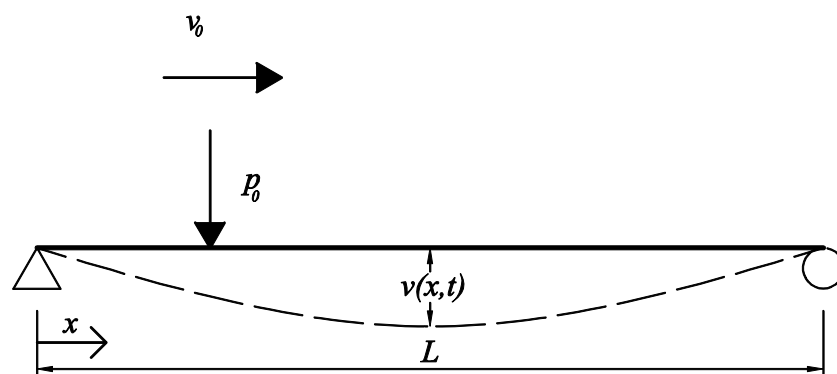
Figure 2.6   Illustration of the moving load problem over a simply supported beam.

The differential equation of motion and boundary conditions from Section 2.4.1 is applicable for this case as well. In addition, the initial condition of the beam is necessary in order to solve the moving load problem. The beam is assumed to be undeformed and at rest when the load is applied. The initial conditions can then be stated as

$$u(x,0) = 0 \qquad\qquad (2.48)$$

$$\dot{u}(x,0) = 0 \qquad\qquad (2.49)$$

The deflection of the beam can be expressed in terms of mode superposition as the sum of the product of the nth mode shape function $\phi_n(x)$ and the nth generalized coordinate $q_n(t)$ according to eq (2.50)

$$u(x,t) = \sum_{n=1}^{\infty} \phi_n(x) q_n(t) \qquad\qquad (2.50)$$

For the given mode shape function in eq (2.47), it can be shown that the complete solution for a simply supported beam subjected to a moving point load can be expressed as

$$u(x,t) = \sum_{n=1}^{\infty} \left[\begin{array}{c} \dfrac{2p_0 L^3 /(EIn^4\pi^4)}{(1-S_n^2)^2+(2\zeta S_n)^2} \cdot \\[2mm] \left[(1-S_n^2)\sin(\Omega_n t) - 2\zeta S_n\cos(\Omega_n t) + e^{(-\zeta\omega_n t)} \cdot \right. \\[2mm] \left. \cdot\left(2\zeta S_n\cos(\omega_{dn}t) + \dfrac{S_n}{\sqrt{1-\zeta^2}}(2\zeta^2+S_n^2-1)\sin(\omega_{dn}t)\right) \right] \end{array} \right] \sin\left(\dfrac{n\pi x}{L}\right) \qquad (2.51)$$

where Ω_n is the exciting frequency given by

$$\Omega_n = \frac{n\pi v_0}{L} \qquad (2.52)$$

and S_n is a non-dimensional speed parameter defined as

$$S_n = \frac{\Omega_n}{\omega_n} = \frac{n\pi v_0}{\omega_n L} \qquad (2.53)$$

The formulation of the beam displacement is only valid when the point load excites the beam i.e. for $0 < v_0 t < L$. A complete derivation of the analytical solution of a simply supported beam subjected to a moving point load can be found in *Vehicle-Bridge Interaction Dynamics – With Applications to High-Speed Railways* (Yang, et al., 2004).

The effect of damping may be neglected when studying the dynamic response of a simply supported beam subjected to a moving point load. The reason is that the damping has a low impact on the response since the acting time of the point load is relatively short (Yang, et al., 2004). By neglecting the influence of damping, eq (2.51) reduces to

$$u(x,t) = \frac{2p_0 L^3}{EI\pi^4}\sum_{n=1}^{\infty}\frac{1}{n^4}\sin\left(\frac{n\pi x}{L}\right)\left(\frac{\sin(\Omega_n t)-S_n\sin(\omega_n t)}{1-S_n^2}\right) \qquad (2.54)$$

3 Dynamic behaviour of railway bridges

The dynamic behaviour of railway bridges is an important subject in bridge design, especially when loads from high-speed trains are to be considered. The dynamic response is influenced by a number of different factors, including the characteristics of the bridge itself as well as the characteristics of the vehicles travelling on the bridge.

This chapter will include an introduction to some dynamic effects of railway bridges as well as a presentation of the most important bridge parameters that may influence the response and how these may be modelled in a dynamic analysis. Furthermore, a presentation of how the dynamic effects are considered in Eurocode 1, SS-EN 1991-2 (CEN, 2003) and in the Swedish national code TRVK-Bro 11 (Swedish Transport Administration, 2011) will be included.

3.1 Dynamic effects to be considered on railway bridges

The mode shapes and corresponding eigenfrequencies of a railway bridge may occur with different characteristics, such as vertical, horizontal transverse, longitudinal and torsional. In Figure 3.1, these mode shapes are illustrated for a simply supported bridge. Dynamic loading from trains induces these kind of vibrations and may cause problems for the structure.
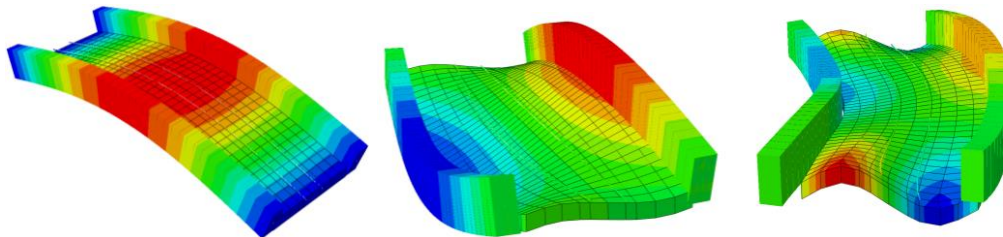
Figure 3.1   Typical natural modes of railway bridges including vertical bending, torsional and horizontal transverse.

The applied load on a railway bridge mainly arise from the trains travelling along the bridge. These vehicles are complex systems subjecting the bridge to forces in many directions, hence exciting the different eigenmodes of the bridge (Frýba, 1996). In addition, the bridge is subjected to wind, snow, earth pressure, temperature differences as well as creep and shrinkage.

The dynamic effects from vertical forces mainly arise from wheel and axle forces of the moving vehicles. In the horizontal transverse plane, centrifugal forces from curved bridges and lateral impacts is dominating the response. The lateral dynamics are significant for high bridges in particular due to the increasing wind loads higher up. The longitudinal forces are a result of accelerations and decelerations of trains and may induce axial vibrations of the deck. Torsional vibrations may be initiated by track eccentricities of a single track or by trains moving along one side of a double track bridge, thus induce twisting moments (Arvidsson & Karoumi, 2014).

All the dynamic effects described above will be magnified in the presence of resonance, which may cause problem for the bridge and compromise the safety of the structure.

3.1.1 Resonance and cancellation effects

For railway bridges subjected to high-speed trains, the effect of resonance needs to be considered. The trains are composed of coaches with regularly spaced axles which excites the bridge with a certain frequency. At high speeds these frequencies may coincide with the natural frequencies (or a multiple of it) of the bridge and resonance will occur. In such case, a dynamic analysis is essential in order to evaluate the response. However, significant resonance effects are unlikely to occur for train speeds below 200 km/h, and in such case it is generally sufficient to magnify the static response with a dynamic amplification factor.

The resonance speed of a bridge may be calculated according to

$$v_n^j = \frac{\omega_n D}{2 j \pi} = \frac{f_n D}{j}, \qquad j = 1,2,3... \qquad (3.1)$$

where v_n^j is the jth resonance speed of the nth mode and f_n is the natural frequency in Hertz (Cho, et al., 2016).

When a train is moving at resonance speed, the dynamic effects will increase every time an axle excites the bridge and the maximum response is generally obtained when the last load has passed. However, for a damped structure, the amplitude will converge towards a maximum value as the number of loads increases (Li & Su, 1999).

Another phenomenon that may occur under specific conditions is cancellation effects which may, on the contrary to resonance, supress the dynamic vibrations. These effects occur for specific span to vehicle length ratios together with a certain train speed.

Both the resonance and cancellation effects may be derived for a simply supported beam in order to illustrate at what conditions these effects may occur. As a result, it is possible to suggest optimal design conditions in order to obtain minimal dynamic response. This have been done in several studies and (Yang, et al., 2004) showed this by deriving the train load as a set of two moving loads with constant intervals, representing the train axles. An expression of the speed parameter of the first mode, $S_1 = \Omega / \omega_1$ was derived in order to state a resonance condition as

$$S_1 = \frac{D}{2iL}, \qquad i = 1,2,3... \qquad (3.2)$$

As can be seen from this expression, a longer beam will obtain a lower speed at which resonance occurs. It was concluded that the most critical condition was obtained when the speed parameter equals 0.5D/L, representing the primary resonance speed. For the higher integers i, the resonance peaks will appear at lower speeds, however, the response is decreased and their influence are generally neglected (Yang, et al., 2004).

From the result it was observed that it is theoretically possible to select a speed at which cancellation effects occur and thus providing a better dynamic performance of the bridge. Similar to the expression for resonance condition, (Yang, et al., 2004) derived the condition of cancellation as

$$S_1 = \frac{1}{2i-1}, \qquad i = 1,2,3...\qquad (3.3)$$

In practise, it is possible to select a suitable vehicle length and span length in order to obtain an optimal dynamic behaviour where the primary resonance response is supressed. By letting the first critical resonance speed, i.e. $S_1 = 0.5D/L$ equal any of the cancellation speeds in eq (3.3), an expression for the optimal span/vehicle length ratio is given by eq (3.4). Noticeable is that this expression is independent of the speed.

$$\frac{L}{D} = i - 0.5, \qquad i = 1,2,3...\qquad (3.4)$$

In order to illustrate the resonance and cancellation effects, the midpoint response of an undamped beam is plotted in Figure 3.2 with two different speeds causing resonance and cancellation. It can be seen that at resonance speed, the response is increasing when more loads are passing the beam. At cancellation speed, there are no amplification effects of the response and as the last load has passed the bridge, no residual response remains even though no damping is applied to the beam (Yang, et al., 2004).
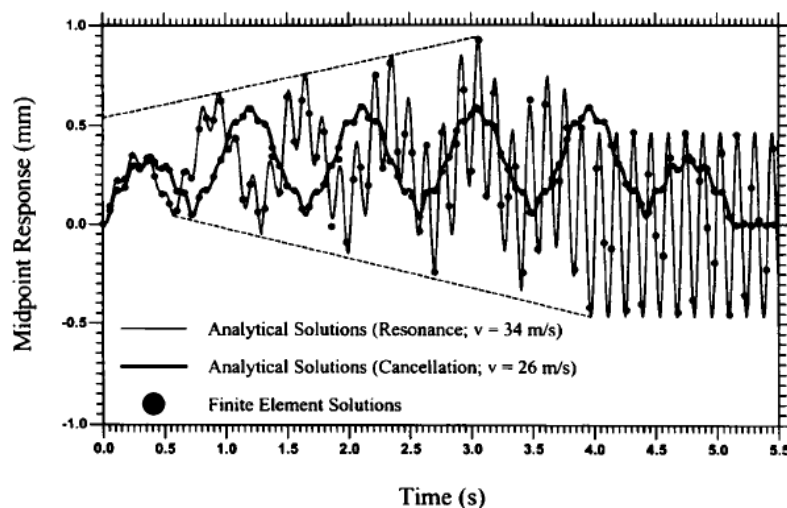
Figure 3.2   Illustration of the resonance and cancellation effects of a simply supported beam subjected to a moving train of 5 cars with identical lengths (Yang, et al., 2004).

Similar results were obtained in a study conducted by (Cho, et al., 2016) where they evaluated resonance and cancellation effects for bridges subjected to high-speed trains. For simply supported bridges the optimal span length was found to be 1.5D, 2.5D, 3.5D etc., which is the same result as in eq (3.4). Moreover, an increased number of spans gave additional optimal design lengths. As an example a two-span continuous bridge had optimal span lengths of D, 1.5D, 2D, 2,5D, etc.

In order to illustrate the cancellation effects, a resonance spectrum F_1^j corresponding to the first mode of the jth resonance speed was introduced in the study by (Cho, et al., 2016). It was defined as the response in terms of the ratio of the distance between loads and the span length of the bridge. The resonance spectrum is plotted against the

span to coach length ratio in Figure 3.3 where the optimal ratios are clearly illustrated. Diagram (b) in the figure corresponds to the envelope resonance spectrum of the first mode, which includes ten resonance spectra. It can be seen that for higher span to coach length ratios, i.e. for longer bridges, the dynamic response is reduced.
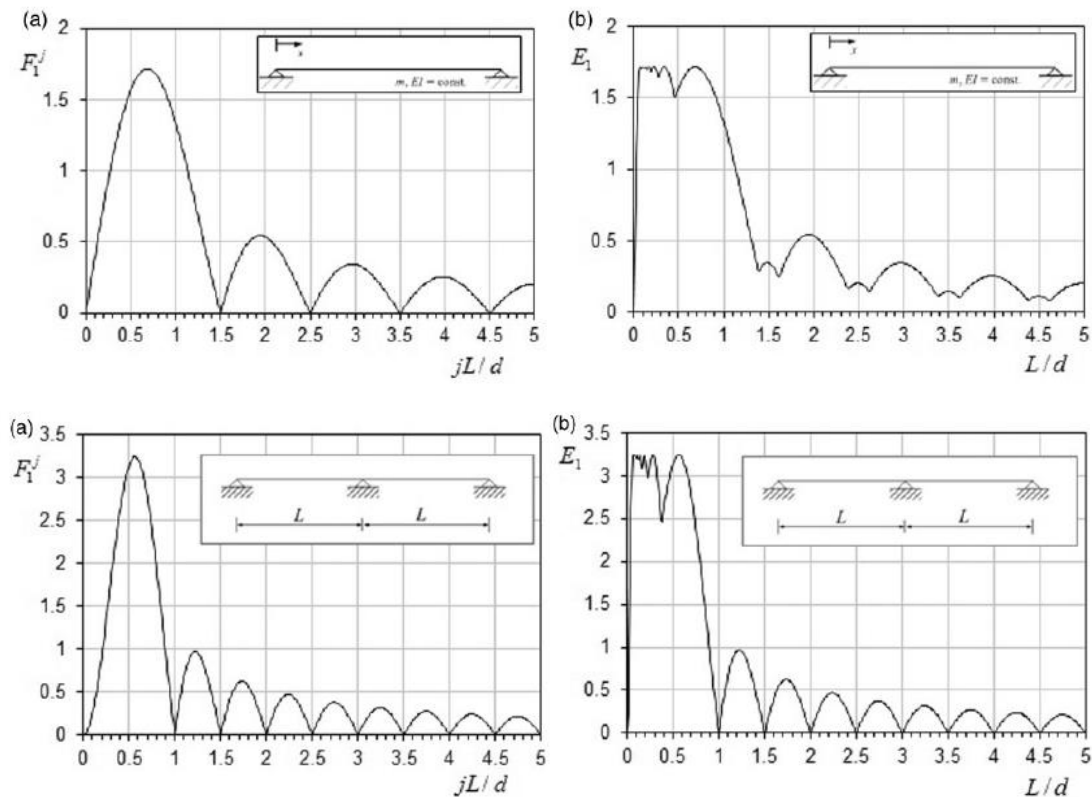
Figure 3.3   Resonance spectrum of single-span and two-span continuous beams for the first mode.

It should be noted that even though it is possible to find an optimal span length for a certain vehicle length or vice versa, the application in a real design case may be difficult since the bridge should most certainly be checked for various train types and loads. As an example, the high-speed load model that should be adopted according to Eurocode 1, SS-EN 1991-2 (CEN, 2003) includes 10 train types, all with different optimal span length.

3.2   Important parameters for dynamic bridge response

There are a lot of different parameters that contributes to the dynamic response of a bridge when it is subjected to dynamic loading. The most obvious ones are the damping, stiffness and mass of the structure that are highly influential, but in addition there are a number of other factors that needs to be considered. In the following section, the most important bridge parameters and their contribution to the dynamic behaviour will be introduced.

3.2.1 Damping

The damping of a railway bridge has a high influence of the dynamic behaviour, especially at resonance, and it is a desirable effect that reduces the dynamic response. A bridge starts to vibrate as soon as a train is passing along and when the train has passed, the bridge will vibrate freely until it eventually reaches equilibrium as a result of the damping property (Frýba, 1996). The effect of damping at resonance peaks is illustrated in Figure 2.3, Section 2.2.

The damping phenomenon is complex and occurs due to energy losses during cycles of oscillation. The energy dissipation is a result of a number of factors such as: friction in the material, friction at supports, deformations of the material, opening and closing of cracks etc. The amount of damping in a specific bridge can vary depending on the amplitude of vibration, temperature, whether the track is ballasted or not and influence of boundary conditions (ERRI, 1999).

Due to the complex nature of damping, it is almost impossible to take all influencing parameters into account when evaluating the damping properties of a bridge. As a result, there are no theoretical equations for determining the damping coefficients to be used in design. Instead, the proposed design values are based on empirical data obtained from real bridge experiments (Frýba, 1996).

Damping is generally expressed as a ratio of critical damping c_{cr} as

$$\zeta = \frac{c}{c_{cr}}\left[\%\right] \tag{3.5}$$

3.2.1.1 Dampers

Additional damping may be applied to the structure if dampers are installed. By tuning the dampers to affect a certain frequency, the response from that frequency will be reduced.

Dampers are categorized into three main categories; active, semi-active and passive control systems. The active control systems needs an external power supply whilst a passive control system uses the motion of the structure to increase the damping (Beygi, 2015).

According to a master thesis from KTH (Beygi, 2015), tuned mass dampers (TMD) installed in the middle of the bridge, could be used to significantly decrease the response. Another master thesis (Rådeström & Tell, 2014) investigated how fluid viscous dampers (FVD) could be applied to decrease the response. The FVD's would be applied at each support and the TMD's at the middle of the bridge. Both systems are passive and can be seen in Figure 3.4.

| a) | b) |
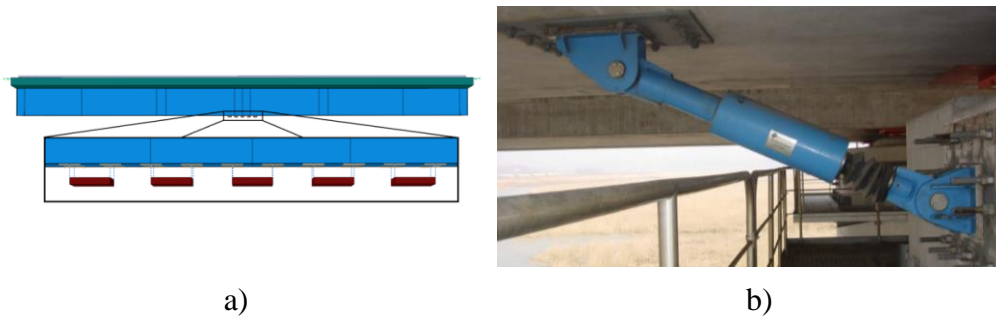
Figure 3.4   Tuned mass dampers a) (Beygi, 2015) and a fluid viscous damper b) (Rådeström & Tell, 2014).

The dampers are passively decreasing the influence of a certain frequency and thus reducing the response as can be seen in Figure 3.5. The reports came to the conclusion that it is possible to significantly decrease accelerations and deflections due to dynamic loading with TMD's and FVD's respectively.
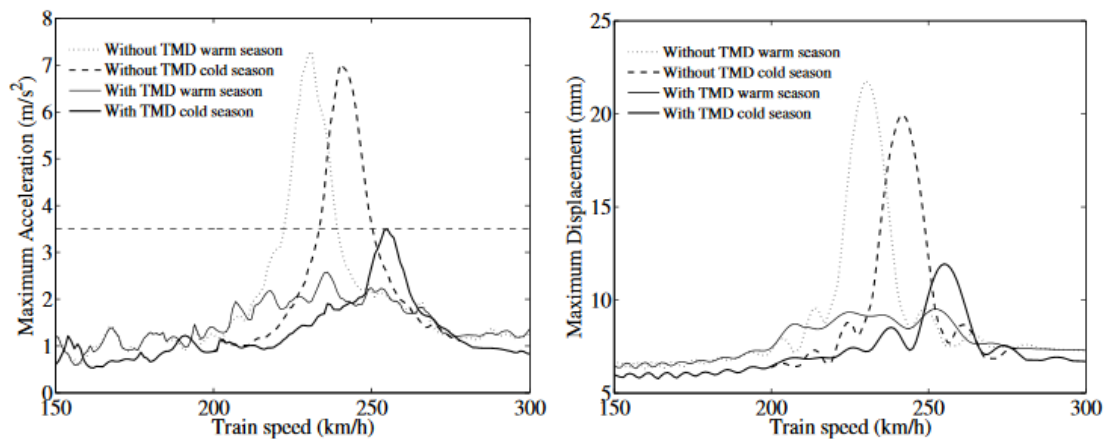
Figure 3.5   Influence of multiple tunes mass dampers on a railway bridge subjected to HSLM-A3 (Beygi, 2015).

3.2.2   Mass

The mass in a structural dynamic problem is related to the acceleration of the structure. If a load is applied at a sufficiently slow rate, the problem can be considered as static since the inertial effects will be negligible. Nonetheless, when the load application is relatively fast i.e. having a high speed, the inertial effects can have a large influence of the structure and needs to be considered. In such case, the mass has a great impact of the dynamic response of the structure.

By looking at the expression for the natural frequency of a simply supported beam given by eq (2.46) in Section 2.4.1, it is clear that the eigenfrequency is inversely proportional to the square root of the mass. An increase in mass will thereby decrease the natural frequency of a structure and thus lower the speed at which resonance occur.

At resonance, the maximum acceleration is inversely proportional to the mass of the structure. Hence, an increase in mass will lower the maximum acceleration. Apart from the regions at which resonance occurs, the dynamic behaviour of the beam is dominated by the response from the first axle load exciting the bridge (ERRI, 1999).

In design situations it is therefore important to assess two cases; one where a lower bound estimate of the mass is considered in order to predict maximum deck accelerations and one where an upper bound is considered to obtain the lowest speed at which resonance is likely to occur (ERRI, 1999).

3.2.3 Stiffness

The natural frequency of a railway bridge is proportional to the square root of the stiffness as can be seen in eq (2.46). Increasing the stiffness of a structure will raise the natural frequency and thus increase the speed at which resonance effects are likely to occur. Furthermore, the deflection will decrease with an increase of stiffness but the acceleration will be unaffected.

The stiffness of concrete structures is generally difficult to predict and it is recommended to use a lower bound value in design. Even though a lower value of the stiffness is conservative it should be noted that it could result in the appearance of new resonance peaks in the considered speed interval. This may result in a need for higher stiffness in order to move the new resonance peak outside the design interval again. Increasing the stiffness can often cause an increase of the mass which in turn will lower the speed at which resonance occur. In conclusion, a too conservative assumption of the stiffness may result in a redundant and uneconomical structure (Andersson, et al., 2010).

3.2.4 Length and number of spans

The influence of variation of length and number of spans has generally shown that the dynamic effects decreases for longer spans as well as for continuous bridges. By changing the span length of a bridge, the natural frequencies will be affected. Furthermore, the relation between the span length and the distance between train axles will be influenced.

In general, the natural frequencies are influenced by stiffness, mass and length as can be seen in eq (2.46). A lower natural frequency means that the speed at which resonance will occur is decreased as well. A parametric study of how the length and number of spans influenced the dynamic response was conducted by (Andersson, et al., 2010) where a number of bridge configurations were evaluated. The study was performed with 1 - 5 spans with a varying length of 8 - 60 meters in addition to other varying parameters. The applied load was the HSLM-A load model from Eurocode 1, SS-EN 1991-2 (CEN, 2003) and the maximum vertical accelerations were studied.

Results from the study regarding varying lengths showed that short bridges with low eigenfrequencies gave the highest accelerations. In order to avoid excessive dynamic effects the eigenfrequencies needs to be high for short bridges and bridges with low eigenfrequencies need to be sufficiently long. Furthermore, it was concluded that the lower limit for the first natural frequency n_0 in Eurocode 1, SS-EN 1991-2 (CEN, 2003), given by Figure 3.15, is a good recommendation in order to avoid excessive dynamic effects (Andersson, et al., 2010).

The obtained reduction of the dynamic effects of longer span bridges can be explained by the fact that if the bridge is longer than the distance between axles of the train, a number of axles will be on the bridge at different phases, hence cancelling effects will

occur. A simple illustration of the influence of span length on deflection for a simply supported bridge can be seen in Figure 3.6 (Calcada, et al., 2009).
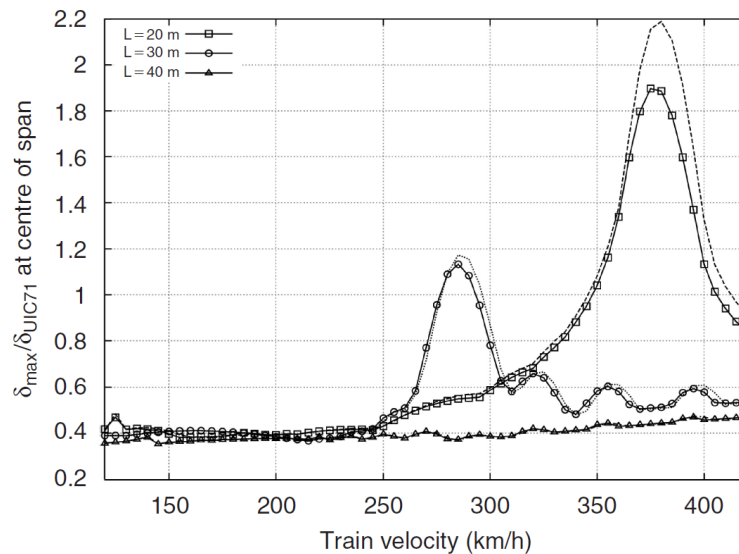
Figure 3.6   *Influence of span length on deflection of a simply supported bridge using a length of 20, 30 and 40 meters. Solid lines represent a moving load model and dashed lines represent a vehicle-bridge interaction model (Calcada, et al., 2009).*

The study by (Andersson, et al., 2010) regarding different number of spans was performed using the same length, mass and stiffness for all spans. It was concluded that for bridges with frequencies within the limits recommended by Eurocode, given in Figure 3.15, the vertical accelerations were decreased compared to single span bridges. Moreover, continuous short span bridges with low eigenfrequencies resulted in higher accelerations compared to single span bridges. As a result, a bridge design with continuity over supports instead of a series of simply supported spans will enhance the dynamic performance (Andersson, et al., 2010).

Similar results have been obtained in other studies as well and (Yau, 2001) concluded in a study that the dynamic response is decreased for continuous beams. Further observations stated that the number of resonance peaks increased with increasing number of spans even though the dynamic response was reduced, which can be observed in Figure 3.7. Moreover, the distribution of frequencies got denser as the number of spans was increased.
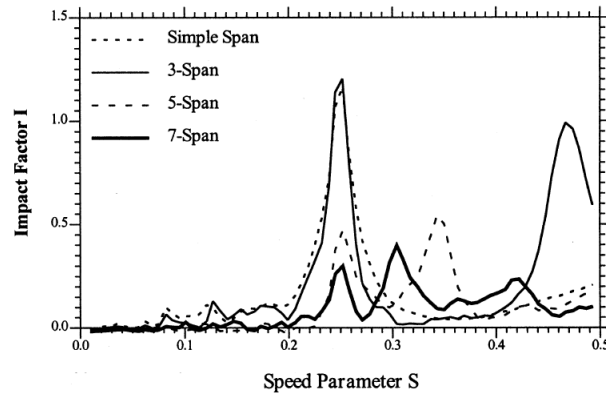
Figure 3.7   *Comparison of dynamic response of continuous beams with different number of spans where the impact response (defined as $I = \frac{R_d(x) - R_s(x)}{R_s(x)}$, where $R_d(x)$ and $R_s(x)$ are the maximum dynamic and static response respectively) is plotted against the speed parameter $S = \Omega/\omega$ (Yau, 2001).*

For simply supported bridges, the dynamic response is dominated by the first eigenfrequency and the corresponding eigenmode, whereas several eigenmodes influence the behaviour of continuous bridges and thus cancel each other out to some extent (Calcada, et al., 2009). Furthermore, the vibration energy can be spread more easily to the adjacent spans when the number of spans are increased and thus reduce the dynamic effects (Yau, 2001).

3.2.5   Ballasted and non-ballasted tracks

Traditionally, railway lines have been constructed using ballast in the supporting sub-structure. The ballast layer contains some sort of granular material which is packed in order to provide a sufficient support for rails and sleepers. Movements and deterioration of the ballast material may occur under loads from moving trains and this may cause irregularities of the track and thus induce additional stresses to the supporting structure as well as the moving vehicle. As a result, regular maintenance is required in order to preserve an accurate track alignment and ensure traffic safety.

An alternative to the traditional ballasted railway track is the non-ballasted track which consists of a solid slab that supports the rail and sleepers. As a result of the absence of ballast, the track will require less maintenance and thus enable high availability. With the increasing traffic intensity in our society it is important that the railway lines are available for trains as much as possible and thus low maintenance is a great advantage. For high-speed applications in particular, the ballasted tracks have shown to require more maintenance, mainly because of damages of wheels and rails from ballast particles that are churned up at high speeds. Furthermore, the non-ballasted tracks provide a lower structural height, lower weight and a higher precision of the track alignment compared to the ballasted alternative. Studies with regard to life-cycle costs have shown that slab tracks are a very good alternative to traditional ballasted tracks (Esveld, 2001).

A comparison of the dynamic behaviour of a railway bridge with ballasted and non-ballasted track was conducted in a study by (Casal, et al., 2011). The study included a bridge segment of four 28.4 meter spans made of pre-stressed concrete. For the

analysis with ballasted track, values of density was adopted with accordance to Eurocode and the ballastless track consisted of Rheda 2000 slabs. Load model HSLM-A10 from Eurocode 1, SS-EN 1991-2 (CEN, 2003) was adopted in the dynamic analysis in order to obtain maximum vertical acceleration and maximum deflection. The results showed that the resonance peak for maximum acceleration of ballasted track was obtained at lower speed compared to the ballastless track. This was mainly due to the fact that the ballastless track resulted in a lower mass and hence a higher speed at which resonance occurs. The maximum acceleration was higher for the ballastless track, however, this does not necessarily have to be a problem since the permissible limits of vertical acceleration is higher for non-ballasted tracks (Casal, et al., 2011). The influence of the mass contribution from ballast is lower for concrete bridges compared to steel and composite bridges since the mass is already high for a concrete bridge, thus the mass ratio between ballast and the concrete bridge will be low (Frýba, 1996).

Moreover, the resulting maximum deflections was not influenced by the choice of railway topology even though they occurred at different speeds. The obtained response of the studied bridge is in line with what was described in Section 3.2.2 with regard to how the mass influence the dynamic behaviour.

An important topic for railway bridges is the end connections which may cause disturbances to the railway. This may be problematic for the non-ballasted slab track subjected to high-speed loads in particular since less movements can take place in such topology. The displacements and rotations must be limited in order to keep the resulting forces at an acceptable level. There are less problems for a ballasted track due to the fact that it allows for movements caused by temperature gradients as well as creep and shrinkage (Calcada, et al., 2009).

3.2.6 Track irregularities

A railway track is never perfectly straight or without imperfections and such irregularities will induce vibrations to the bridge during a passage of a train. Track irregularities can occur in both the vertical and horizontal plane and thus induce vertical, horizontal and torsional vibrations. Some typical track irregularities is illustrated in Figure 3.8. Factors that may cause track irregularities are for instance wheel defects, rail joints, turnouts, transition zones (between bridges and abutments for instance) (Frýba, 1996).
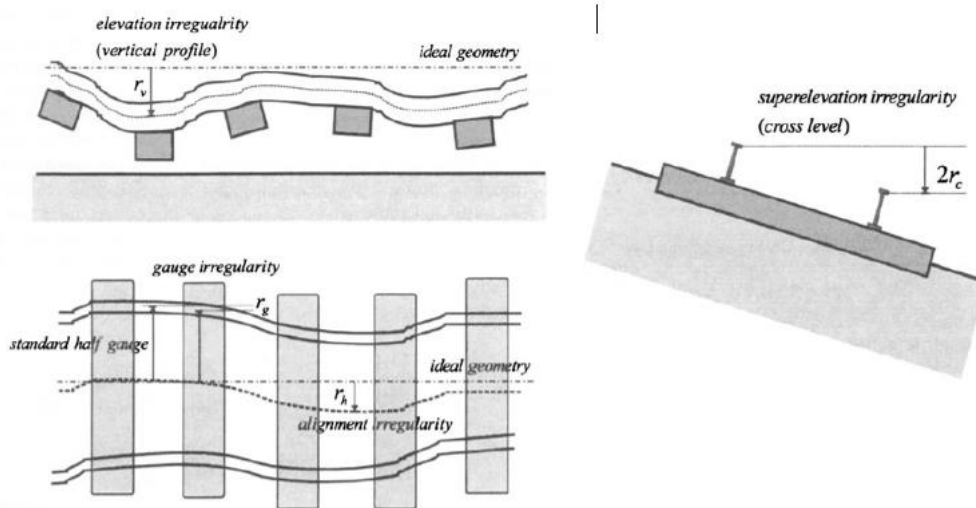
Figure 3.8   Typical irregularities of a rail track (Yang, et al., 2004).

The transition zones between bridges and abutments or between different railway superstructures such as ballasted and non-ballasted tracks (see Figure 3.9) may cause increased dynamic effects. This is due to the fact that the vertical stiffness is abruptly changed, leading to impact loading of the wheels of the vehicle as well as the rails. As a result, it is important to take this problem into consideration when designing transition zones. It can be achieved by gradually change the stiffness over a sufficiently long distance in order to avoid the abrupt change in stiffness (Meng, et al., 2015). Failure to deal with this problem may lead to excessive maintenance requirements. Studies have shown that the maintenance frequency can be five times higher for transition zones than for regular tracks (Arvidsson & Karoumi, 2014).
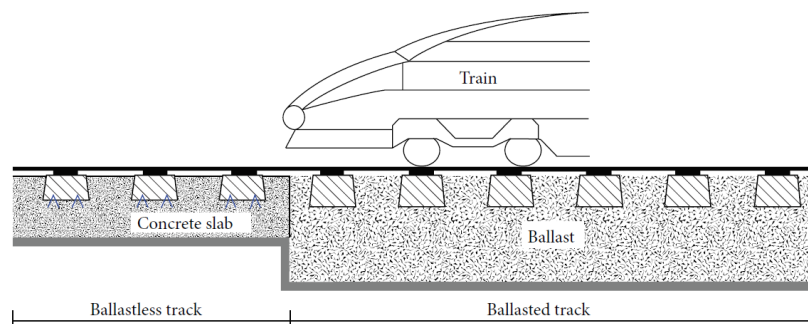
Figure 3.9   Illustrative example of a transition zone between ballasted and non-ballasted track (Meng, et al., 2015).

In dynamic calculations of railway bridges, track irregularities may be considered in a simplified way by using a factor φ''. This factor was a result from investigations conducted by the ORE committee D23 and additional studies by the ERRI committee D214 concluded that the factor φ'' lead to conservative results (Arvidsson & Karoumi, 2014).

Track irregularities may as well be modelled in a dynamic analysis to evaluate the dynamic effects. However, in such case the train-bridge interaction is necessary in the model and thus the computational effort may be extensive. Train-bridge interaction models will be discussed further in Section 3.5.

3.2.7 Train parameters

The most important parameter affecting the dynamic response of a railway bridge is the speed of the train. Generally, the dynamic behaviour increases with an increased speed (Frýba, 1996). A train travelling at low speed are unlikely to induce any significant dynamic stresses to the bridge.

The configuration of the moving train has also a substantial impact on the dynamic behaviour. A train can have different car lengths, masses, suspension system etc. and all will affect the bridge response to some extent. A certain span to length ratio together with a certain speed can either influence the structure in a favourable way or in an unfavourable way as described in Section 3.1.1.

3.3 Different bridge types for high-speed railway lines

Since the first high-speed railway line started to operate in Japan in 1964, many countries have introduced high-speed railways into their infrastructure (UIC, 2015). Bridges play an important role in the railway system and each country have developed their own design in order to fulfil the dynamic requirements that arise with high speed.

The high-speed railway bridges in Europe consists of a high number of prestressed concrete bridges. Box girders are a commonly used profile which provides high bending and torsional stiffness in addition to efficient use of material, see Figure 3.10 b). The prestressed box girders are typically used for span lengths up to 60 meters both for simply supported and continuous bridges. The majority of the bridges in Spain and Italy consists of different prestressed box girder solutions. For short span bridges of 20-30 meters, a typical solution in Spain is a prestressed voided slab, see Figure 3.10 a) (Calcada, et al., 2009). The prestressed box girder profile is also a common solution in the German high-speed railway network (Dai, et al., 2015).
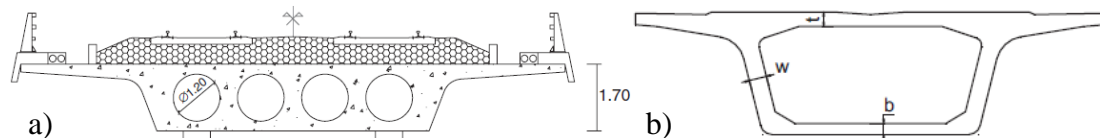
Figure 3.10   a) Prestressed voided slab deck used in the Spanish high-speed network for span lengths 20-30 m (Calcada, et al., 2009). b) Prestressed box girder bridge typically used for span lengths up to 60 meters (Dai, et al., 2015).

In the initial stage of the development of the French high-speed railway system, reinforced and prestressed concrete bridges were designed in order to ensure an appropriate dynamic behaviour. However, in recent years the majority of the designed bridges consists of steel-concrete composite for span lengths above 40 meters. The most commonly used profile is the twin girder with spans up to 75 meters, see Figure 3.11. For longer spans, steel trusses and tied-arch bridges have been constructed. For short span bridges below 30 meters, reinforced and prestressed concrete solutions are still typically used (Calcada, et al., 2009).
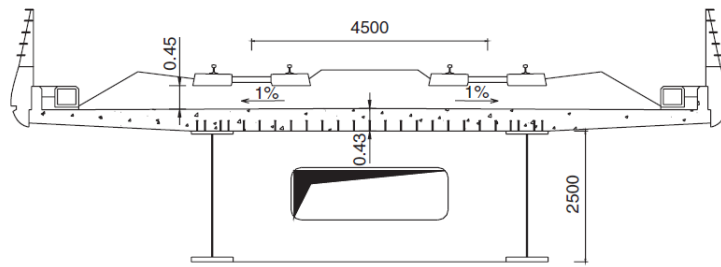
Figure 3.11   Steel-concrete composite twin girder bridge used in a continuous bridge in the French TGV Nord line with maximum span length of 40 meters (Calcada, et al., 2009).

The Chinese high-speed railway system has expanded significantly in recent years and they have utilized a high number of simply supported short span bridges with standard profiles in order to provide rapid construction. Typical span lengths are 24, 32 and 40 meters where prestressed concrete box girders have been used (Dai, et al., 2015). For medium and long span bridges other solutions have been used such as steel arch bridges, rigid frame bridges and cable-stayed truss girder bridges, see Figure 3.12 (Dai, et al., 2014).

Figure 3.12   Railway bridges in the Chinese high-speed network for medium and long spans. a) Tied steel arch bridge (Tingsihe Bridge, main span 140 m), b) Cable-stayed bridge with truss girder (Tianxingzhou Bridge, main span 504 m), c) Steel truss arch bridge (Dongping Bridge, main span 242 m), d) Rigid frame bridge (Tianluo Bridge, main span 160 m) (Dai, et al., 2014).

The Swedish railway network does not yet include many bridges designed for high-speed trains. However, the bridges along the Bothnia Line between Kramfors and Umeå are supposed to handle train speeds up to 250 km/h. The construction of this railway line was initiated in 1999 and the requirement of checking the dynamic behaviour of bridges with intended line speed above 200 km/h was introduced into the Swedish regulations in 2004, meaning that the majority of the bridges along the Bothnia Line are not designed for high-speed loads.

A study to assess these bridges when subjected to the high-speed load model HSLM from Eurocode 1, SS-EN 1991-2 (CEN, 2003) was later conducted by (Andersson, et al., 2011). Simplified 2D-analyses were performed for 76 of the bridges with regard to vertical accelerations. The analyses included portal frame bridges, steel-composite bridges as well as reinforced concrete beam and slab bridges and the results indicated that 41 of the bridges did not fulfil the dynamic requirements. Beam and slab bridges designed with end shields showed high accelerations, because of a transient response induced by the train load at the end of the end shields. Steel-concrete composite bridges showed high accelerations as a result of low bending stiffness and low mass. The response of the analysed portal frame bridges was shown to be highly dependent of the foundation conditions and 75 % of these bridges exceeded the permissible acceleration limit.

According to *Technical system standard for high-speed tracks* (Swedish Transport Administration, 2016), the following recommendations are given with regard to different bridge types for high-speed applications:

- Suspension bridges, cable-stayed bridges or arch bridges with suspension struts should be avoided due to the risk of resonance

- Steel-concrete composite bridges may result in excessive vibrations due to a combination of low mass and low natural frequency

- There is a risk of high levels of vibration in bridges designed with end shields since a transient response may be induced by the impact from the train loads at the end of the end shields

- Short bridges located at soft foundations may result in high vibrations even if the load-bearing structure is rigid

3.4 Dynamic effects according to Eurocode

The dynamic effects of railway bridges are considered in Eurocode 1, SS-EN 1991-2 (CEN, 2003) Section 6.4, Dynamic effects (including resonance). The general design criteria states that a static analysis shall be carried out with the load model LM71 in Figure 3.13, together with load models SW/0 and SW/2 if required. The load models should also be multiplied by a factor α if required in order to account for heavy rail traffic (CEN, 2003). TRVK Bro 11 (Swedish Transport Administration, 2011) states that the α should be taken as $\alpha = 1.60$ for railway lines where heavy freight traffic is intended and $\alpha = 1.33$ for other lines (Swedish Transport Administration, 2011).
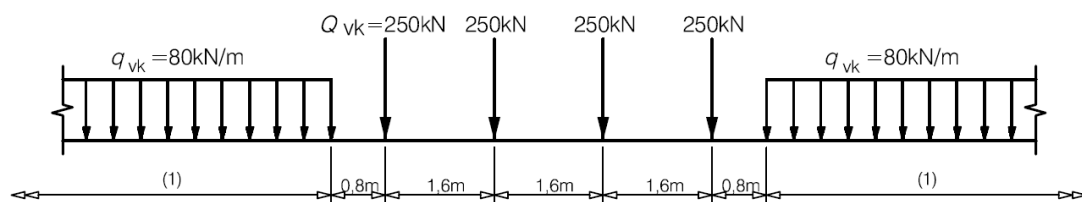
Figure 3.13   Load model LM71 from Eurocode to be considered in static design of railway bridges (CEN, 2003).

Whether a dynamic analysis is required or not is determined by the flowchart in Figure 3.14. Where a dynamic analysis is not required, the dynamic loads may be considered as quasi-static by magnifying the static load by a dynamic factor Φ.

Eurocode defines a quasi-static load as a dynamic load represented as an equivalent static load, which is obtained by the dynamic amplification factor Φ (CEN, 2003).
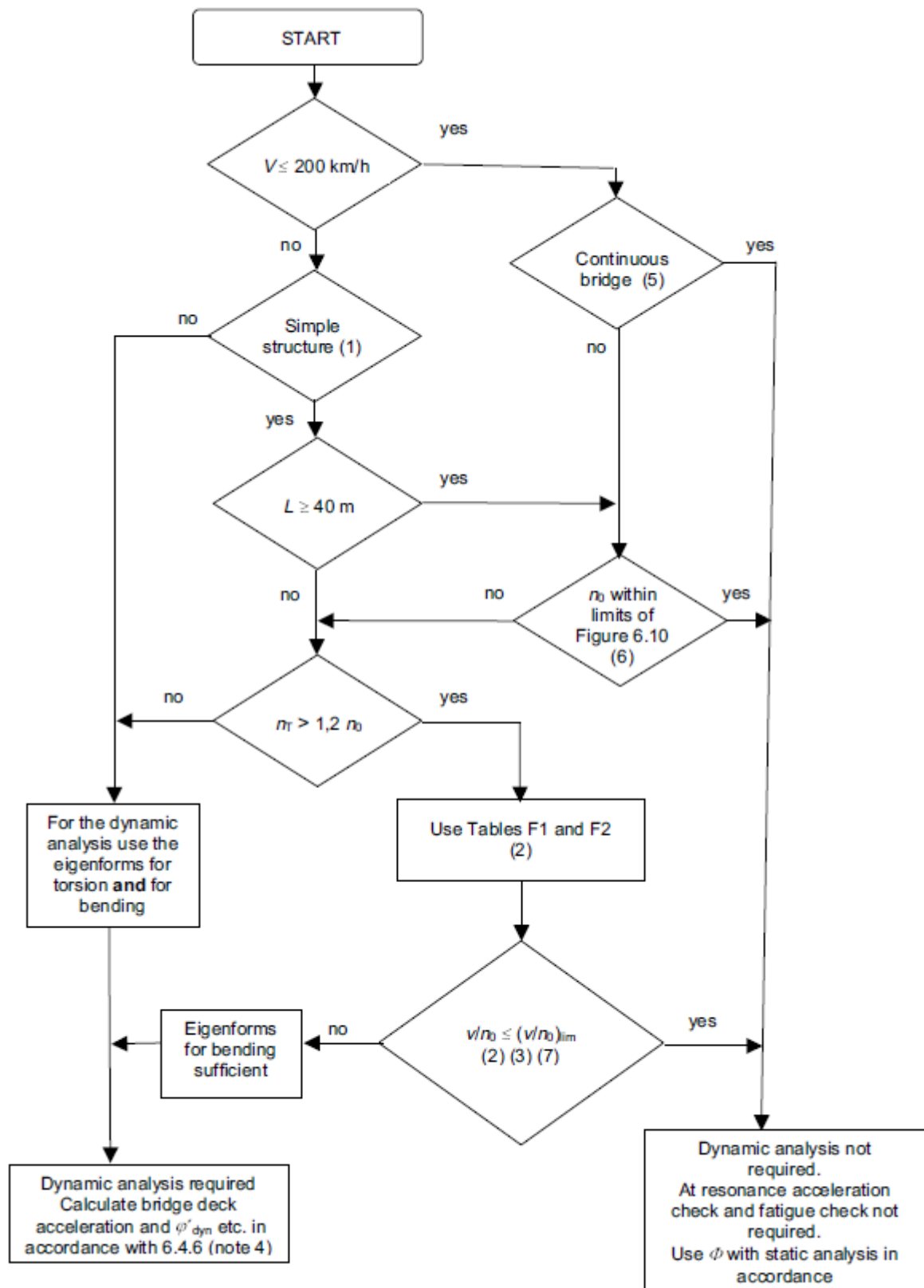
Figure 3.14   Flow chart used to determine whether a dynamic analysis is required or not (CEN, 2003).

where

V	is the maximum line speed [km/h]
L	is the span length [L]
n_0	is the first natural bending frequency of the bridge [Hz]
n_T	is the first natural torsional frequency of the bridge [Hz]
v	is the maximum nominal speed [m/s]
$(v/n_0)_{lim}$	is defined in Annex F in Eurocode

The limits of the first natural bending frequency of the bridge n_0 is given by Figure 3.15. The upper limit is determined by dynamic enhancements due to track irregularities and is defined as

$$n_0 = 94.76 L^{-0.748} \tag{3.6}$$

The lower limit is determined by dynamic impact criteria, defined as

$$n_0 = \frac{80}{L} \qquad\qquad \text{for } 4\text{m} \leq \text{L} \leq 20\text{m} \tag{3.7}$$

$$n_0 = 23.58 L^{-0.592} \qquad\qquad \text{for } 20\text{m} < \text{L} \leq 100\text{m} \tag{3.8}$$
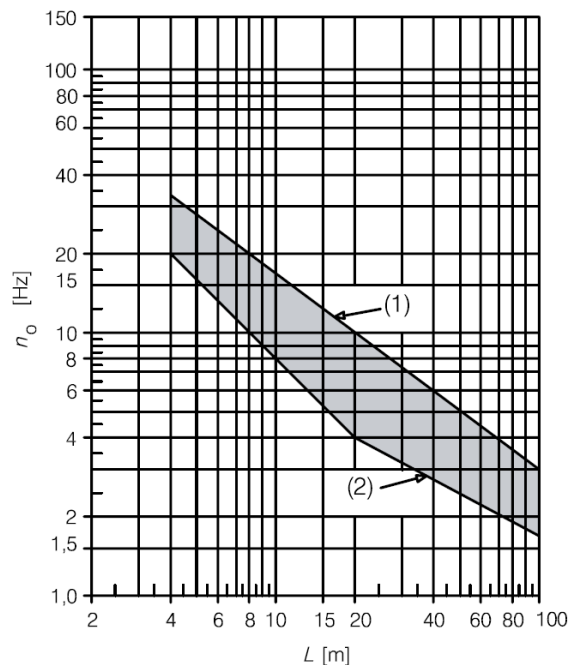
Key
(1) Upper limit of natural frequency
(2) Lower limit of natural frequency

Figure 3.15   Limits of the fundamental natural frequency (CEN, 2003).

These limits are based on results from experimental tests of 113 railway bridges of different categories. According to the test results, the fundamental frequency of all bridges appeared within the grey zone in Figure 3.15, and the lower and upper limits were determined accordingly (Frýba, 1996).

In order to estimate the first natural frequency n_0 for a simply supported bridge subjected to bending, Eurocode 1, SS-EN 1991-2 (CEN, 2003) suggest to use the following equation:

$$n_0 = \frac{17.75}{\sqrt{\delta_0}} \text{ [Hz]} \tag{3.9}$$

where δ_0 is the deflection at the middle of the span when the bridge is loaded by permanent actions (CEN, 2003).

3.4.1   Dynamic factor

The dynamic factor Φ may be applied on the static load models LM71, SW/0 and SW/2 in order to consider the dynamic magnification of stresses and vibrations in the structure. However, it does not take resonance effects into account. When a dynamic analysis is required in accordance with the flowchart in Figure 3.14, the resonance effects can be evaluated.

The dynamic factor should be taken as either eq (3.10) or (3.11) depending on the quality of track maintenance. For carefully maintained tracks, Φ_2 should be applied and for tracks with standard maintenance Φ_3 should be applied.

$$\Phi_2 = \frac{1.44}{\sqrt{L_\Phi} - 0.2} + 0.82 \qquad 1.00 \le \Phi_2 \le 1.67 \tag{3.10}$$

$$\Phi_3 = \frac{2.16}{\sqrt{L_\Phi} - 0.2} + 0.73 \qquad 1.00 \le \Phi_3 \le 2.00 \tag{3.11}$$

where L_Φ is the determinant length defined in Table 6.2 in Eurocode 1, SS-EN 1991-2 (CEN, 2003). The expressions for the dynamic factor were established for simply supported girders and in order to use the expressions for other cases, the determinant length is applicable.

A reduction of the dynamic factor can be used for arch bridges and concrete bridges if the cover is greater than 1.00 m. However, this is only valid for bridges with a single track and for bridges with more tracks no reduction can be applied (CEN, 2003).

3.4.2   Requirements for a dynamic analysis

3.4.2.1   Loads and load combinations

The excitation from real trains may be modelled as a series of moving point forces and vehicle-structure interaction may be neglected. According to Eurocode 1, SS-EN 1991-2 (CEN, 2003), the loading from real trains, which intend to use the bridge, should be adopted using characteristic values. Furthermore, load model HSLM should

be implemented in the analysis for bridges designed of international lines (CEN, 2003). According to TRVK Bro 11 (Swedish Transport Administration, 2011), HSLM is the only load model that should be adopted in the dynamic analysis. Load model HSLM includes two different load model compositions, HSLM-A and HSLM-B. HSLM-A is a combination of 10 different train configurations according to Figure 3.16 and Table 3.1.
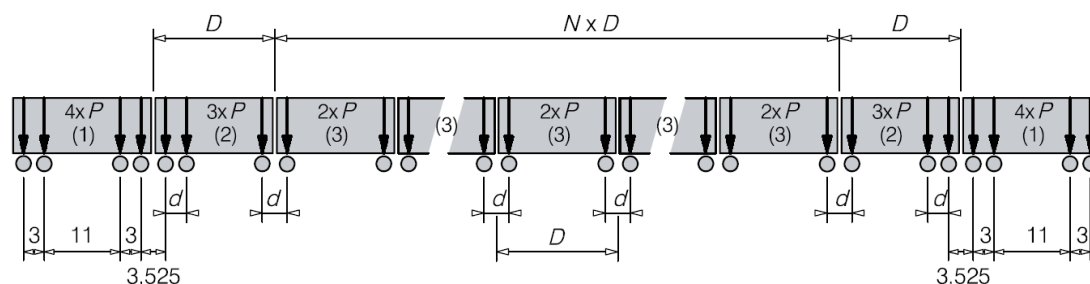
Figure 3.16   HSLM-A train configuration, where (1) is the power car, (2) is the end coach and (3) is the intermediate coaches (CEN, 2003).

Table 3.1   Specified values of the ten different train configurations included in HSLM-A (CEN, 2003).

Universal train	Intermediate coaches N	Coach length D [m]	Bogie axle spacing d [m]	Point force P [kN]
A1	18	18	2.0	170
A2	17	19	3.5	200
A3	16	20	2.0	180
A4	15	21	3.0	190
A5	14	22	2.0	170
A6	13	23	2.0	180
A7	13	24	2.0	190
A8	12	25	2.5	190
A9	11	26	2.0	210
A10	11	27	2.0	210

HSLM-A should be used when designing continuous bridges and for all simply supported bridges with a span longer than 7 m. For simply supported bridges with a span shorter than 7 m, HSLM-B should be applied. HSLM-B is a series of point loads of 170 kN with identical spacing between each one.

The train speeds to be considered in the dynamic analysis should be a series of speed steps starting from 40 m/s (144 km/h) up to 1.2 times the maximum intended line speed. In regions close to resonance speeds, smaller speed steps should be used in order to acquire the resonance peaks with sufficient accuracy.

Load distribution from the rails, sleepers and ballast may be taken into account in a dynamic analysis for load model HSLM-A. The longitudinal distribution of a point load may be distributed over three sleepers and the distribution from the sleepers through the ballast can be accounted for by using a ratio of 4:1. The longitudinal load distribution is presented in Figure 3.17. Furthermore, the load may be distributed transversely through the ballast with the ratio of 4:1. These effects may be taken into account for all span lengths but they are most important for loaded lengths of less than 10 m (CEN, 2003).
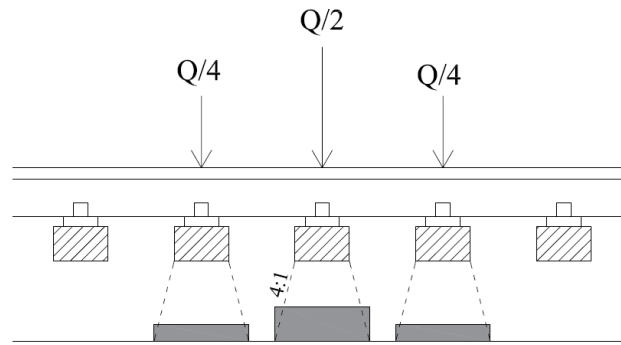
Figure 3.17   Principle of longitudinal load distribution of the axle loads according to Eurocode 1, SS-EN 1991-2 (CEN, 2003).

If the dynamic load effects exceed the effects from static loading on a track, the dynamic load effects should be combined with the horizontal load effects on the track that was loaded in the dynamic analysis. Furthermore, if the dynamic load effects exceed the static ones the dynamic load effects should be combined with the vertical and horizontal load effects on the other tracks in accordance with Section 6.8.1 and Table 6.11 in Eurocode 1, SS-EN 1991-2 (CEN, 2003). For bridges with more than one track, the vertical acceleration of the bridge deck and passenger comfort criteria should be checked with one track loaded while for vertical and horizontal deformation of the deck as well as deck twist, the load should be applied on the number of tracks giving the most critical response.

In addition, the dynamic rail loading effects (bending and twisting moments, shears, deformations etc.) should be enhanced by the partial factors specified in Eurocode, SS-EN 1990 (CEN, 2002) whenever the dynamic effects exceed the static effects. However, partial factors should not be applied when determining the bridge deck accelerations (CEN, 2003).

3.4.2.2   Specifications of bridge parameters

There are several different parameters that influence the dynamic behaviour of a railway bridge and according to Eurocode 1, SS-EN 1991-2 (CEN, 2003), there are several factors that are considered to be most influential. The important parameters related to the train is the speed, number of axles, axle load, spacing of axles, suspension characteristics and vehicle imperfections. The important factors of the bridge is span length, mass, damping and natural frequencies (related to the stiffness) (CEN, 2003).

3.4.2.2.1   Damping

The amount of damping in a structure influence the dynamic response to a great extent and in order to ensure safe predictions of the peak response, it is important to adopt lower bound values in the dynamic analysis. Table 3.2 shows the appropriate values of damping for different bridge types that should be assumed in the design phase (CEN, 2003). The recommended values are based on empirical data from a number of tests of railway bridges (ERRI, 1999).

Table 3.2   *Lower bound values of the structural damping to be used in design of railway bridges (CEN, 2003).*

Bridge Type	ζ Lower limit of percentage of critical damping [%]	
	Span $L < 20$m	Span $L \geq 20$m
Steel and composite	$\zeta = 0.5 + 0.125 \, (20 - L)$	$\zeta = 0.5$
Prestressed concrete	$\zeta = 1.0 + 0.07 \, (20 - L)$	$\zeta = 1.0$
Filler beam and reinforced concrete	$\zeta = 1.5 + 0.07 \, (20 - L)$	$\zeta = 1.5$

The peak response at resonance has a tendency to be reduced for bridges with a span less than 30 meters when vehicle-structure interaction effects are considered. This may be accounted for by either performing a dynamic analysis with vehicle-bridge interaction, or to increase the damping of the structure according to eq (3.12) and Figure 3.18. For continuous bridges, the smallest value of all spans should be used (CEN, 2003).

$$\zeta_{TOTAL} = \zeta + \Delta\zeta \tag{3.12}$$

where

$$\Delta\zeta = \frac{0.0187L - 0.00064L^2}{1 - 0.0441L - 0.0044L^2 + 0.000255L^3} \tag{3.13}$$
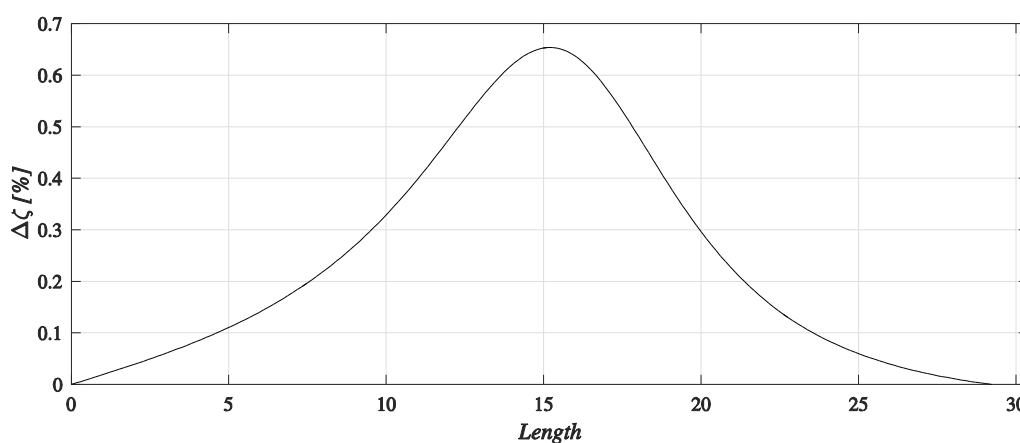
Figure 3.18   *Graph showing the assumed increase in damping due to vehicle-structure interaction according to eq (3.13).*

The additional damping is a result of analyses performed by the ERRI Committee D214 where a moving constant force model was compared with a simplified vehicle-bridge interaction model for simply supported beam bridges with a span length of 0 - 30 meters. The moving constant force model was given additional damping in order to obtain the same response as the simplified vehicle-interaction model. The curve given by Figure 3.18 is a lower bound of the results (ERRI, 1999).

3.4.2.2.2 Mass

The mass is an important factor for the dynamic response of a bridge and both the bridge acceleration and the resonance speed will be affected by a change in mass. The maximum acceleration of a bridge is inversely proportional to its mass at resonance. An underestimation of the mass will overestimate the natural frequency and the resonance speed.

Two specific cases should be evaluated in order to predict the maximum deck accelerations and the lowest resonance speed. A lower bound estimate of the mass should be adopted to predict the maximum deck acceleration, using minimum thickness and dry clean density of ballast. An upper bound should be adopted to obtain the lowest resonance speed, using maximum saturated density of dirty ballast (CEN, 2003). For fixed track systems, it is allowed to perform only one analysis with a nominal mass (Swedish Transport Administration, 2016).

3.4.2.2.3 Stiffness

As for the mass and damping, the stiffness has a great influence on the dynamic behaviour of a bridge. An overestimation of the stiffness will overestimate the natural frequency and the resonance speed. A lower bound of the stiffness should be adopted in accordance with Eurocode 2, SS-EN 1992 to Eurocode 4, SS-EN 1994 (CEN, 2003).

3.4.2.3 Verifications of the limit states

The dynamic bridge response should be verified with respect to serviceability limit state and ultimate limit state. Moreover, a control of the fatigue should be included in the verification of the dynamic response of a bridge. In the serviceability limit state verifications, the following effects should be checked:

- Vertical deck acceleration
- Vertical displacements and rotations of the deck
- Horizontal displacements and rotations of the deck
- Deck twist

When designing a railway bridge, the most unfavourable value of eqs (3.14) and (3.15) should be considered.

$$\left(1 + \varphi'_{dyn} + \frac{\varphi''}{2}\right) \cdot \begin{pmatrix} \text{HSLM} \\ \text{or} \\ \text{RT} \end{pmatrix} \tag{3.14}$$

$$\Phi \cdot (\text{LM71"+"SW/0}) \tag{3.15}$$

where φ'_{dyn} is a dynamic enhancement factor determined from the dynamic analysis:

$$\varphi'_{dyn} = \max \left| y_{dyn} / y_{stat} \right| - 1 \tag{3.16}$$

y_{dyn} is the maximum dynamic response and y_{stat} is the corresponding maximum static response. φ'' is an increase of the dynamic response with regard to vehicle imperfections and track irregularities defined as:

$$\varphi'' = \frac{\alpha}{100}\left[56e^{-\left(\frac{L_\Phi}{10}\right)^2} + 50\left(\frac{L_\Phi n_0}{80} - 1\right)e^{-\left(\frac{L_\Phi}{20}\right)^2}\right] \geq 0 \tag{3.17}$$

where $\alpha = 1$ for speeds above 22 m/s (79.2 km/h), L_Φ is the determinant length and n_0 is the fundamental natural frequency (CEN, 2003).

3.4.2.3.1 Vertical deck accelerations

The vertical deck accelerations should be limited in order to ensure traffic safety and prevent track instability. The maximum limits according to Eurocode SS-EN 1990 (CEN, 2002) are given by eqs (3.18) and (3.19), where γ_{bt} is applicable for ballasted tracks and γ_{df} is used for non-ballasted tracks.

$$\gamma_{bt} = 3.5\,\text{m/s}^2 \tag{3.18}$$

$$\gamma_{df} = 5.0\,\text{m/s}^2 \tag{3.19}$$

The maximum vertical acceleration in the dynamic analysis should be carried out by including all natural frequencies and corresponding mode shapes up to the highest value of either 30 Hz, 1.5 times the first natural frequency or the third natural frequency (CEN, 2002).

The limiting values of the vertical accelerations are based on field measurements and laboratory tests where it was concluded that ballast instability was initiated for deck accelerations of 7-8 m/s^2. A safety factor of two was then used to obtain a design value (ERRI, 1999).

3.4.2.3.2 Vertical displacements and rotations of the deck

The vertical deflection of the bridge deck should be limited with regard to traffic safety and passenger comfort. For static loads, the maximum vertical deflection should not exceed $L/600$ for railway bridges loaded by characteristic values in accordance with Eurocode 1, SS-EN 1991-2 (2003). TRVK Bro 11 (Swedish Transport Administration, 2011) states that the maximum permissible deflection is $L/800$, which is applicable for both vertical and horizontal deflection (Swedish Transport Administration, 2011).

Furthermore, the vertical displacement δ_v between the end of a bridge deck and adjacent structures should be limited in order to avoid excessive stresses, see Figure 3.19. The limiting value is 2 mm for train speeds above 160 km/h (CEN, 2002).
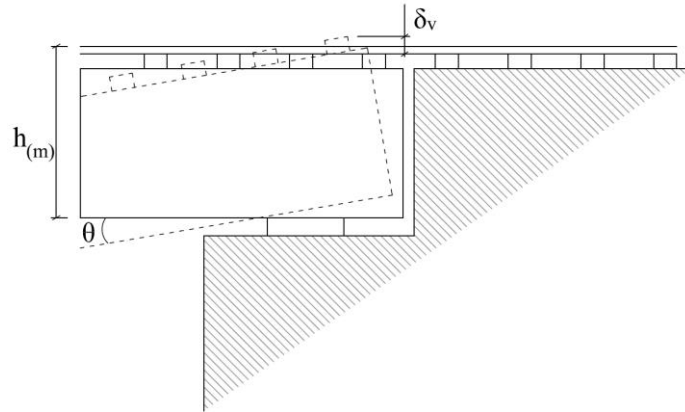
Figure 3.19   Definition of the vertical displacement δ_v, the bridge end rotation θ and the distance from the bottom of the superstructure to the top of the rail h_(m) (Calcada, et al., 2009).

In addition, the vertical rotation θ between the end of a bridge deck and the abutment should be limited according to eq (3.20) (Swedish Transport Administration, 2011).

$$\theta_1 = \frac{2 \cdot 10^{-3}}{h_{(m)}} \tag{3.20}$$

The rotation between two bridge decks should be limited to

$$\theta_2 = \frac{4 \cdot 10^{-3}}{h_{(m)}} \tag{3.21}$$

Figure 3.20   Definition of the vertical rotation of the bridge deck (CEN, 2002).

These values are valid for ballasted tracks in accordance with TRVK Bro 11 (Swedish Transport Administration, 2011). There are no specific value given for a non-ballasted track, instead it is stated that the corresponding rotation limits may be given by the constructor (Swedish Transport Administration, 2011).

3.4.2.3.3 Vertical deflection with regard to passenger comfort

Passenger comfort is dependent on the vertical acceleration b_v inside the train and Eurocode, SS-EN 1990 (CEN, 2002) recommends the values given by Table 3.3 in order to ensure a good travelling experience.

Table 3.3   Recommended comfort levels (CEN, 2002).

Level of comfort	Vertical acceleration b_v [m/s²]
Very good	1.0
Good	1.3
Acceptable	2.0

The vehicle acceleration may be determined by performing a dynamic analysis with vehicle-bridge interaction taken into account. Alternatively, the limits for passenger comfort can be controlled by checking the maximum deflection δ along the centreline of a track as a function of span length, train speed, number of spans and bridge configuration (simply supported, continuous). Limits of maximum deflection L/δ of a railway bridge with three or more simply supported spans is given by Figure 3.21 and the values corresponds to a very good level of comfort i.e. $b_v = 1$ m/s². If a lower level of comfort is desired, the values of L/δ in Figure 3.21 can be divided by the corresponding limits of vertical vehicle acceleration. For a bridge composed of one or two simply supported spans, the values of L/δ in Figure 3.21 should be multiplied by 0.7, the same value is relevant for two continuous spans. The values for continuous bridges with three or more spans, should be multiplied by 0.9. Note that the values of L/δ should not be lower than 600 (CEN, 2002).
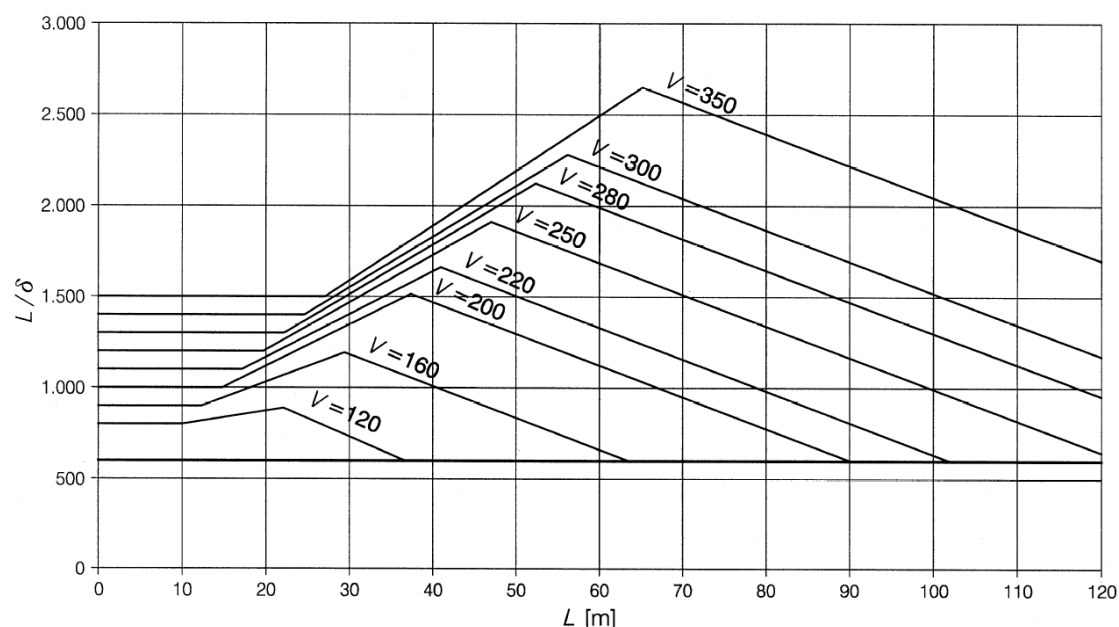
Figure 3.21   Maximum deflection limits L/δ for railway bridges with three or more spans, corresponding to a vertical vehicle acceleration of $b_v=1$ m/s² i.e. very good level of comfort (CEN, 2002).

3.4.2.3.4 Horizontal displacement and rotations of the deck

The horizontal deflection and vibration should be checked in order to guarantee a safe structure. The horizontal deflection should be checked with regard to angular rotation at the end of the deck as well as change in radius of curvature. For train speeds above 200 km/h, the maximum horizontal rotation at support is $\alpha = 0.0015$ rad and the maximum change in radius of curvature is $r = 14\ 000$ meters for a single track bridge or $r = 17\ 500$ meters for a multi-span bridge. The curvature variation can be determined by the following expression:

$$r = \frac{L^2}{8\delta_h} \tag{3.22}$$

where δ_h is the horizontal deflection.

Furthermore, the lowest horizontal natural frequency should not be lower than the recommended value $f_{h0} = 1.2$ Hz in order to avoid lateral resonance (CEN, 2002).

3.4.2.3.5 Deck twist

Deck twist for a track gauge with a width of $s = 1.435$ meters measured over a length of 3 meters should not exceed $t = 1.5$ mm/3 m where train speeds above 200 km/h is intended. Deck twist is defined in Figure 3.22.
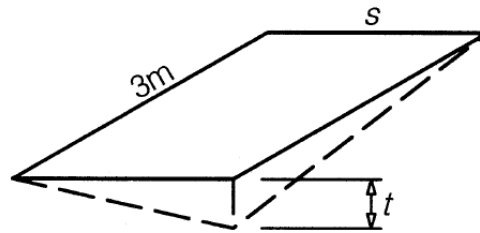
Figure 3.22 Definition of deck twist (CEN, 2002).

3.5 Dynamic analysis of railway bridges

In a dynamic analysis it is possible to adopt simplified models of the applied load as well as the structure itself in order to obtain sufficient accuracy of the result. The different choices depends on the purpose of the analysis and it is important to understand under what conditions a certain model would be suitable. In the following section different modelling choices will be presented and how these may influence the result of the analysis.

3.5.1 Train models

In order to analyse a railway bridge, the train load may be represented by simplified load models, either by moving constant forces or with vehicle-bridge interaction models. Figure 3.23 illustrates such models with increasing complexity.
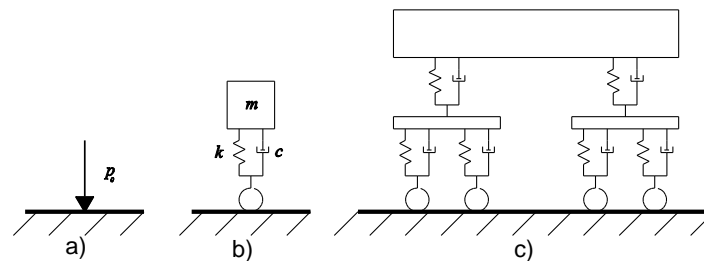
Figure 3.23   Different complexity of load models. a), a vertical moving force acting on the rail. b), a damped spring-mass system. c), a composition of damped spring-mass systems representing a coach.

In reality the interaction between the train and bridge is a non-linear, coupled and time-dependant dynamic problem since the contact forces between the train wheels and the rail is not constant in time and their magnitude is varying. A model representing the vehicle-bridge interaction would then reflect the real behaviour in a better way (Yang, et al., 2004).

The moving constant force model is generally used when designing railway bridges, and it is usually a good representation when the vehicle-bridge mass ratio is small and the elastic and inertial effects can be neglected. However, the choice of load model can have a significant influence on the result of an analysis and it is important to be aware of the consequences when choosing a specific model. The response of the train cannot be represented without the vehicle-bridge interaction and for railway bridges subjected to high-speed trains, the vertical and lateral accelerations of the train is essential when evaluating the riding comfort of the passengers (Yang, et al., 2004).

A number of studies have been carried out in this topic in order to get a better understanding of when and why a certain load model should be adopted. (Arvidsson & Karoumi, 2014) reviewed a number of publications dealing with the effect of train-bridge interaction models and it was concluded that the effect was only relevant for bridges with intermediate lengths. A train-bridge interaction model does only imply a considerable reduction of the bridge response at resonance whereas the difference is negligible outside the resonance range, which can be seen in Figure 3.24 (Arvidsson & Karoumi, 2014). The reason is that the energy from the bridge is partially transferred into the vehicle, thus resulting in a reduction of the dynamic response. For longer bridges the difference between the load models is small, which could be observed in Figure 3.6, Section 3.2.4 (ERRI, 1999).
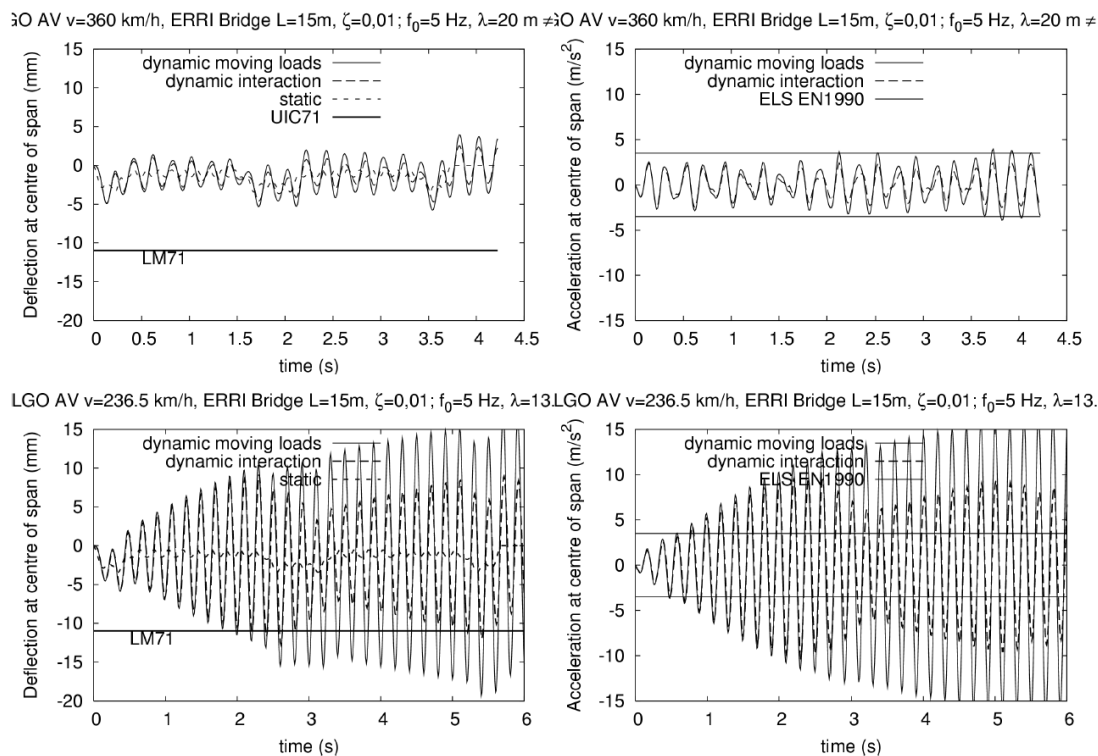
Figure 3.24   Results from a study conducted by the ERRI Committee D214 where the dynamic behaviour of a simply supported bridge was evaluated when using moving force model and bridge-vehicle interaction. Resonance speed (v=236.5 km/h) was compared with non-resonance speed (v=360 km/h). Deflections and accelerations was studied and compared with quasi-static deflection as well as acceleration limits given by Eurocode (Gabaldón, et al., 2006).

Further details can be adopted in the bridge-vehicle interaction model by introducing 3D-models. In such case it is possible to simulate the dynamic response in the lateral and longitudinal direction as well.

3.5.2   Bridge models

In addition to the train models, it is possible to model the track as well in order to introduce an even more realistic model. By doing so, the axle forces from the train is distributed along the track rather than acting at one point. The load distribution has a tendency to reduce the dynamic response of the bridge.

For a ballasted track, the rail may be modelled as beam elements on top of the sleepers that may be represented by suspended masses. The pads and ballast properties can be idealised as spring-damper systems. An example of such a track model is given by Figure 3.25. A non-ballasted track may be modelled in a similar way by letting the slab be represented by beam elements (Casal, et al., 2011).
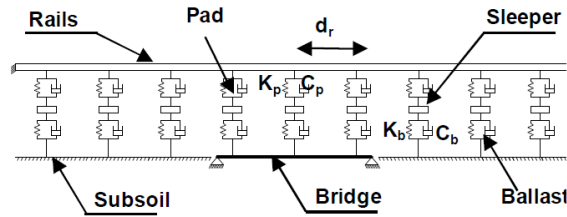
Figure 3.25   An example of how a ballasted track may be modelled in a dynamic analysis (Casal, et al., 2011).

According to Eurocode 1, SS-EN 1991-2 (CEN, 2003) it is allowed to account for load distribution in a dynamic analysis by the principle discussed in Section 3.4.2.1. In a study of the influence of load distribution conducted by (Andersson, et al., 2011) it was concluded that the dynamic effects were significantly reduced for short span bridges with a high fundamental frequency. For longer spans the reduction was negligible (Andersson, et al., 2010).

Track irregularities may be included in the dynamic analysis in order to account for different defects of the rail. This can be done by implementing different mathematical models that describes the irregularities or using real measured data for existing bridges. As a consequence of including track irregularities in the analysis, the dynamic response is somewhat increased for the bridge whereas the effects are higher for the train. How much the result is influenced depends on how the track irregularities are implemented in the analysis (Arvidsson & Karoumi, 2014).

3.5.3   Boundary conditions

There are a lot of different railway bridges out there with different configurations and support conditions. The support conditions may have a great influence of the dynamic behaviour of a bridge. The dynamic response of a simply supported bridge is different from a bridge with fixed support conditions. In addition, the soil-bridge interaction can be very important for the response of a bridge by affecting the stiffness and damping properties of the structure. This is especially true for short and stiff structures such as portal frame bridges, which are surrounded by soil (Ülker-Kaustell, 2009). By including the soil-bridge interaction, the natural frequencies of a bridge are generally reduced, thus lowering the train speed at which resonance occurs. Consequently, an assumption of non-flexible supports may lead to non-conservative results as higher resonance speeds may be obtained in the dynamic analysis (Karoumi & Ülker-Kaustell, 2008).

In a study of a 12 meter simply supported bridge including soil-bridge interaction (Domínguez, et al., 2013), it was concluded that the resonance speed was lowered compared to the case where soil-bridge interaction was not considered. The magnification of the dynamic response at resonance was also lowered. This indicates that the soil-bridge interaction is an important topic in bridge dynamics (Domínguez, et al., 2013).

4 Case studies of reinforced concrete bridges

The case studies in this thesis includes several different reinforced concrete bridges subjected to high-speed trains. A dynamic analysis was carried out for each bridge in order to evaluate their dynamic response. The study included the following bridges:

- Simply supported reinforced concrete slab bridge (with and without end shields)

- Simply supported reinforced concrete trough bridge (with and without end shields)

- Continuous reinforced concrete slab bridge (two-span and three-span)

Each bridge type was analysed by considering four different span lengths of 16, 24, 32 and 40 meters. This chapter provides some general information about each bridge and how they were modelled in the finite element analyses.

4.1 General conditions and simplifications

The FE-analyses were carried out in accordance with the specifications given by Eurocode 1, SS-EN 1991-2 (CEN, 2003). The results were carried out using modal analysis including mode shapes and corresponding frequencies up to $f_{max} = \max(30 \text{ Hz}, 1.5f_1, f_3)$ where f_1 and f_3 are the first and third bending frequency of the bridge respectively. The damping was determined by summing up the value given by Table 3.2 and the additional damping given by eq (3.13). The same damping coefficient were provided for all natural modes.

The structure was assumed to behave linearly, thus mode analysis could be adopted when computing the dynamic response. Moreover, geometric nonlinearities were not considered since the bridges were assumed to experience small deformations. The cross-section was treated as constant along the length of the bridge even though it varied slightly for the real bridges. The boundary conditions were modelled as inflexible throughout the analyses.

Approximations of the stiffness and mass were determined from the available drawings and the considered densities for reinforced concrete and ballast were 2500 kg/m³ and 2000 kg/m³ respectively. Rails, sleepers and railings were included as an additional mass contribution, thus they did not influence the stiffness of the bridge.

The applied load was the HSLM-A load model from Eurocode 1, SS-EN 1991-2 (CEN, 2003) and the considered train speeds were 144 - 384 km/h. The upper speed was taken as the maximum intended speed for the planned Swedish high speed railway line, which is 320 km/h. This value was then multiplied by a factor of 1.2 in accordance with Eurocode 1, SS-EN 1991-2 Section 6.4.6.2 (CEN, 2003). The time step was set to be 5 km/h and for regions close to resonance it was adjusted to 1 km/h in order to obtain sufficient accuracy of the peak values. The time increment per speed step was chosen according to the Brigade/Plus manual (Scanscot Technology, 2015) after the principle that it should not be greater than a tenth of the highest eigenfrequency, which resulted in a value of 3.3 ms for $f_{max} = 30$ Hz. This time increment was used throughout the analyses even though higher frequencies than

30 Hz was included for some cases. The obtained results were magnified with $1 + \frac{\varphi''}{2}$ in order to account for track irregularities, where φ'' is given by eq (3.17).

Horizontal loads such as wind and braking forces were not considered in the dynamic analysis. Only single track bridges were evaluated and the train were modelled to travel along the centreline of the bridge without any track eccentricities. As a consequence, lateral and torsional mode shapes did not contribute to the dynamic response, thus only vertical bending modes were affecting the bridge behaviour.

In order to be able to compare the different bridge types, four different span length was analysed for each bridge. The considered span lengths were 16, 24, 32 and 40 meters. The FE-models were generated from two existing bridges where the real span lengths were 24 meters for the concrete slab bridge and 29 meters for the concrete trough bridge. In order to evaluate the other span lengths it was necessary to adjust the corresponding cross-sections accordingly, hence, unreasonable bridge configurations were avoided. The cross-sectional adjustment were done by considering the ratio between the static deflection δ_s and the span length L of the original design. The cross-section of the adjusted bridge were then changed to obtain a stiffness corresponding to the same ratio. The considered loads for the static analysis were self-weight of the bridge and train load model LM71 from Eurocode 1, SS-EN 1991-2 (CEN, 2003). More details about the adjusted cross-section is described for each bridge when they are presented below.

Furthermore, longitudinal load distribution was introduced by distributing each point force over three sleepers according to Section 3.4.2.1.

4.2   Simply supported reinforced concrete slab bridge

The first bridge to be studied was a simply supported concrete slab bridge with end shields. It is crossing the river Aspan in Nordmaling and it carries a single railway track. Some general information of the bridge is presented in Table 4.1. The total length is 38.6 meters including end shields as well as wing walls and the span length is 24 meters. An elevation of the bridge is presented in Figure 4.1 and its cross-section is shown in Figure 4.2. The complete drawings of the bridge may be found in Appendix C.

Table 4.1   General information of the slab bridge over the river Aspan.

Name	Bridge over the river Aspan
Construction number	3500-5778-1
Bridge type	Simply supported bridge with end shields
Material	Concrete C40/50
Span length [m]	(1.7) + 24 + (1.7)
Number of tracks	1
Location	Nordmaling
Year of construction	2004
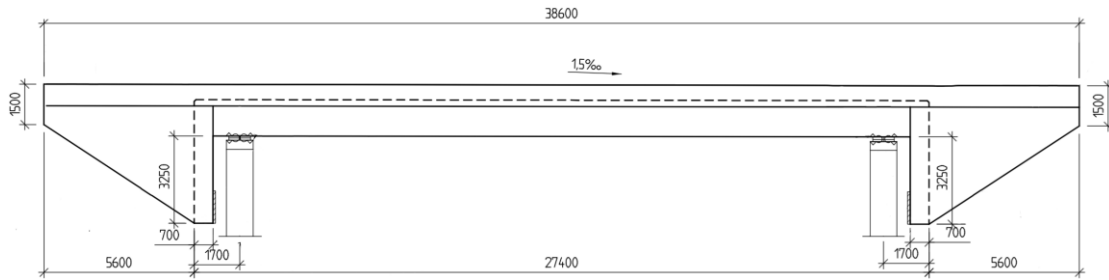
Figure 4.1   Elevation of the reinforced concrete slab bridge over the river Aspan (Swedish Transport Administration, 2016a).
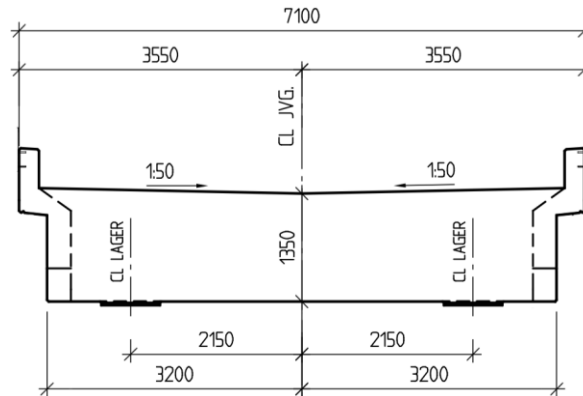
Figure 4.2   Cross-section of the reinforced concrete slab bridge over the river Aspan (Swedish Transport Administration, 2016a).

4.2.1   FE-models

In order to evaluate the influence of the end shields and wing walls with regard to vertical dynamic response, the bridge was modelled considering two cases; one where the bridge was modelled without the end shields and one where the end shields were included. Figure 4.3 shows the principle model of the two cases. Each case was analysed for the four considered span lengths of 16, 24, 32 and 40 meters. The real cross-section was modified in order to obtain a reasonable bridge configuration. The height of the bridge deck was changed until a stiffness corresponding to the same static deflection as for the real bridge was obtained. A more detailed description of the procedure may be found in Appendix A. The resulting cross-sections of the FE-models for each span length is presented in Figure 4.4. For the case when the end shields and wing walls were included, the cantilever length of the real bridge was considered for all span lengths, i.e. 1.7 meters.

Figure 4.3   Principle models of the bridge over the river Aspan where Model 1 represent the case without end shields and Model 2 represent the case with end shields and wing walls.

In addition to the single span case, this slab bridge was used in order to evaluate the dynamic behaviour of continuous two-span and three-span bridges. The same cross-

sections and span lengths as for the single span case were considered for the evaluation. Furthermore, the end shields and wing walls were included for all the continuous cases.
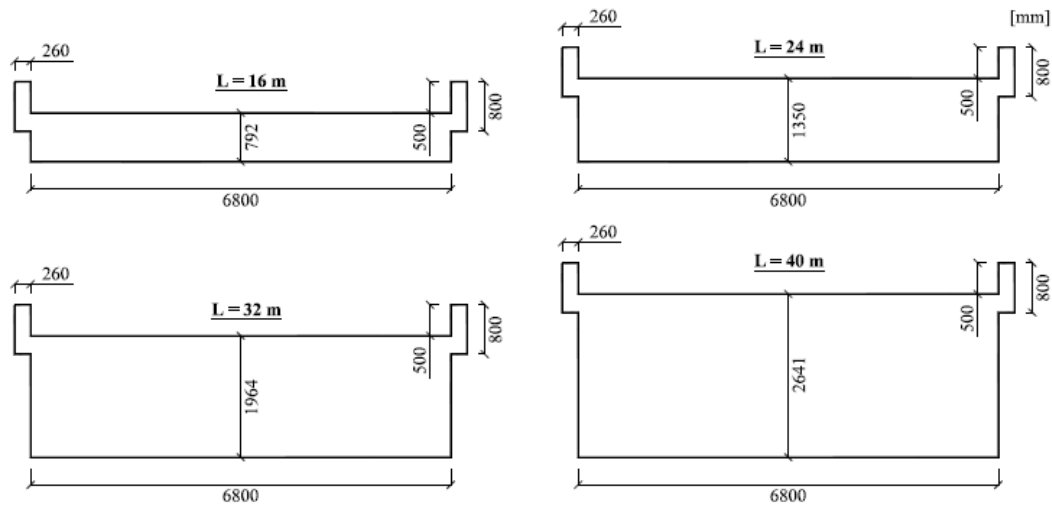
Figure 4.4   Considered cross-sections for the different span lengths of the slab bridge over the river Aspan in the FE-analyses.

According to Eurocode 1, SS-EN 1991-2 (CEN, 2003) a lower bound estimate of the stiffness should be used. For these cases the concrete were assumed to be cracked and thus a reduction of the stiffness were considered. Reducing the bending stiffness with 40 % is a conservative approach (Swedish Transport Administration, 2016). The damping for each bridge length was determined according to Table 3.2 and Figure 3.18, resulting in:

$$16 \text{ meter:} \qquad \zeta_{tot} = 2.417\,\%$$

$$24 \text{ meter:} \qquad \zeta_{tot} = 1.586\,\%$$

$$32 \text{ meter:} \qquad \zeta_{tot} = 1.500\,\%$$

$$40 \text{ meter:} \qquad \zeta_{tot} = 1.500\,\%$$

The bridge deck was modelled using 3D shell elements while the edge beams were modelled as 3D beam elements. The outermost nodes on the long side of the deck were tied with a stiff connection to the beam elements to ensure complete interaction. For the single span case, the columns were not considered in the model and the support conditions were assumed to be fixed in vertical and transverse translation. The longitudinal translation was restrained at one support and free at the other. The boundary conditions are modelled as line boundaries over a width of 585 mm and no restrictions were set for the rotational degrees of freedom. The transverse distance between the supports were set to be 4.3 meters. The track was modelled as 3D beam element without stiffness in the middle of the deck. The mesh and boundary conditions of the FE-model for the 24 meter bridge without end shields can be seen in Figure 4.5.
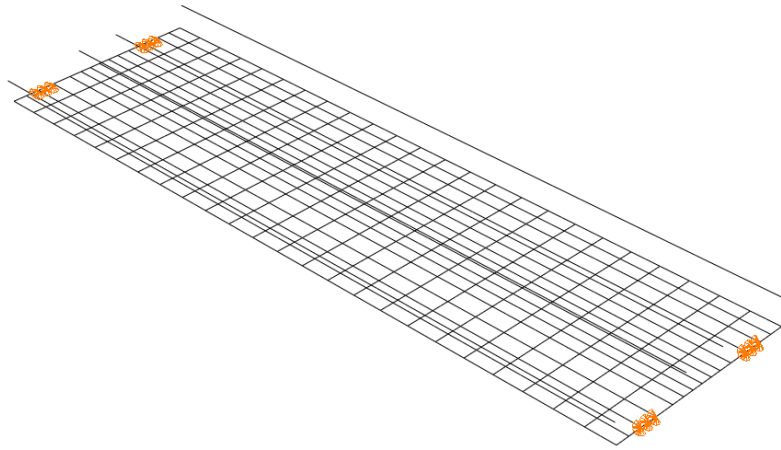
Figure 4.5   Mesh of the concrete slab bridge where the end shields were disregarded.

The FE-model of the case with end shields was generated from the first model by extending the bridge deck and adding the end shields. The cantilevering part of the deck extends 1.7 meters over the supports. The end shields goes 3.25 meters below the deck with a thickness of 700 mm. The wing walls extend 5.6 meters from the end of the bridge deck with a thickness of 500 mm. More details about the dimensions of the end shields and wing walls may be found in Appendix A. The mesh of the model where the end shields were included is illustrated in Figure 4.6.
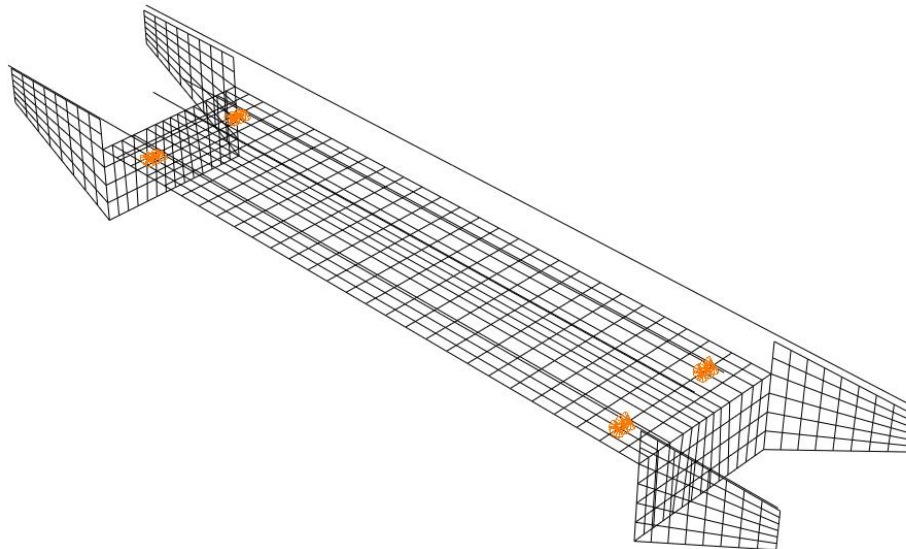
Figure 4.6   Mesh of the concrete slab bridge with end shields included.

The continuous models were generated from the single span model with end shields by adding another span. For the analyses with different span lengths, the boundary conditions were modelled as simply supported. However, the bridge with 24 meter spans were also modelled with fixed columns as mid-support in order to evaluate how this would affect the dynamic response. This was done for both the two-span case and the three-span case. The meshes of the two-span continuous bridge for the simply supported case and the case with a fixed column are illustrated in Figure 4.7. The modelling principle is the same for the three-span case but with an additional span.
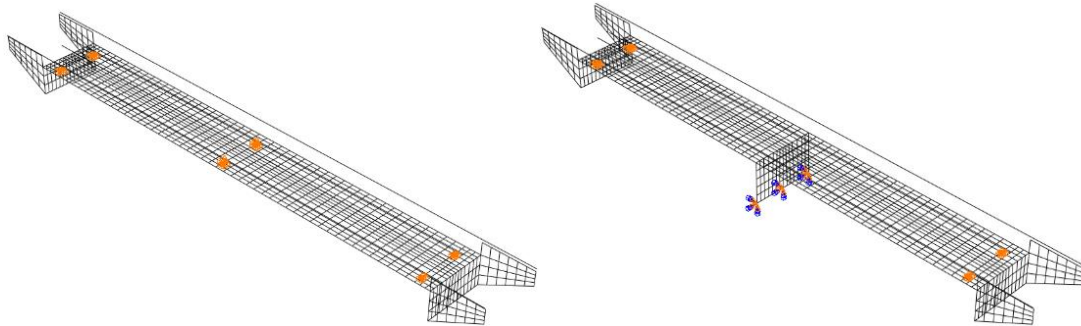
Figure 4.7   Mesh of the continuous two span bridges.

4.3   Simply supported reinforced concrete trough bridge

The second bridge was a simply supported concrete trough bridge with end shields located in Umeå as a part of the Bothnia Line and it is crossing the river Norrmjöleån. It has a total length of 41.4 meters and the distance between supports are 29 meters as can be seen in the elevation of the bridge given by Figure 4.8. The cross-section can be seen in Figure 4.9 where the height of the edge beams are 2724 mm. More detailed information about the bridge dimensions may be found in Appendix B. Table 4.2 summarizes some general information of the bridge.

Table 4.2   General information of the bridge over the river Norrmjöleån.

Name	Bridge over the river Norrmjöleån
Construction number	3500-5798-1
Bridge type	Simply supported bridge with end shields
Material	Concrete C35/45
Span length [m]	(2.26) + 29 + (2.26)
Number of tracks	1
Location	Umeå
Year of construction	2009
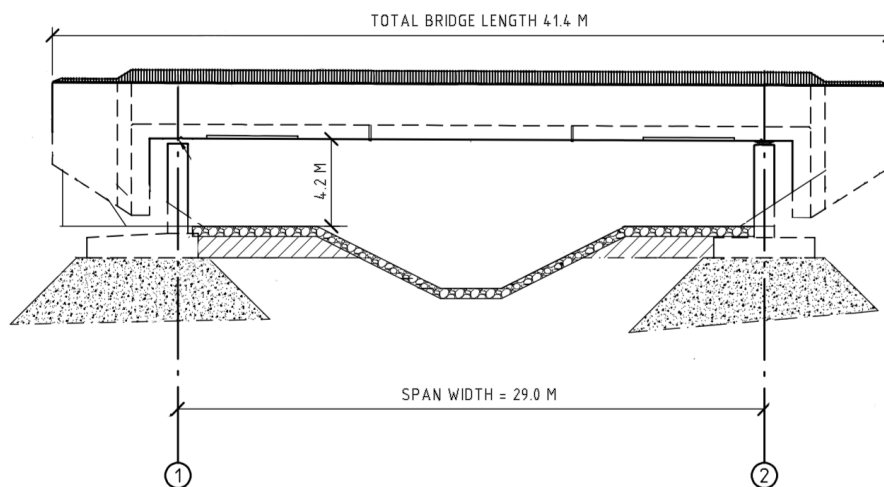
Figure 4.8   Elevation of the concrete trough bridge over the river Norrmjöleån (Swedish Transport Administration, 2016b).
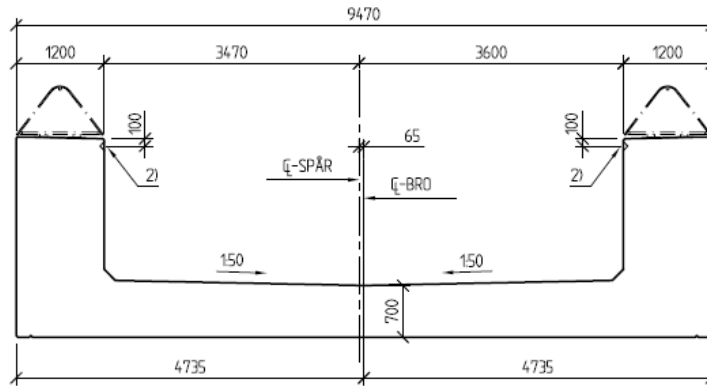
Figure 4.9   Cross-section of the concrete trough bridge over the river Norrmjöleån where the height of the edge beams are 2724 mm (Swedish Transport Administration, 2016b).

4.3.1   FE-models

As for the previous bridge, this one was also modelled considering two cases where the end shields were disregarded for one case. The analysed span lengths in the model were 16, 24, 32 and 40 meters and since the original bridge length was 29 meters the cross-section was adjusted accordingly. The adjustment was made so that the ratio between the width and height of the edge beams stayed the same for the new cross-section as for the original one. The thickness of the deck remained constant for all cases. A complete description of the calculations for the adjusted cross-sections can be found in Appendix B. The considered cross-section of the four bridge models is illustrated in Figure 4.10.
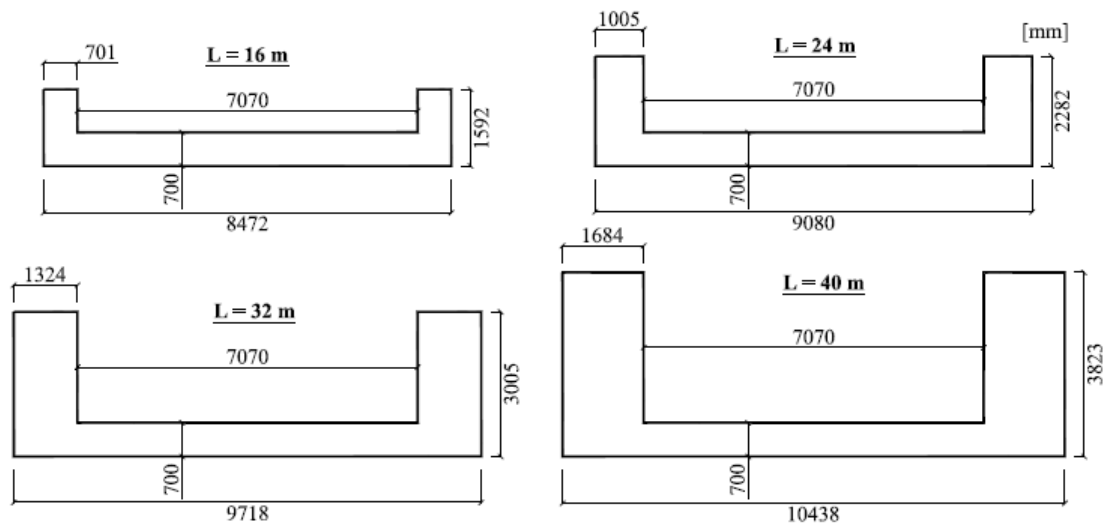
Figure 4.10   Considered cross-sections of the four span lengths for the concrete trough bridge.

A lower bound estimate of the stiffness was used and the concrete was assumed to be cracked, thus reducing the bending stiffness with 40 % as for the previous bridge. The damping for each bridge length was determined according to Table 3.2 and Figure 3.18, resulting in:

$$16 \text{ meter:} \qquad \zeta_{tot} = 2.417\,\%$$

24 meter: $\zeta_{tot} = 1.586\,\%$

32 meter: $\zeta_{tot} = 1.500\,\%$

40 meter: $\zeta_{tot} = 1.500\,\%$

The bridge deck was modelled using 3D shell elements while the edge beams were modelled as 3D beam elements. The supports of the real bridge were located at the bottom of the edge beams below their centrelines. However, in the FE-model the boundary conditions were applied in the midpoint of the edge beams, leading to a slight increase of the transverse distance between supports for the longer spans since these were wider. The track was modelled as 3D beam elements without stiffness and tied to the deck. The FE-model of the case without end shields with the mesh and boundary conditions can be seen in Figure 4.11.
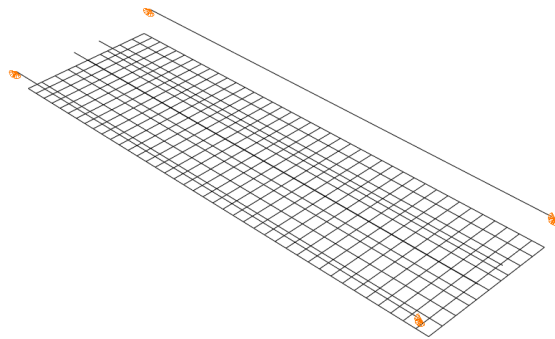
Figure 4.11   Mesh of the trough bridge where the end shields were disregarded.

The FE-model of the case with end shields were generated from the first model by extending the deck over the supports. The length of the cantilevering part was set to 2.3 meters and this length was used for all considered spans. The end shields have a height of 3.8 meters and a thickness of 900 mm. The wing walls extends 3.9 meters from the end of the bridge deck and the thickness is 500 mm. More details of the dimensions of the end shields and wing walls may be found in Appendix B. The mesh of the model with end shields are presented in Figure 4.12.
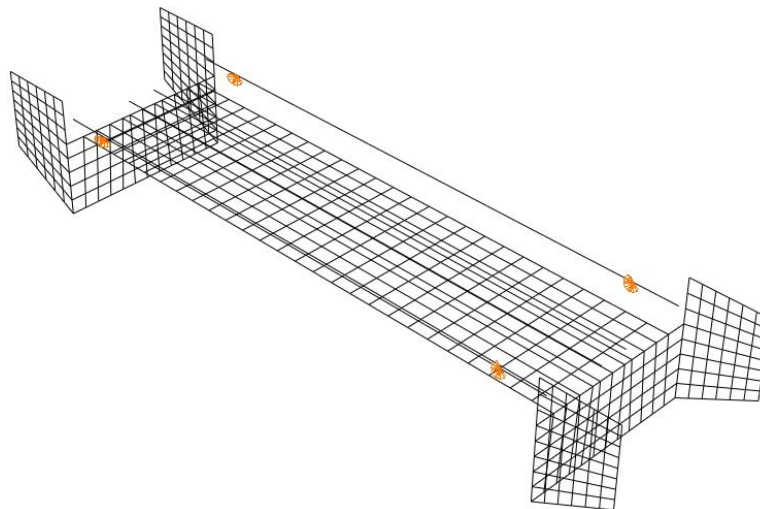
Figure 4.12   Mesh of the trough bridge with end shields.

5 Results

The following chapter includes the results from dynamic analyses of the reinforced concrete bridges. The vertical accelerations and vertical deflections were evaluated with regard to the specified limits according to Eurocode SS-EN 1990 (CEN, 2002) and SS-EN 1991-2 (CEN, 2003). The general layout of the dynamic analysis was firstly to perform a convergence study to ensure a sufficiently fine mesh, secondly the models were compared to an analytical solution. Finally, the vertical accelerations and vertical deflections could be extracted and evaluated. The maximum values were obtained in different regions of the bridge deck depending of the bridge type. A principal illustration of where the maximum response were obtained in the deck is presented in Figure 5.1.
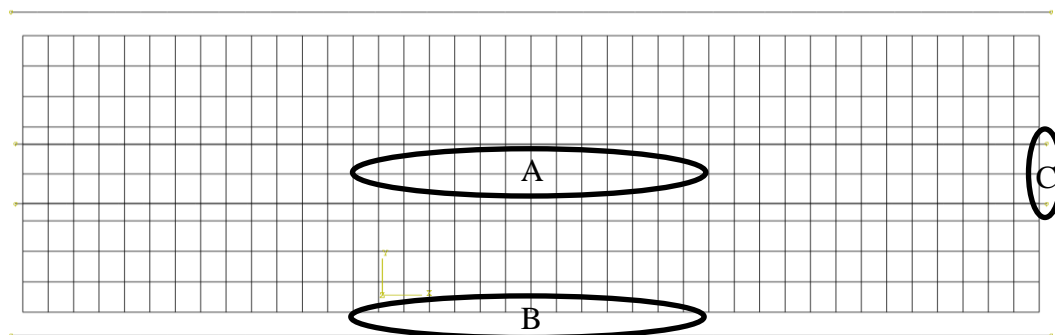
Figure 5.1   Principal plan of a bridge, illustrating where maximum response was obtained.

In order to verify the FE-model, a comparison with an analytical solution was performed with regard to static deflection due to self-weight as well as the first three natural frequencies that corresponded to the first three vertical bending mode shapes. The dynamic response of the single-span bridges was also compared to an analytical solution for a case when a point load passed along the track at constant speed. This was done in order to verify the dynamic response of the bridge but also to better understand the dynamic behaviour before including a series of point loads.

The analytical solution was based on Bernoulli-Euler theory and the FE-model was based on Kirchhoff plate theory for shell elements and Bernoulli-Euler theory for beam elements. For bridges with a span length longer than 8 meters, shear deformations have generally a negligible effect on the response (ERRI, 1999).

The analyses included a parametric study of some of the main parameters that may influence the dynamic response. Each considered factor were altered one at a time while the others stayed constant. This was done in order to obtain a clear picture of how each parameter affected the dynamic response. In reality, a change of one parameter will often affect another to some extent and thus more factors will influence the behaviour of the bridge. A variation of stiffness for instance will probably change the mass of the structure as well. This is especially true when studying a variation of the span length and cross-section since both the stiffness and mass are heavily affected as well.

In the analysis of the simply supported concrete slab bridge, the parametric study was performed thoroughly by considering the influence of variations of damping, mass and stiffness. The principle of changing the damping, mass and stiffness individually is the same independent of the bridge type, thus these factors is only evaluated for the

slab bridge. However, different span lengths will basically affect all the considered parameters to a great extent in reality and therefore all these changes should be considered. Therefore, a variation of the span length was included in the analyses for all bridges, considering all the other factors that was influenced as well. Moreover, the influence of load distribution was evaluated for the single span bridges.

5.1 Simply supported concrete slab bridge

The first bridge in the analysis was the simply supported slab bridge where the end shields were excluded to begin with. The verification of the FE-models was done for these single-span bridges and the more complex models, i.e. the continuous cases as well as the case where the end shields were considered, were generated from this one. A convergence study of the first three natural frequencies was performed for all models. The verification and convergence study of the 24 meter FE-model will be presented in the section below and others were checked in the same manner.

5.1.1 Convergence study and verification of FE-model

A convergence was performed for the 24 meter FE-model in order to ensure that the mesh of the FE-model was sufficiently fine. The first three natural frequencies was studied for different number of element in x-direction (longitudinal) and y-direction (transverse). A mesh with 24 elements in x-direction and 14 elements in y-direction was considered to provide sufficiently accurate results.

The FE-model was verified against an analytical solution regarding static deflection, natural frequencies and dynamic response of the bridge when excited by a point load. The analytical analysis resulted in a static deflection of $\delta_s = 38.166$ mm when considering the deadweight only. In the FE-model, the static deflection was slightly lower, $\delta_{s,FEM} = 38.089$ mm. Since the FE-model consists of shell elements, which introduce transverse bending of the deck, the deflection value was taken as the average over the transverse midline of the deck. The value from the analytical solution and the FE-solution is therefore somewhat different.

The natural frequency analysis resulted in 7 mode shapes with a corresponding frequency within the cut-off limit of 30 Hz. The first three vertical bending frequencies are presented in Table 5.1 and the corresponding mode shapes are illustrated in Figure 5.2. As can be seen the results are very similar between the analytical solution and the FE-solution, especially for the first frequency. The small difference that can be observed mainly arise from the additional transverse bending that was included in the FE-model.

Table 5.1   Natural frequencies of the first three vertical bending modes for the analytical and FEM solution of the real bridge over Aspan.

Mode number (vertical bending)	Analytical solution [Hz]	FEM solution [Hz]
1st	2.873	2.872
2nd	11.493	11.247
3rd	25.859	24.141
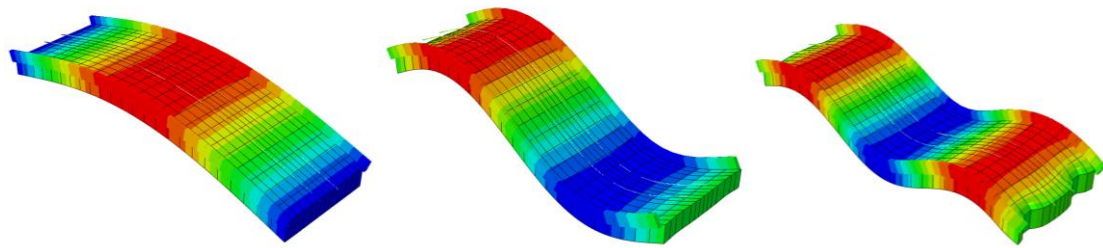
Figure 5.2   First three vertical bending modes of the bridge over Aspan.

In order to verify that the dynamic response of the FE-model was reasonable, it was evaluated for a case when a moving point load of constant speed excited the bridge. This could then be compared with the analytical solution of the same case. The considered point load was $p_0 = 200$ kN which corresponds to an axle load of the train model HSLM-A1 and the considered speed was $v_0 = 150$ km/h. The results are presented as midpoint deflection and midpoint acceleration in Figure 5.3. Since the analytical solution is only valid when the point load excites the bridge, the response is only plotted over the time it took for the load to cross the bridge i.e. from $t = 0$ s to $t_{max} = 0.576$ s.

The displacement plot of the dynamic response shows that the analytical solution and the FE-solution match up quite well. Observe that the initial behaviour of the bridge when the load enters indicate a positive displacement of the midpoint i.e. an upward movement. This is clearly indicated in the acceleration plot where the initial acceleration is positive. This phenomenon was due to the fact that as the load entered the bridge it excited all vertical bending modes. However, the ones with a high frequency had a negligible effect of the response. Therefore, the positive deflection that was observed in the first time steps of Figure 5.3 mainly resulted from the third mode shape. Note that the bending modes with even numbers did not affect the midpoint response as they were anti-symmetrical, see the second mode in Figure 2.5 as an example. As the point load continued to cross the bridge, the response was dominated by the first mode shape.

The comparison of the analytical solution and the FE-solution with regard to midpoint acceleration in Figure 5.3 shows that they are in quite good agreement with each other. It can be seen that the FE-solution of the bridge response corresponds well to the first mode shape of the analytical solution due to the similarities between their first natural frequencies. The third mode shape can be observed in the diagram as it oscillates around the first mode. In the initial stage, the third mode shape of the FE-solution follows the analytical case quite well but as the load keeps crossing the bridge the two cases gets out of phase. This can be explained by the differences in the higher natural frequencies. The third natural frequency of the analytical solution was slightly higher than the FE-solution, which is why the time period between oscillations was smaller for the analytical case.

Further observations were that the first mode shape resulted in negative acceleration of the midpoint in the initial stage. Nonetheless, when including the third mode shape the initial acceleration were positive due to the same reason as described earlier for the deflection.

For the given results, the FE-model was considered to provide reasonable results and could be used for more complex analyses.
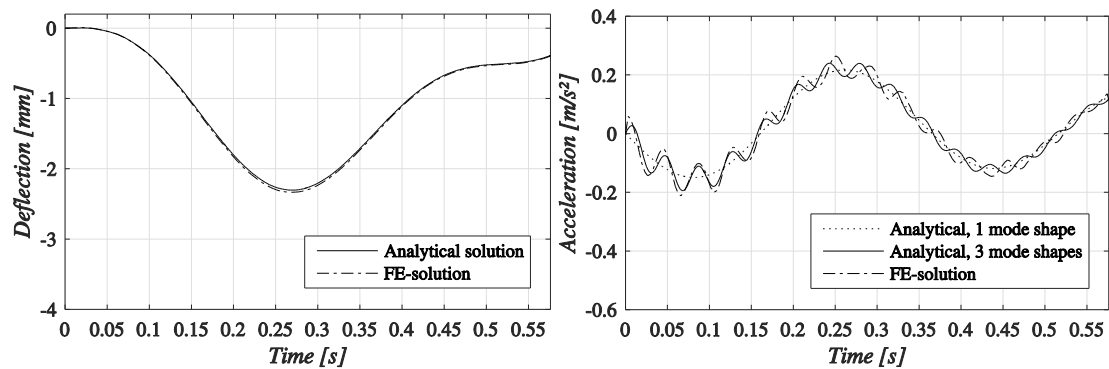
Figure 5.3   *Comparison of the analytical solution and the FE-solution for midpoint displacement and acceleration of the bridge over Aspan due to a moving point load.*

5.1.2 Dynamic response from HSLM-A

The results from the dynamic analysis of the 24 meter slab bridge when subjected to load model HSLM-A (defined in Figure 3.15 and Table 3.1) are presented as maximum vertical accelerations in Figure 5.4 and maximum deflections in Figure 5.5. The maximum response were obtained in the edge of the long side of the bridge deck, i.e. region B) in Figure 5.1.

The bridge response indicated very high accelerations at resonance peaks that were well beyond the Eurocode limit of 3.5 m/s² for all train configurations, except HSLM-A1. All peak values appeared when the loading frequency coincided with the first natural frequency of the bridge. The first resonance peak within the considered speed range occurred at a speed of approximately 186.5 km/h for HSLM-A1. As the coach length got longer for the following trains, their peak values occurred at higher speeds. Moreover, the response was increased for the following trains, which can be explained by the span to coach length ratios. The shorter trains were closer to the optimal design ratio of 1.5, which was discussed in Section 3.1.1, and thus the response were reduced. This phenomenon will be further discussed when different span lengths are compared in Section 5.1.4.

Additional observations was that for HSLM-A1 and HSLM-A10, there was an extra peak in the acceleration plot within the considered speed range that occurred at a speed of approximately 365 km/h. This peak arose when the loading frequency coincided with a multiple of the second eigenfrequency of the bridge.

The deflection of the bridge is presented in Figure 5.5 where two horizontal lines are included which corresponds to the limits given by Eurocode SS-EN 1990 (CEN, 2002) . The lower line corresponds to very good level of comfort given by Figure 3.21 and the upper line corresponds to the static limit of *L*/600. The deflection from the first three HSLM trains fulfilled the limit of very good level of comfort. All HSLM trains fulfilled the deflection limit that corresponded to acceptable level of comfort. However, the acceptable level of comfort limit exceeded the static limit of *L*/600, which is why this value was taken as the maximum limit in the diagram. It was only the last two HSLM trains that exceeded this limit.
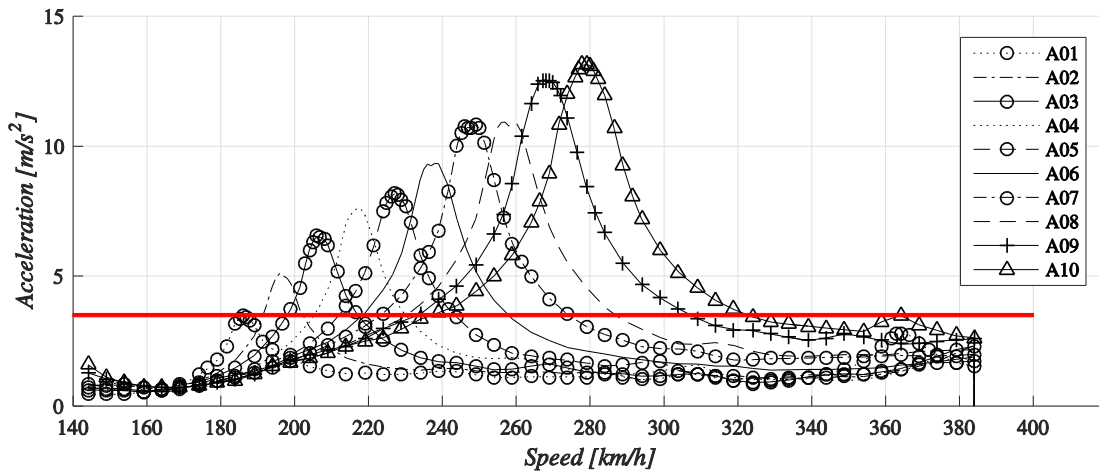
Figure 5.4   Maximum vertical acceleration of the slab bridge over the river Aspan when subjected to the HSLM trains from Eurocode. The maximum allowable acceleration limit is indicated in the figure as a solid horizontal line.
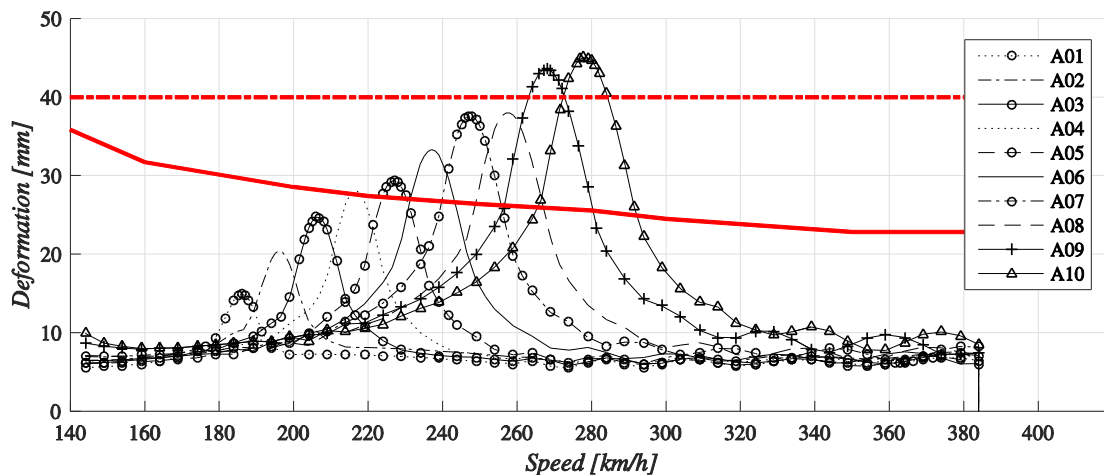
Figure 5.5   Maximum deflection of the bridge over Aspan when subjected to the HSLM trains from Eurocode. The doted horizontal line represent the static deflection limit of L/600 and the solid horizontal line represent a deflection corresponding to very good level of comfort given by Eurocode, SS-EN 1990 (CEN, 2002).

The response of the bridge when subjected to HSLM-A4 is plotted in Figure 5.6 where the maximum vertical acceleration of a resonance speed is compared to a non-resonance speed. A similar comparison is made for maximum deflection in Figure 5.7. It is clear that the response at resonance increased for each axle pair crossing the bridge. Maximum response was obtained right after the first boogie of the end coach has passed the middle of the bridge span. For a non-resonance speed, the response did not increase for each pair of axles passing the bridge, instead the response remained relatively low. When the train had left the bridge, the bridge would vibrate freely and eventually reach equilibrium again as a result of damping.
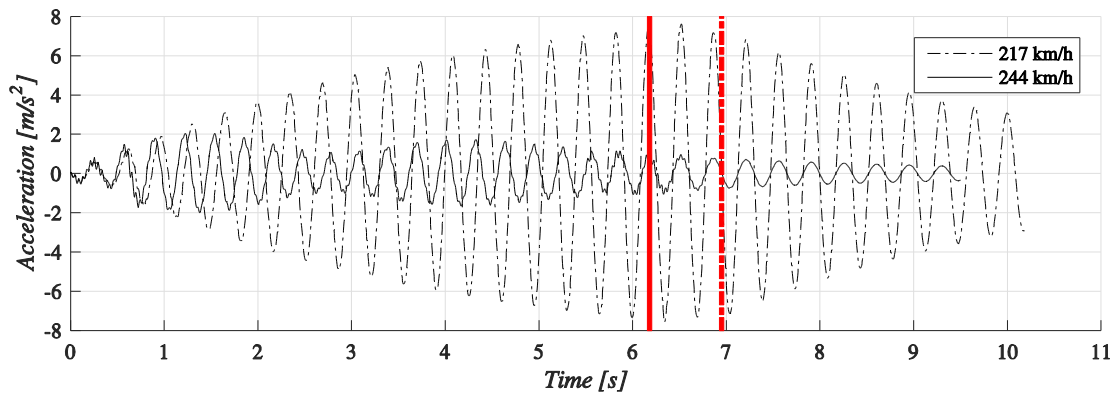
Figure 5.6   Maximum vertical acceleration of the bridge over Aspan during the passage of HSLM-A4 at resonance speed of 217 km/h and non-resonance speed of 244 km/h. The vertical doted line indicates when the last axle pair of the train travelling at resonance speed exit the bridge. The vertical solid line corresponds to the exit of the train at non-resonance speed.
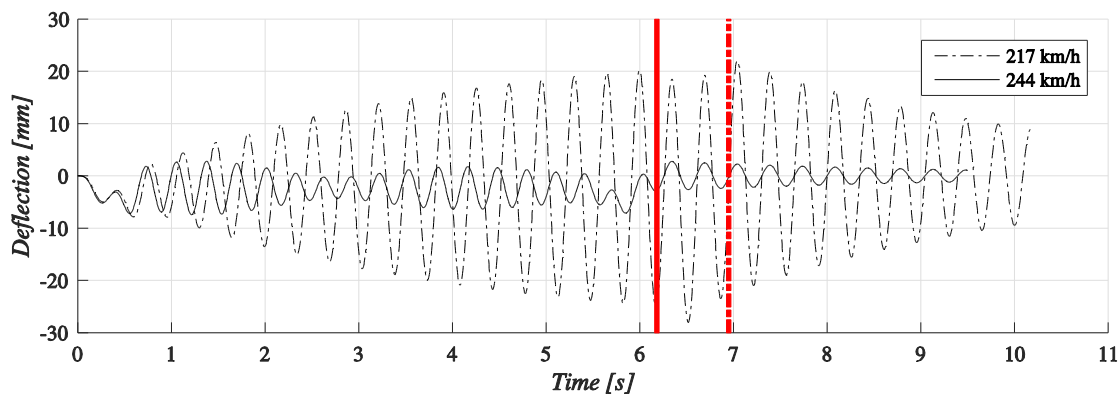
Figure 5.7   Deflection of the bridge over Aspan during the passage of HSLM-A4 at resonance speed of 217 km/h and non-resonance speed of 244 km/h. The vertical doted line indicates when the last axle pair of the train travelling at resonance speed exit the bridge. The vertical solid line corresponds to the exit of the train at non-resonance speed.

In order to illustrate how the dynamic response increases at resonance for each train axle that excited the bridge, a time sequence of HSLM-A4 is presented in Figure 5.8 when it was crossing the bridge. A downward deflection was initiated as the first pair of axles enters the bridge at a) and the deck started to vibrate. At b) ¼ of the bridge's oscillation (i.e. period) was completed and it started to move upwards again. Since the wheel loads were as far away from the middle of the bridge as they could be at c) when the bridge had returned to its original position, it was allowed to continue its movement upwards. At the moment when the bridge reached its highest position at d) and wanted to move down again, the next pair of axles reached the middle of the span. Consequently, the deck was pushed down by the wheel loads just at the same moment as it wanted to move down by itself. This procedure was repeated for every pair of axles that excited the bridge, thus the response was increased and caused resonance.
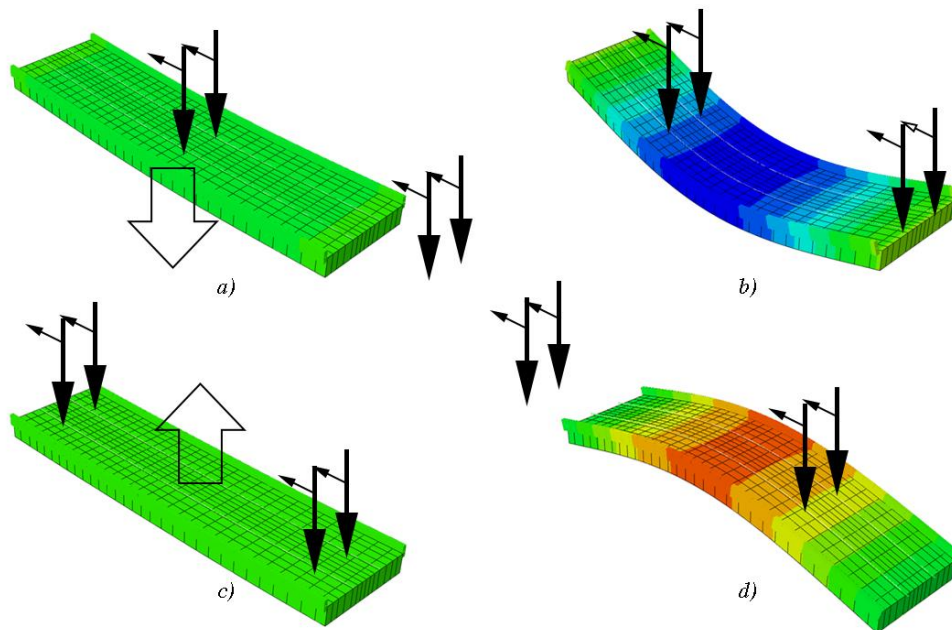
Figure 5.8   Train axles moving over the bridge at resonance speed.

5.1.3   Parametric study

A parametric study was carried out for the 24 meter slab bridge over the river Aspan without considering the end shields. The study was performed using HSLM-A4 and the other trains was not considered since they would provide similar results. The included parameters were; mass, stiffness and damping.

5.1.3.1   Mass

The first parameter to be evaluated was the mass, which was studied by changing the density of the material in the model. The density of reinforced concrete is 2500 kg/m³ and the considered densities in the parametric study were 1500 kg/m³, 2000 kg/m³, 2500 kg/m³, 3000 kg/m³ and 3500 kg/m³. The results are presented in Figure 5.9 and Figure 5.10 as maximum vertical acceleration and maximum deflection. Each increment of density corresponds to an increase in mass of 4.77 ton/meter.
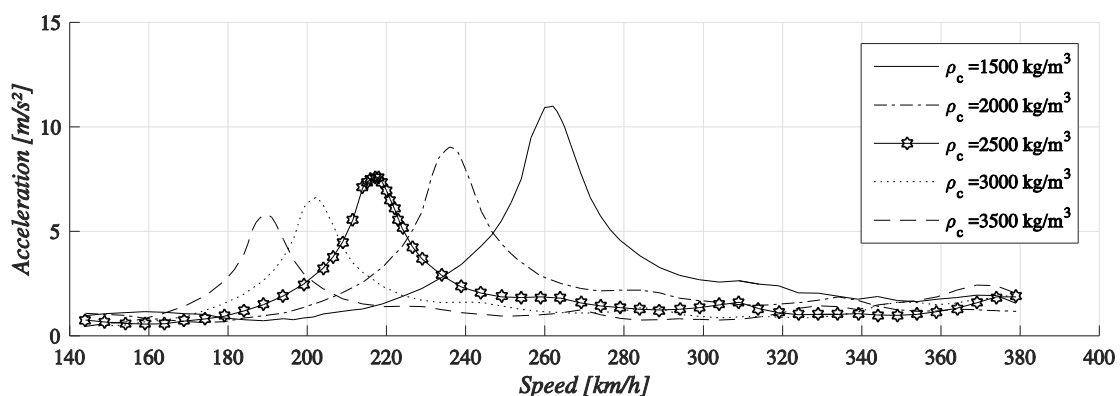
Figure 5.9   Maximum vertical deck acceleration for different densities of the concrete.
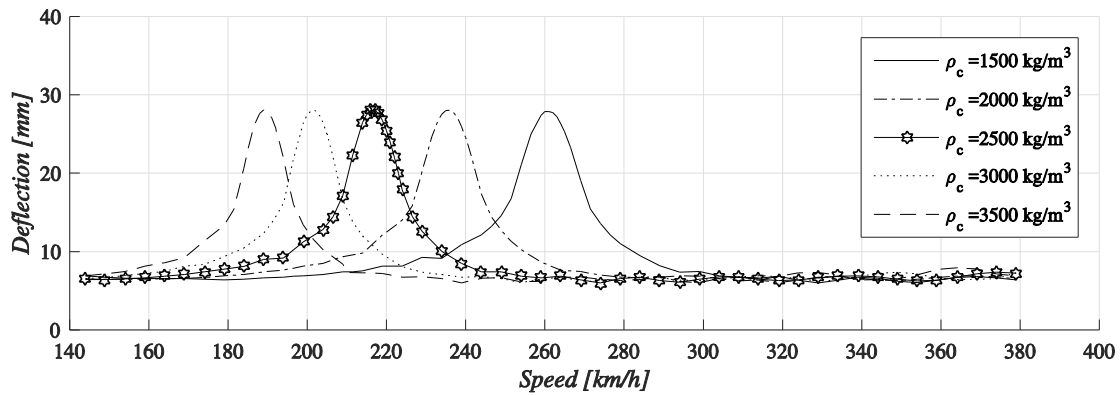
Figure 5.10   Maximum deflection of the deck for different densities of the concrete.

As can be seen in the acceleration diagram, the response was reduced when the mass was increased and the resonance peaks appeared at lower train speeds. In the deflection plot, the resonance peaks were moved to lower train speeds as for the accelerations, however, the same peak values appeared independent of the mass. The deadweight of the bridge was not included in the deflection analysis and it only influenced the natural frequencies of the bridge, which is why the peak values remained the same in the diagram.

The influence of increasing the mass of a bridge may be summarized in the following bullet points:

- Natural frequencies and critical resonance speeds decreases

- Maximum accelerations at resonance decreases

- Maximum accelerations at resonance are inversely proportional to the mass of the bridge

- Maximum deflections at resonance are unchanged

5.1.3.2   Stiffness

The influence of stiffness was studied for five different values of the elastic modulus, with 14 GPa, 21 GPa, 28 GPa, 35 GPa and 42 GPa. The result is presented in Figure 5.11 and Figure 5.12 where the maximum vertical acceleration and maximum deflection are shown.
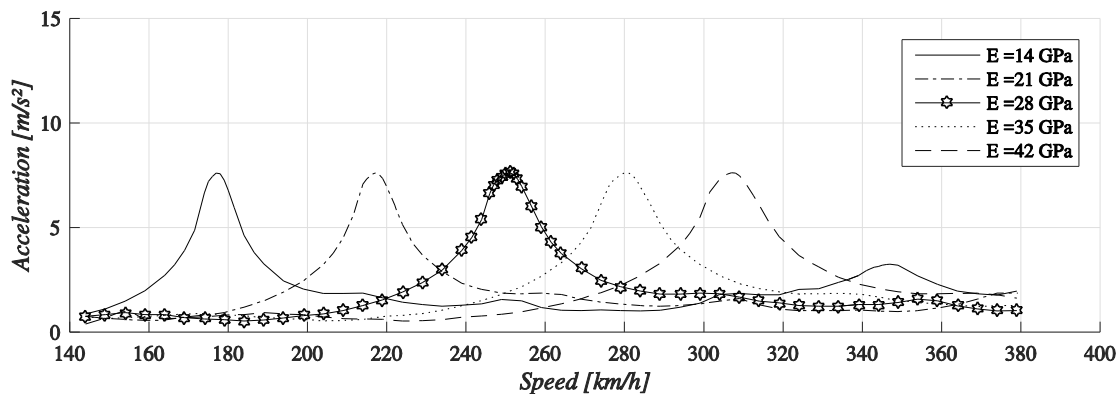
Figure 5.11   Maximum vertical acceleration of the bridge deck for different stiffness.
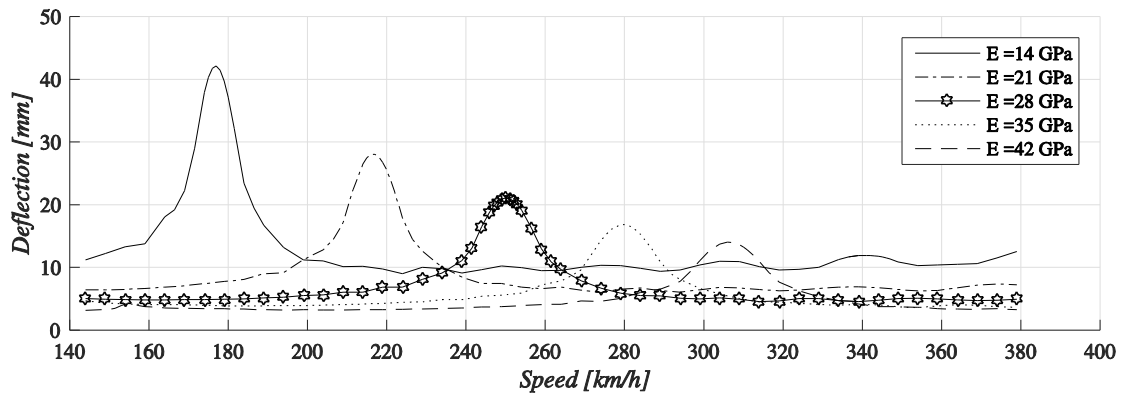
Figure 5.12   Maximum deflection of the bridge deck for different stiffness.

The maximum vertical acceleration occurred at higher train speeds when the stiffness was increased. Nonetheless, the peak values were unaffected by the change in stiffness. In the deflection diagram it is clear that a lower stiffness resulted in higher deflection at lower train speed.

The influence of increasing the stiffness of a bridge may be summarized in the following bullet points:

- Natural frequencies and critical resonance speeds increases
- Maximum accelerations at resonance are unchanged
- Maximum deflections at resonance decreases
- Maximum deflections at resonance are inversely proportional to the bending stiffness of the bridge

5.1.3.3   Damping

Different damping coefficients were studied in order to evaluate their influence of the bridge response. The maximum vertical acceleration and maximum deflection of the deck is plotted in Figure 5.13 and Figure 5.14. A higher damping resulted in lower dynamic response both for the acceleration and deflection. The resonance peaks appeared at the same train speed independent of the damping value.
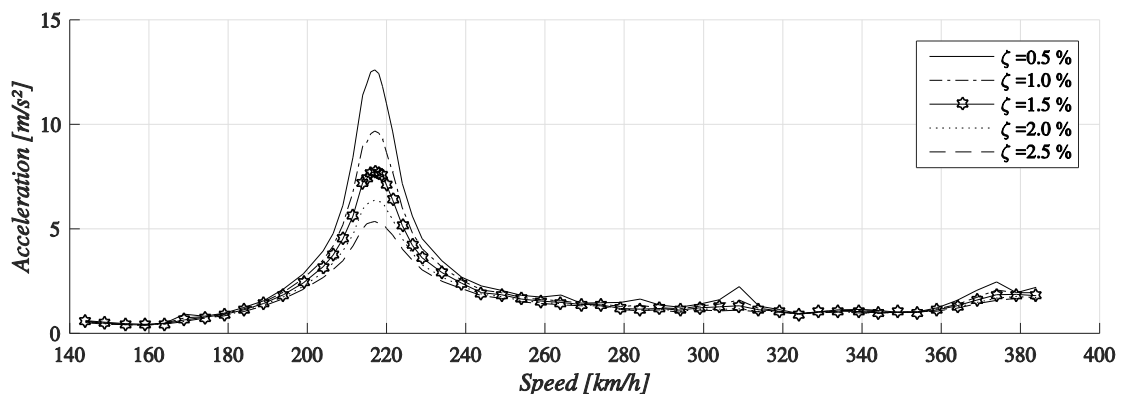
Figure 5.13   Maximum vertical acceleration of the deck for different damping values.
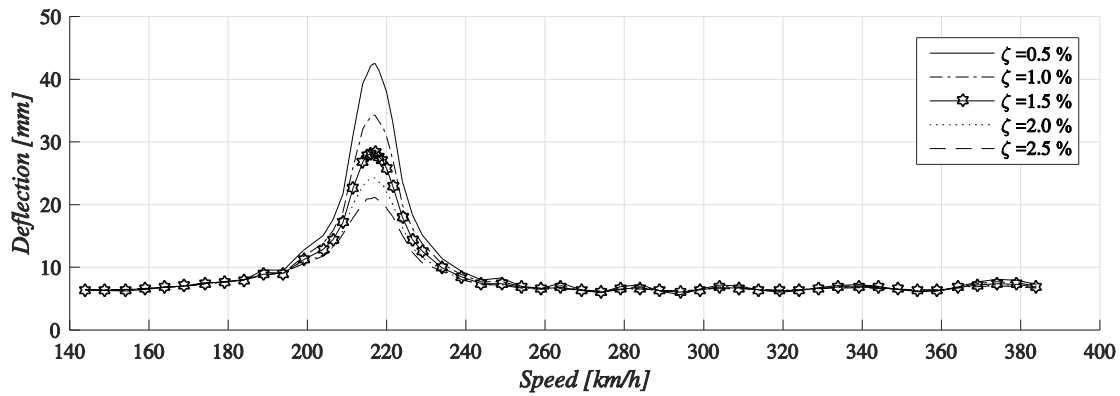
Figure 5.14   Maximum deflection of the deck for different damping values.

The influence of increasing the damping of a bridge may be summarized in the following bullet points:

- Natural frequencies and critical resonance speeds are unchanged

- Maximum accelerations at resonance decreases

- Maximum deflections at resonance decreases

5.1.4   Dynamic response of different span lengths

The concrete slab bridge without end shields was evaluated for four different cases where the span length and cross-section were changed simultaneously. The considered span lengths were 16, 24, 32 as well as 40 meters and the corresponding cross-sections are presented in Section 4.2.1. The dynamic analyses of the four cases were performed in two steps, the first in which the influence of load distribution according to Section 3.4.2.1 was excluded. The second step included the load distribution in order to evaluate its effect on the dynamic behaviour.

The properties of the four bridge spans, which affected the dynamic behaviour are shown in Table 5.2. The results indicated that the natural frequencies decreased for a longer bridge.

Table 5.2   Dynamic properties of the four considered span lengths for the concrete slab bridge without end shields.

Span length [m]	Bending stiffness [GNm^2]	Mass [ton/m]	1st bending frequency [Hz]	2nd bending frequency [Hz]	3rd bending frequency [Hz]
16	8.92	21.45	3.959	15.156	31.756
24	34.29	30.92	2.872	11.247	24.515
32	99.07	41.35	2.374	9.295	20.226
40	233.10	52.86	2.062	8.056	17.483

The maximum vertical accelerations and maximum deflections of the four bridge configurations are presented in Figure 5.15 and Figure 5.16 respectively. Observe that in order to make the resonance peaks visible in the plots, the scale of the y-axis is different for all acceleration cases. The maximum response was obtained in the edge of the long side of the bridge deck, i.e. in region B) of Figure 5.1.

The acceleration and deflection plots represents the complete response from the case where longitudinal load distribution was considered according to Section 3.4.2.1. The envelope of the response from the cases where the axle loads were applied as single point loads are included as a red line in the same figures.

By studying the acceleration plots in Figure 5.15 it can be seen that the response decreased as the bridge span got longer. The 16 meter bridge obtained the highest response and the resonance peak values were well beyond the permitted limit. The resonance peaks occurred at higher train speeds as the bridge span got shorter, which can be explained by the fact that the natural frequency was increased for the shorter bridges. The peak value of HSLM-A10 was almost moved outside the considered speed range for the 16 meter bridge. The 24 meter bridge experienced very high accelerations as well, however, the first HSLM train were just at the allowable limit.

For the 32 meter bridge, the accelerations for the first HSLM trains were below the maximum limit of 3.5 m/s^2 and it was only the last two trains that exceeded the limit. The 40 meter bridge showed a very good dynamic behaviour and the peak values were well below the permitted limit. Due to a low eigenfrequency of this bridge, the peaks from the first two trains appeared outside of the considered speed range.

The dynamic response was highly related to the cancellation effects and the optimal bridge span to train coach length ratio that was explained in Section 3.1.1. For a simply supported bridge the first optimal ratio appears at $L/D = 1.5$. The ratio for the 16 meter span varied from 0.59 for HSLM-A10 to 0.89 for HSLM-A1. As a result the response of this bridge was lower for the shorter trains since they were closer to the optimal ratio. For the 24 meter bridge the ratios between the bridge span and train coach length varied from 0.89 for HSLM-A10 to 1.33 for HSLM-A1. Consequently, the response was lower than for the 16 meter bridge. The span to coach ratios of the 32 meter bridge varied from 1.19 for HSLM-A10 to 1.78 for HSLM-A1. The acceleration plot for the 32 meter bridge clearly shows that HSLM-A10 resulted in the highest response and then the peak values got lower and lower as the coach lengths got shorter until there were no visible peaks at all for HSLM-A4 and HSLM-A5. The reason was that the ratio was very close to 1.5 for these two trains and the response was effectively suppressed. As the coach length got even shorter for the remaining trains the response increased again since the ratio moved away from 1.5 once again. The last diagram which corresponds to the 40 meter bridge indicated, on the contrary to the other three bridges, that the response was higher for the shorter trains. This was due to the fact that the ratio between the span length and the train coach went from 1.48 for the longest train to 2.22 for the shortest one.

In addition to the cancellation phenomenon, there were other factors that influenced the response. At resonance the maximum accelerations are inversely proportional to the mass of the bridge and higher mass would result in lower dynamic response. Since the mass increased as the cross-sectional area increased for the longer span lengths, the response was higher for the shorter bridges. Moreover, the magnitude of the moving point loads in load model HSLM was generally higher for the trains with longer coaches. For the longer bridge spans, there were more axle pairs that excited the bridge simultaneously and they cancelled each other out to some extent.

By studying the response of the four bridges it can be seen that the peak values for the 16 meter bridge were quite similar whereas the relative difference increased for the longer bridges. This was also a result of the cancellation effects since the relative

difference between each span length to train coach ratio was small for the 16 meter bridge and then it increased for the longer bridges.

It can be observed that in addition to the primary resonance peaks, which were related to the fundamental natural frequency, there were other peak values in the considered speed range. These peaks arose from a multiple of the natural frequencies, however, their response were lower than for the primary resonance. The additional peaks that appeared in the speed range of 160-200 km/h for the 16 meter bridge were a result of the second resonance speed of the first natural frequency. This means that the loads excited the bridge every other oscillation instead of every oscillation as for the primary resonance.
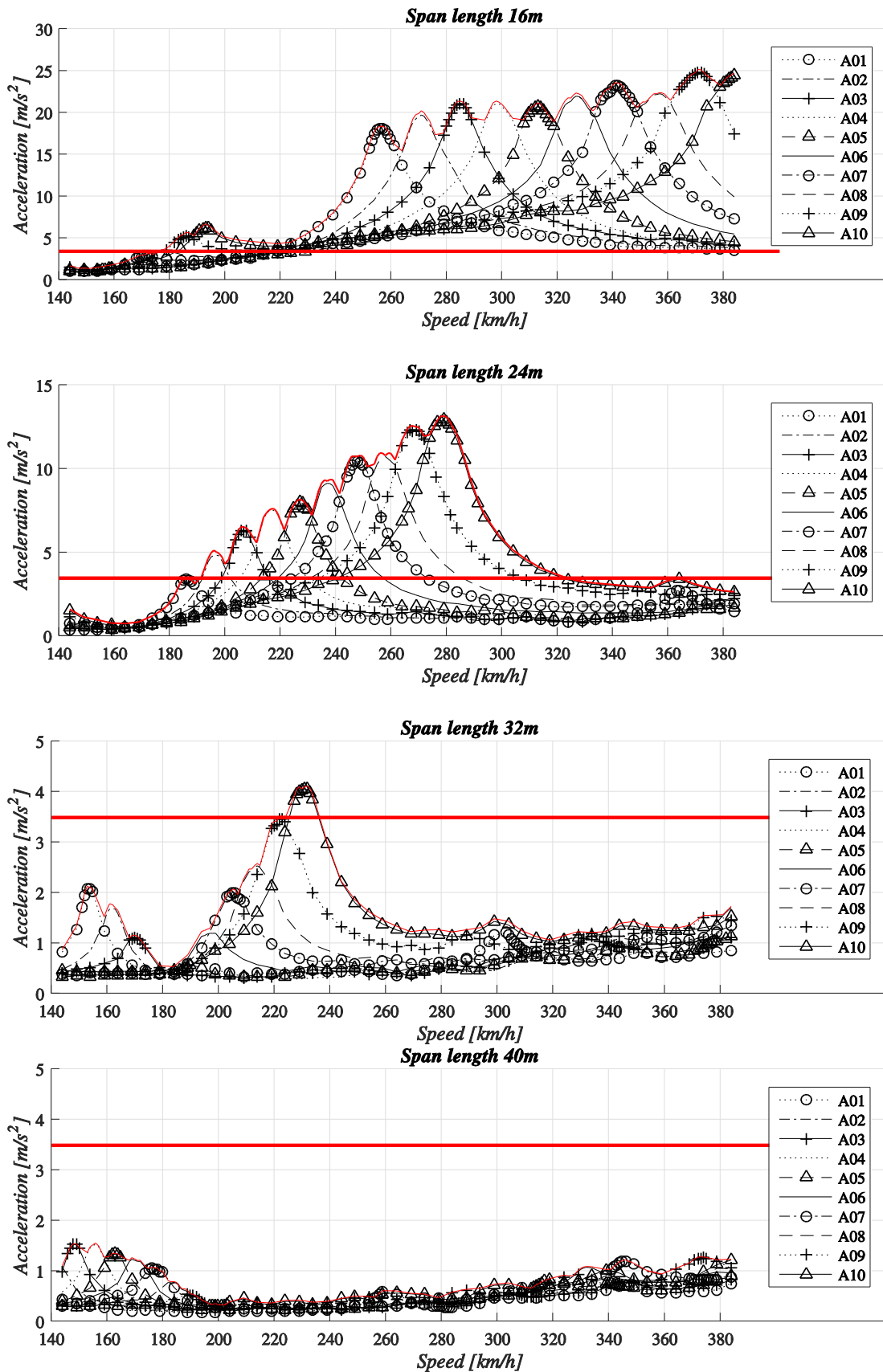
Figure 5.15 Maximum vertical accelerations of the four considered span length for the concrete slab bridge without end shields. Note that the scale of the y-axis differs. The horizontal line represents the maximum allowable acceleration limit according to Eurocode.

In the deflection plots in Figure 5.16 it is clear that the primary resonance peaks appeared at the same train speeds as for the accelerations. Nonetheless, the smaller acceleration peaks that occurred at speeds above the primary resonance speed for the 32 and 40 meter bridges were not apparent in the deflection plots, whereas the additional peaks that appeared at lower speeds for the 16 meter bridge were still present. This can be explained by the fact that the peaks that occurred at lower speed were caused by a multiple of the first natural frequency whereas the peaks at higher speeds were caused by a multiple of the third natural frequency. The dynamic response was mainly dependant of the first natural frequency, thus causing the bridge to vibrate with large amplitudes. The higher frequencies on the other hand, vibrated with much smaller amplitudes which is why they affected the accelerations but not the deflections.

The permissible deflection limit corresponding to very good level of comfort is included in the deflection diagrams and the limit was greatly exceeded for the 16 and 24 meter bridges. The 32 and 40 meter bridges indicated satisfactory dynamic deflections and the peak values were within the allowable limits.

Regarding the effect of load distribution, it can be seen that the response was basically the same whether the axle loads were taken as single point loads or when they were distributed over three sleepers.
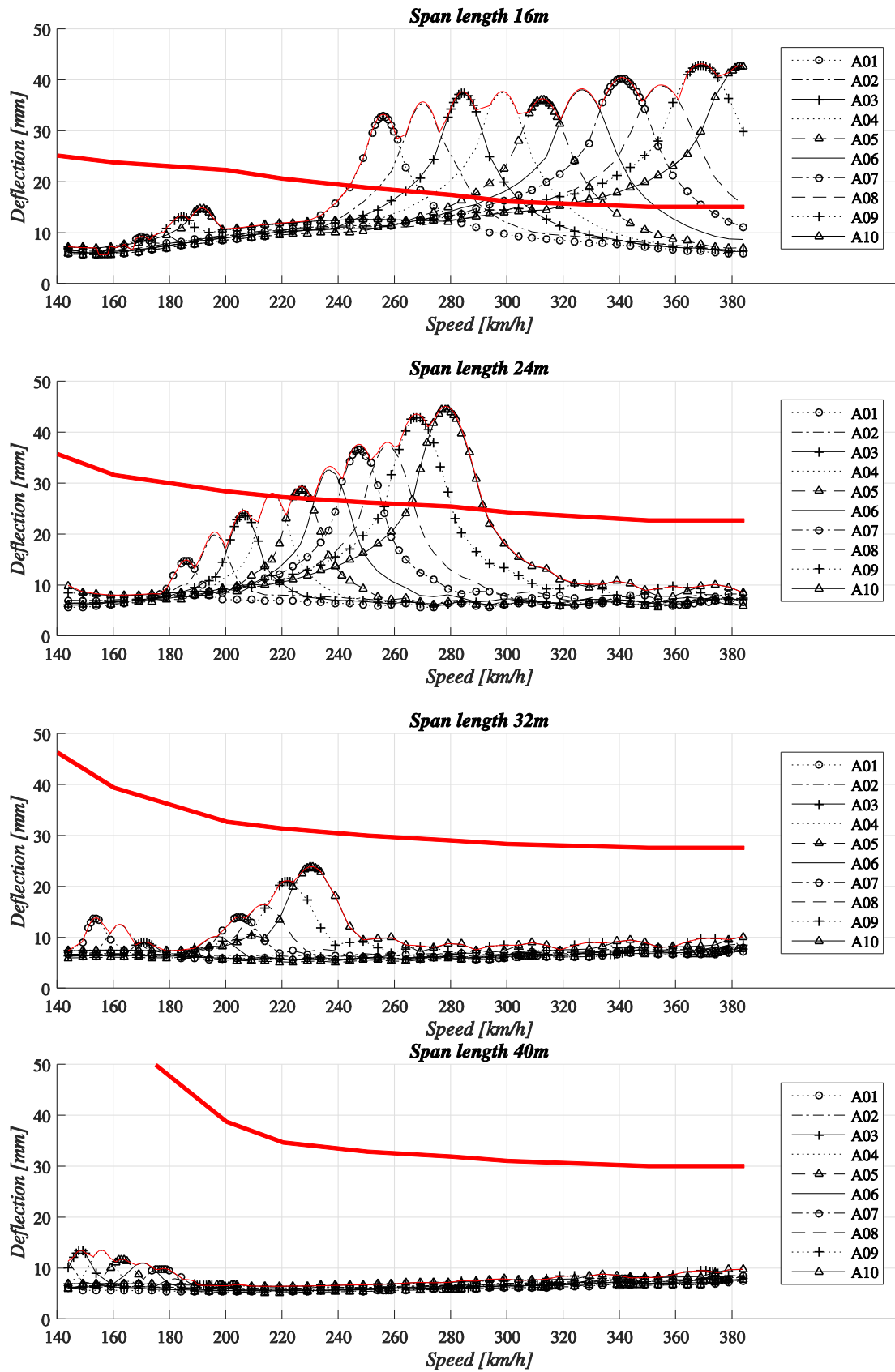
Figure 5.16   Maximum vertical deflections of the four considered span lengths for the concrete slab bridge without end shields. The horizontal line represent the maximum limit corresponding to a very good level of comfort.

5.2 Simply supported concrete slab bridge with end shields

The following section includes the result of the dynamic analysis of the simply supported concrete slab bridge when the end shields and wing walls were considered. The applied load was the HSLM-A load model from Eurocode 1, SS-EN 1991-2 (CEN, 2003), defined in Figure 3.15 and Table 3.1.

5.2.1 Dynamic response of different span lengths

The studied span lengths were the same as for the case when the end shields where excluded, i.e. 16, 24, 32 and 40 meters. The cantilevering length of the end shields were the same for all four bridges, that is 1.7 meters. The dynamic properties are shown in Table 5.3 and it can be seen that the fundamental natural frequency decreased for longer spans. In comparison to the case without end shields, the natural frequencies have decreased slightly when the end shields were included. The mass per meter and stiffness were the same for both cases but since the end shields and wing walls provided an additional mass at the end of the cantilevering part, the natural frequencies were decreased. The first six vertical bending mode shapes of the 24 meter bridge are presented in Figure 5.17 and the other span lengths had similar mode shapes.

Table 5.3   Dynamic properties of the four considered span lengths for the concrete slab bridge when considering the end shields.

Span length [m]	Bending stiffness [GNm²]	Bridge mass [ton/m]	Mass of end shields [ton]	1st bending frequency [Hz]	2nd bending frequency [Hz]	3rd bending frequency [Hz]
16	8.92	21.45	159.55	3.088	6.348	8.031
24	34.29	30.92	175.16	2.694	8.590	11.688
32	99.07	41.35	192.36	2.287	7.988	12.244
40	233.10	52.86	211.32	1.998	7.120	11.364
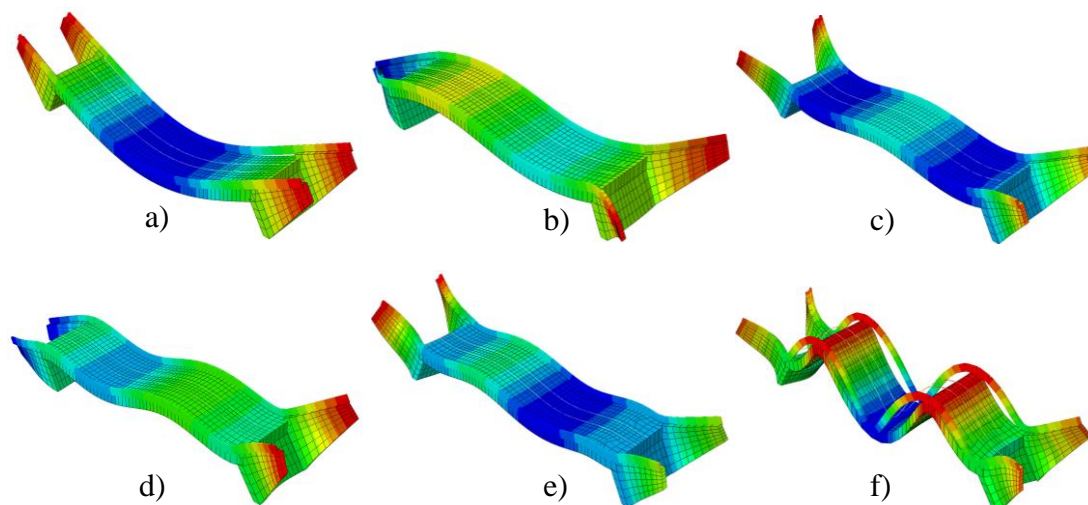
Figure 5.17   The first six vertical bending mode shapes of the 24 meter slab bridge with end shields.

The four considered bridge configurations were loaded with load model HSLM-A and the resulting maximum vertical accelerations and deflections can be seen in Figure 5.18 and Figure 5.19. As for the case without end shields, the influence of load distribution was studied for this bridge type. The complete response from load distribution is presented in the diagrams whereas the single point load case is illustrated as a red line, corresponding to the envelope of the response.

The appearance of the diagrams are quite similar to the case where the end shields were excluded since the relation between the span length and the coach length was identical. The resonance peaks appeared at lower train speeds as a result of the decreased natural frequencies. The maximum accelerations were lower compared to the case without end shields and the difference was more significant for the 16 meter bridge. The difference decreased as the bridge span got longer and for the 40 meter bridge, there were practically no difference at all between the two cases.

The reason that the response was higher for the case without end shields was that the additional mass from the end shields reduced the accelerations. The influence of the extra mass was more significant for the 16 meter bridge since it had the lowest mass to start with. The longer the bridge got the lower was the influence of the additional mass.

The resulting deflections of the four bridges with end shields are plotted in Figure 5.19 and the maximum response occurred at the edge in the middle of the deck, i.e. region B) in Figure 5.1. The result showed that the peak response were similar to the case without end shields and the only visible difference could be spotted for the 16 meter bridge whereas the others were basically unaffected by the end shields, except the fact that the resonance peaks occurred at lower train speed. This can be explained by studying the effect of the mass in Section 5.1.3.1 where it was clear that a change in mass only influenced the accelerations and not the deflections. Since the end shields only provided the bridge with additional mass and no stiffness in the span, the deflections were basically the same as for the case without end shields.

The influence of load distribution was very low for this bridge type as well and the maximum dynamic response was practically the same. Slightly lower accelerations could be observed for the 16 meter bridge.
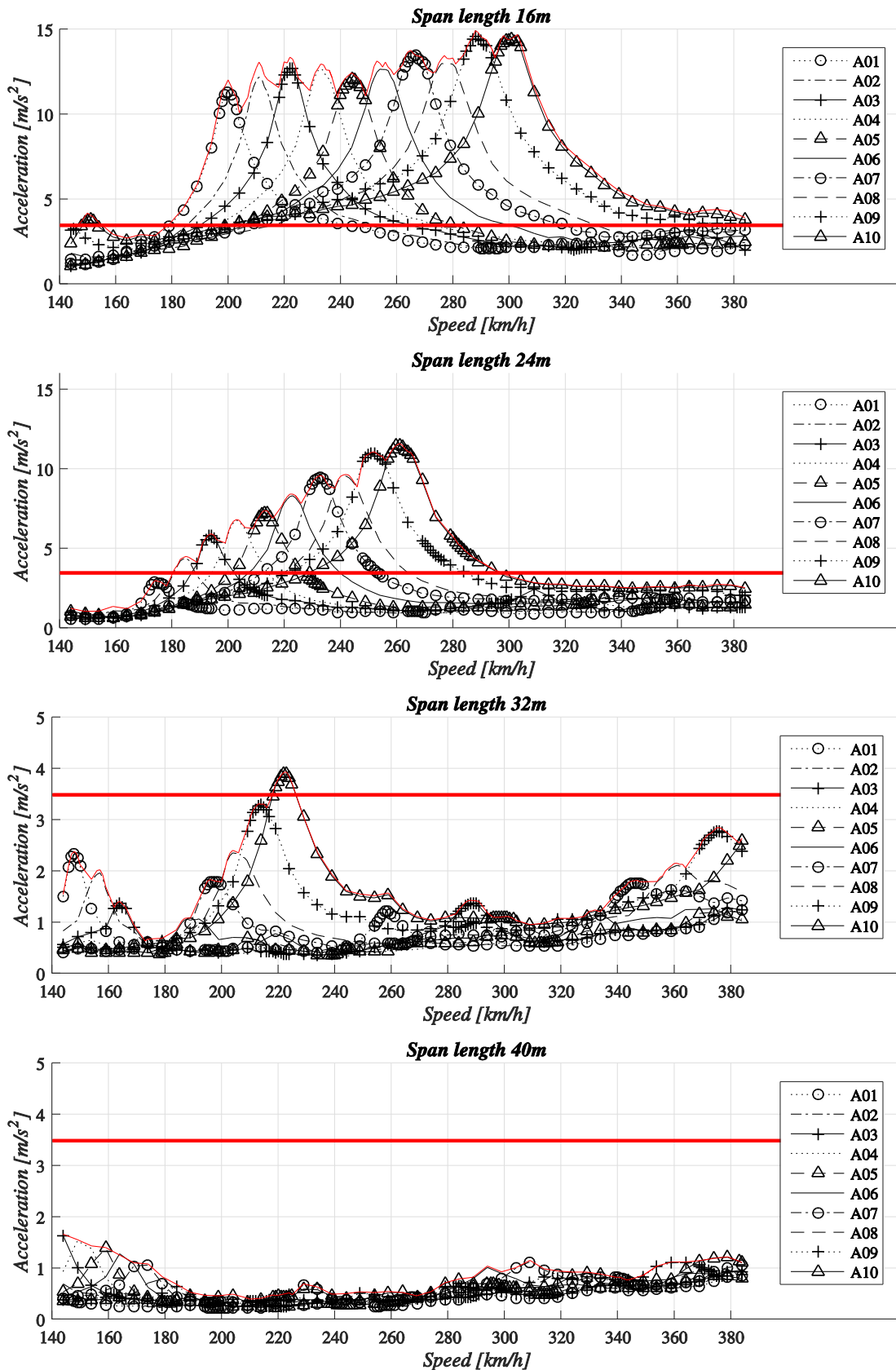
Figure 5.18 Maximum vertical accelerations of the four considered span lengths for the concrete slab bridge with end shields. Note that the scale of the y-axis differs. The horizontal line represents the maximum allowable acceleration limit according to Eurocode.
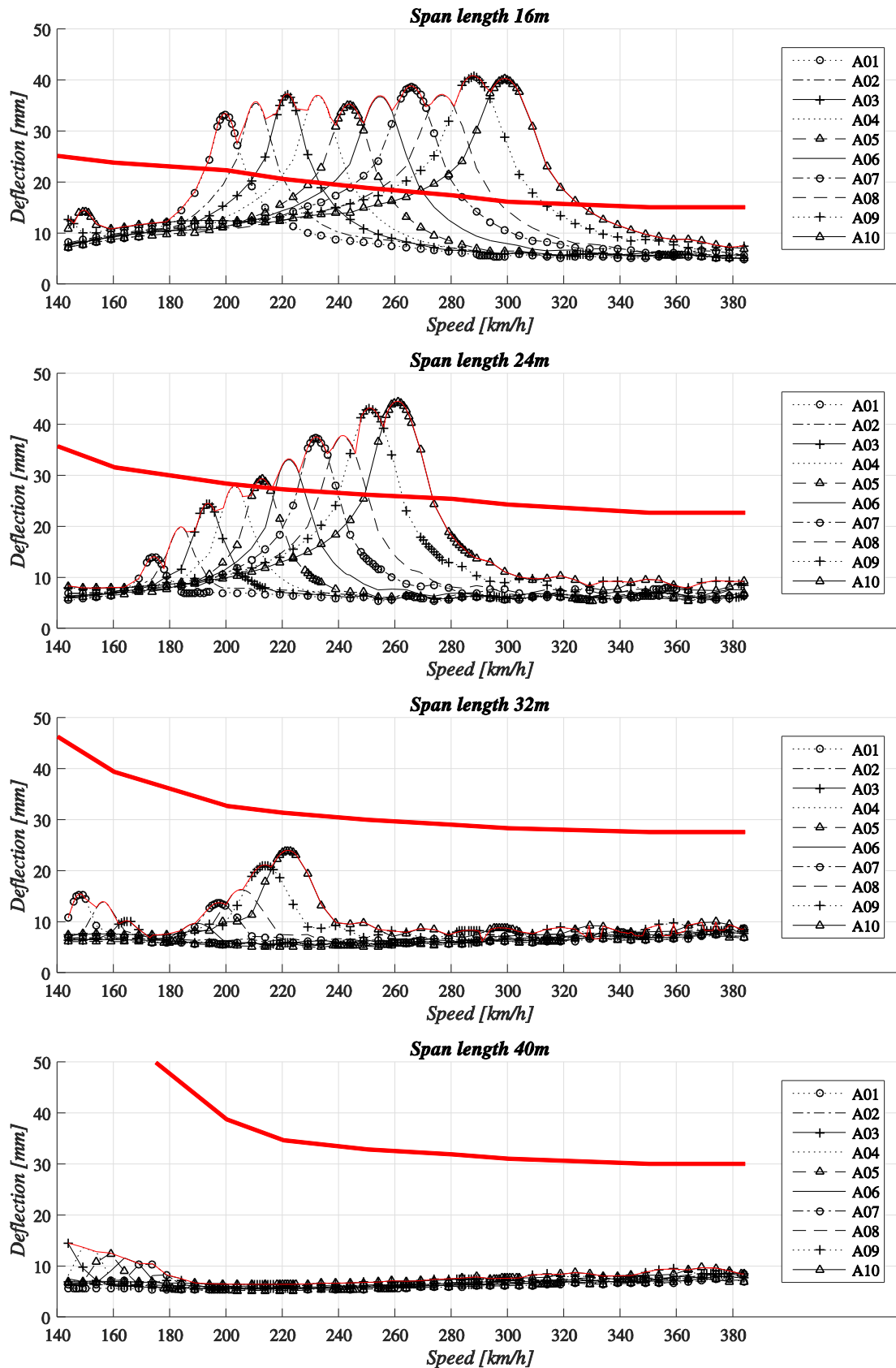
Figure 5.19   Maximum vertical deflections of the four considered span lengths for the concrete slab bridge with end shields. The horizontal line represent the maximum limit corresponding to a very good level of comfort.

5.3   Simply supported concrete trough bridge

This section presents the dynamic analysis of the simply supported trough bridge where the end shields and wing walls were excluded to begin with. The verification of the FE-models was done for these single-span bridges and the more complex models, i.e. the case where the end shields were considered, were generated from this one. A convergence study of the first three natural frequencies was performed for all models. The verification and convergence study of the 24 meter FE-model will be presented in the section below and others were checked in the same manner.

5.3.1   Convergence study and verification of FE-model

The first three natural frequencies were studied in order to ensure that the model had converged. Different number of element in x-direction (longitudinal) and y-direction (transverse) was evaluated. The mesh with 40 elements in x-direction and 10 elements in y-direction was considered to give sufficiently accurate results.

The static deflection due to self-weight for the analytical solution resulted in a value of $\delta_{s.an}$ = 17.731 mm. According to the FE-model, the static deflection was $\delta_{s.FEM}$ = 17.702 mm, which was in good agreement with the analytical value. The values for deflection in the FE-model were taken from the middle node in one of the edge beams in order to exclude the transverse deflection of the bridge deck that arose from the usage of shell elements. Thereby a more reasonable comparison with the analytical solution could be made.

The natural frequencies of the first three vertical bending modes are presented in Table 5.4 where the first frequency of the FE-model was quite in good agreement with the analytical solution. However, the difference for the other two was quite significant, especially for the third frequency. The reason can be explained by the fact that the FE-model with shell elements was more flexible and thus the vertical bending modes included not only vertical bending in the longitudinal plane but also in the transverse plane. The transverse behaviour affected this bridge much more compared to the slab bridge since the transverse stiffness was much lower for this bridge. This was also the reason that there were more vertical bending mode shapes within the considered frequency limit (see Figure 5.20) in comparison to the slab bridge where only three mode shapes were included.

By looking at the first vertical bending mode a) it is clear that the longitudinal bending was dominant and the bridge deflected as a whole, which was why the corresponding frequency was in better agreement with the analytical value. When studying the second vertical bending mode b) it can be observed that the deformation in the deck increased in the transverse direction between the edge beams, while the edge beams themselves experienced smaller displacements. Consequently, the bridge experienced more local bending rather than global deformations as for the first mode. This phenomenon got even more significant for the third mode c) that mainly involved transverse bending of the deck. This is why the corresponding frequency was even further away from the analytical value.

Table 5.4   *Natural frequencies of the first three vertical bending modes for the analytical solution and the corresponding frequencies of the FE-solution for the concrete trough bridge.*

Mode number (vertical bending)	Analytical solution [Hz]	FEM solution [Hz]
1st	4.215	4.153
2nd	16.861	15.075
3rd	37.938	18.440[1]
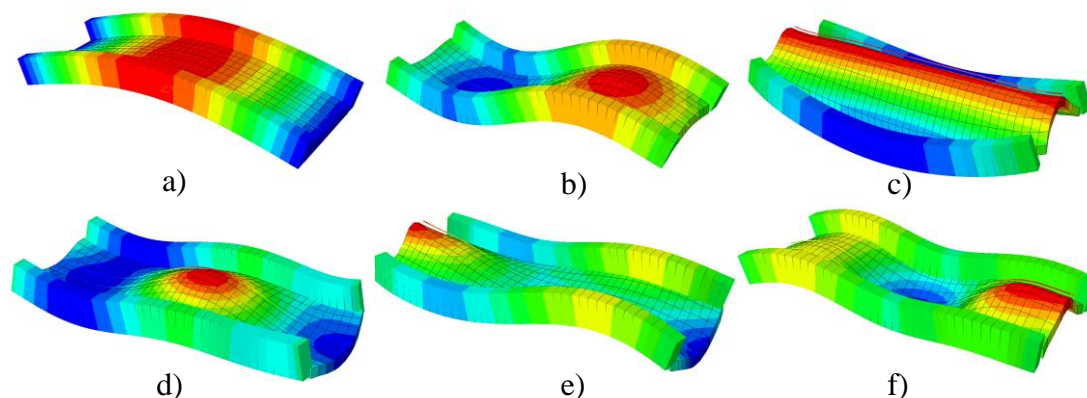
Figure 5.20   *First six vertical bending modes of the concrete trough bridge.*

The dynamic response of the bridge when subjected to a point load $p_0 = 200$ kN at constant speed $v_0 = 200$ km/h was evaluated for the FE-model and compared with an analytical solution. The midpoint deflection and midpoint acceleration are plotted in Figure 5.21. The point load leaves the bridge at time $t_{max} = 0.432$ s.

The midpoint deflection of the FE-model was in good agreement with the analytical solution. The FE-model resulted in a slightly larger maximum deflection due to the transverse bending of the deck. As for the previous bridge, the initial response indicated a positive deflection and acceleration, which was a result of the same reason as explained before in Section 5.1.1.

The diagram of midpoint acceleration shows that the FE-solution of the bridge behaviour were in good agreement with the analytical solution when comparing the contribution from the first mode shape. However, the higher modes were not in good agreement and they were out of phase with each other. The FE-solution oscillated more rapidly and with larger magnitude, since the difference between the corresponding eigenfrequencies was quite large and the transverse bending resulted in higher accelerations. One of the curves in the acceleration diagram corresponded to the behaviour when only mode shapes with mainly longitudinal bending were considered. It was still some transverse bending included in these modes but not as much as for mode c) in Figure 5.20 for instance. When including all modes the response was increased quite a lot which indicates how much the transverse bending

---

[1] For the FE-solution, the third eigenfrequency corresponds to Figure 5.20c. The analytical solution does not take transverse bending into account thus the modes are not the same.

influence the accelerations. The influence of the higher modes on the deflections was negligible since they vibrated with a low amplitude, which is why the deflections were in better agreement with the analytical solution.
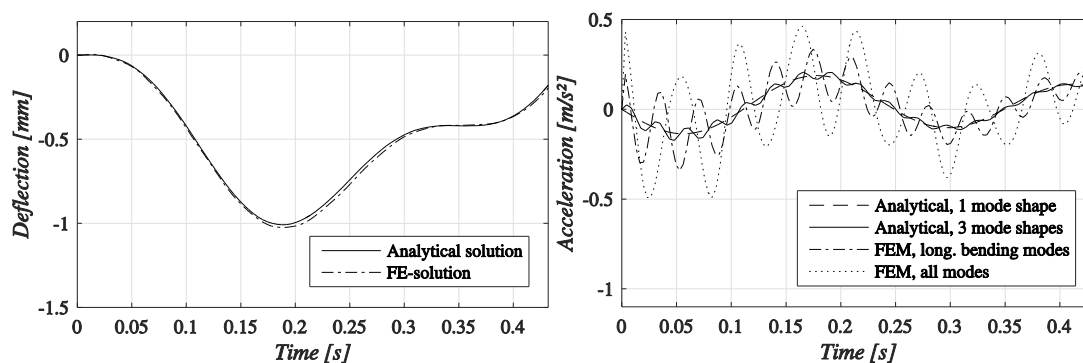
Figure 5.21   Comparison of the analytical solution and the FE-solution for midpoint deflection and acceleration of the concrete trough bridge due to a moving point load.

5.3.2   Dynamic response of different span lengths

The dynamic response of the simply supported trough bridge without end shields and wing walls was studied for four different span lengths as for the previous bridge, i.e. 16, 24, 32 and 40 meter. The dynamic properties for each bridge are presented in Table 5.5 and the first six vertical bending mode shapes for the 24 meter bridge are shown in Figure 5.20. Similar mode shapes were valid for the other span lengths as well, however, their corresponding frequencies were different. Noticeable was that for the 40 meter bridge, mode shape c) appeared before b), which can be explained by the fact that the transverse distance between supports were increased for the longer bridges. Since the frequencies were decreasing for the longer bridges, there were a few more mode shapes within the cut-off limit of 30 Hz in addition to the ones presented in the figure.

Table 5.5   Dynamic properties of the four considered span lengths for the concrete trough bridge without end shields and wing walls.

Span length [m]	Bending stiffness [GNm²]	Mass [ton/m]	1st bending frequency [Hz]	2nd bending frequency [Hz]	3rd bending frequency [Hz]
16	19.10	25.55	5.305	17.834	20.790
24	72.91	31.44	4.153	15.075	18.440
32	205.03	39.86	3.479	13.129	14.542
40	495.86	52.16	3.027	11.225	11.691

In comparison to the concrete slab bridge without end shields, the stiffness for each span lengths was much larger for the trough bridge whereas the mass per meter was similar. Consequently, the fundamental natural frequencies were higher for the trough bridge and thus the resonance peaks occurred at higher train speed. However, the third eigenfrequencies were lower than for the slab bridge, which may be explained by the fact that the third mode shape that appeared for the trough bridge, c) in Figure 5.20, was mainly involving transverse bending of the deck, on the contrary to the slab bridge which had a third mode shape as shown in Figure 5.2. The reason that the

transverse bending was more influential for the trough bridge was that the deck was rather thin and the distance between the supports in the transverse direction was relatively long.

The results of the dynamic analyses for the concrete trough bridge when subjected to load model HSLM-A are presented in Figure 5.23 and Figure 5.24 as maximum vertical accelerations and maximum vertical deflections. The bridges were evaluated for the case when the axle loads were taken as single point loads as well as when load distribution over three sleepers were accounted for. The single point load case is included as an envelope of the maximum response for all trains, presented as a red line in the diagrams. The complete response of the load distribution case is plotted in the same diagrams in order to see the difference.

The acceleration diagrams indicated that the maximum values were slightly lower for the three longest trough bridges in comparison to the slab bridges, when studying the load distribution case. The 16 meter trough bridge however, got slightly higher peak values. The mass of each span length was similar between the trough bridges and the slab bridges, which is why the maximum accelerations were similar. The difference in mass was more significant for the 16 meter span where the mass of the trough bridge was approximately 4 ton/m higher than the slab bridge. Consequently, the mass affected this span length more than the others.

Even though the mass was quite similar between the two bridge types, the appearance of the acceleration plots were not as smooth as for the slab bridge, especially for the 16 and 24 meter bridges. This was because of the dissimilarities of the mode shapes where the trough bridge had more transverse bending involved. The maximum accelerations for the slab bridge at resonance were progressively built up for each axle load exciting the bridge, which was shown in Figure 5.6 and at non-resonance speed the response was kept rather low.

For the trough bridge, the maximum acceleration at resonance was obtained in the middle of the span (region A in Figure 5.1) whereas it was obtained at the short ends of the deck between the supports for non-resonance speeds (region C in Figure 5.1). Figure 5.22 a) shows the accelerations of the short end of the bridge at a non-resonance speed for the 24 meter bridge. The maximum values occurred when the closely placed axle loads of the power car and end coach passed the short edge, see Figure 5.22 b). The maximum response is indicated with rings in the history plot a) and the arrows pointing upwards in b), illustrates the corresponding train location over the short end.
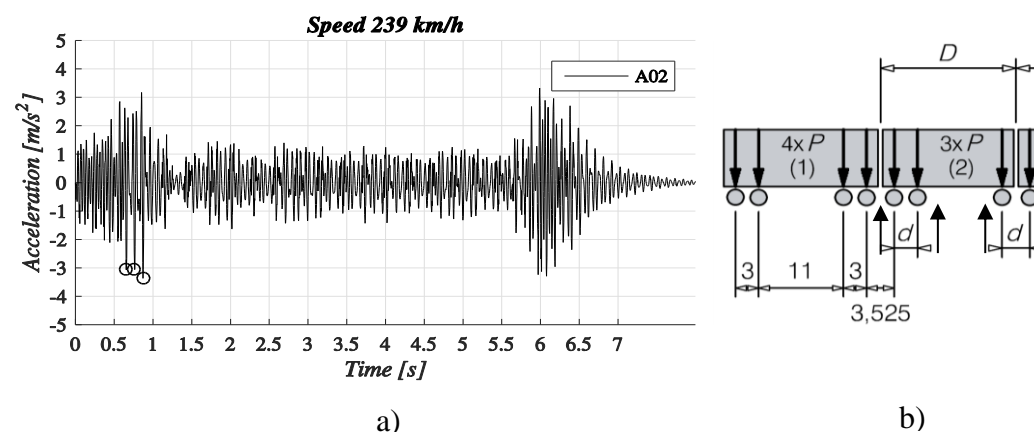
Figure 5.22   Time history plot of a non-resonance speed for the 24 meter bridge.

When the closely placed axle pairs passed the edge of the bridge they stimulated the higher mode shapes, which highly effected the vibrations in the short edge. Hence, they induced transient vibrations in the deck with high peak values. Since the distance between these axle pairs were similar for all the HSLM trains, the response was similar for all trains outside of resonance. For the resonance peaks, the same phenomena with the short edge of the bridge occurred but the accelerations in mid-span were eventually higher as more axle loads excited the bridge.

The deflection of the different span lengths for the trough bridge without end shields are shown in Figure 5.24 and the results were almost overall satisfactory. The allowable limit was only slightly exceeded for the 16 meter bridge at speeds above 340 km/h. The deflection plots were much smoother than the acceleration plots since the maximum values were obtained in the middle of the span. In addition, the higher mode shapes had a negligible effect on the deflection. In comparison to the slab bridge, the deflections were much lower since the stiffness was a lot larger for the through bridge.

The effect of load distribution was much higher for this bridge type where there were significant accelerations at the short edges of the bridge. The transient response that were induced got even higher when the applied load was taken as single point loads. The difference between the load distribution case and the single point load case was less for the resonance peaks. This may be explained by the fact that the resonance response was obtained in mid-span where the effect of the transient response was lower. The deflections plots on the other hand showed no difference at all between the two cases. The reason was that the maximum deflections were obtained in the middle of the span where the influence from the higher modes were negligible.
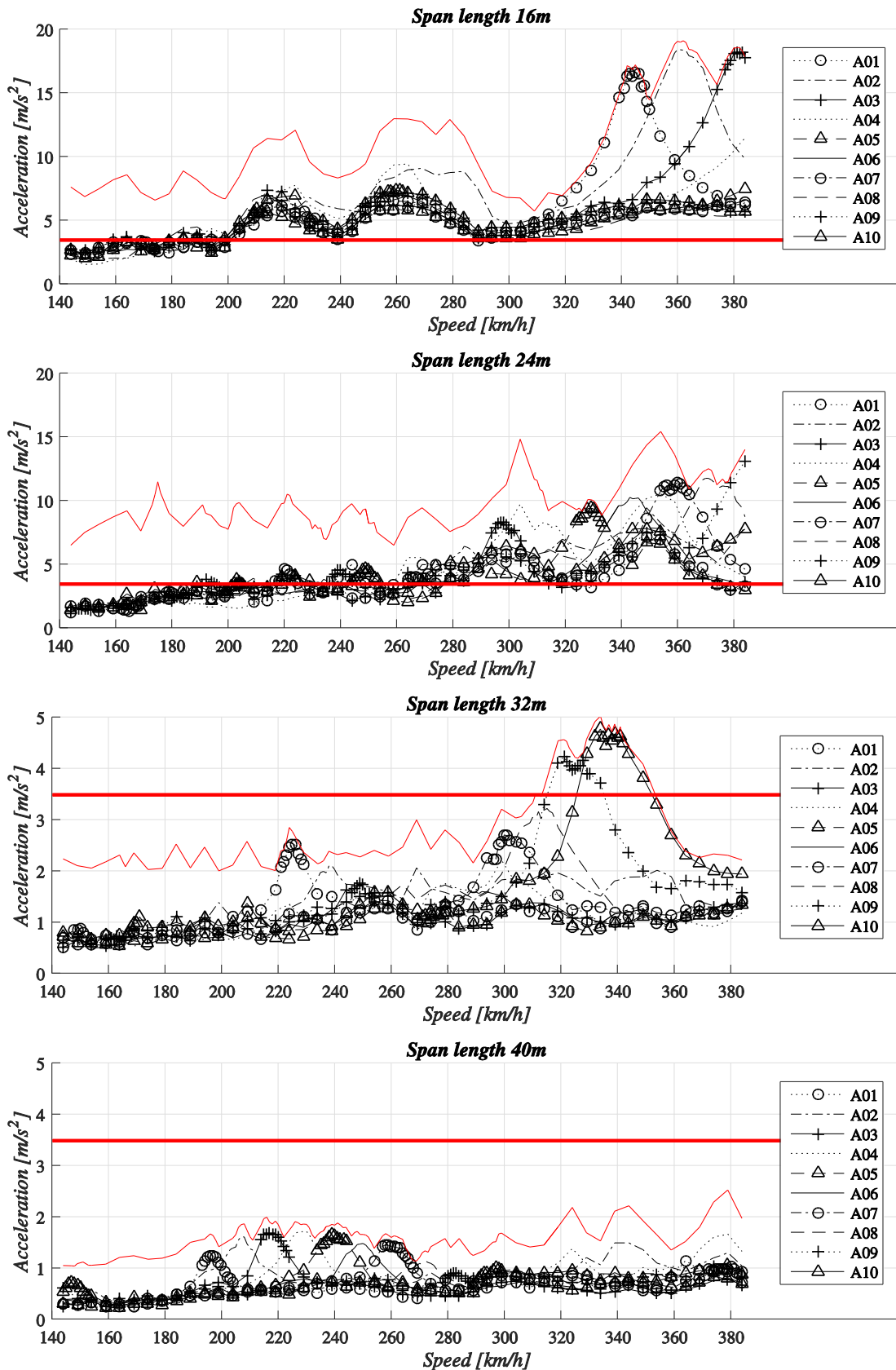
Figure 5.23   Maximum vertical accelerations of the four considered span lengths for the concrete trough bridge without end shields. Note that the scale of the y-axis differs. The horizontal line represents the maximum allowable acceleration limit according to Eurocode.
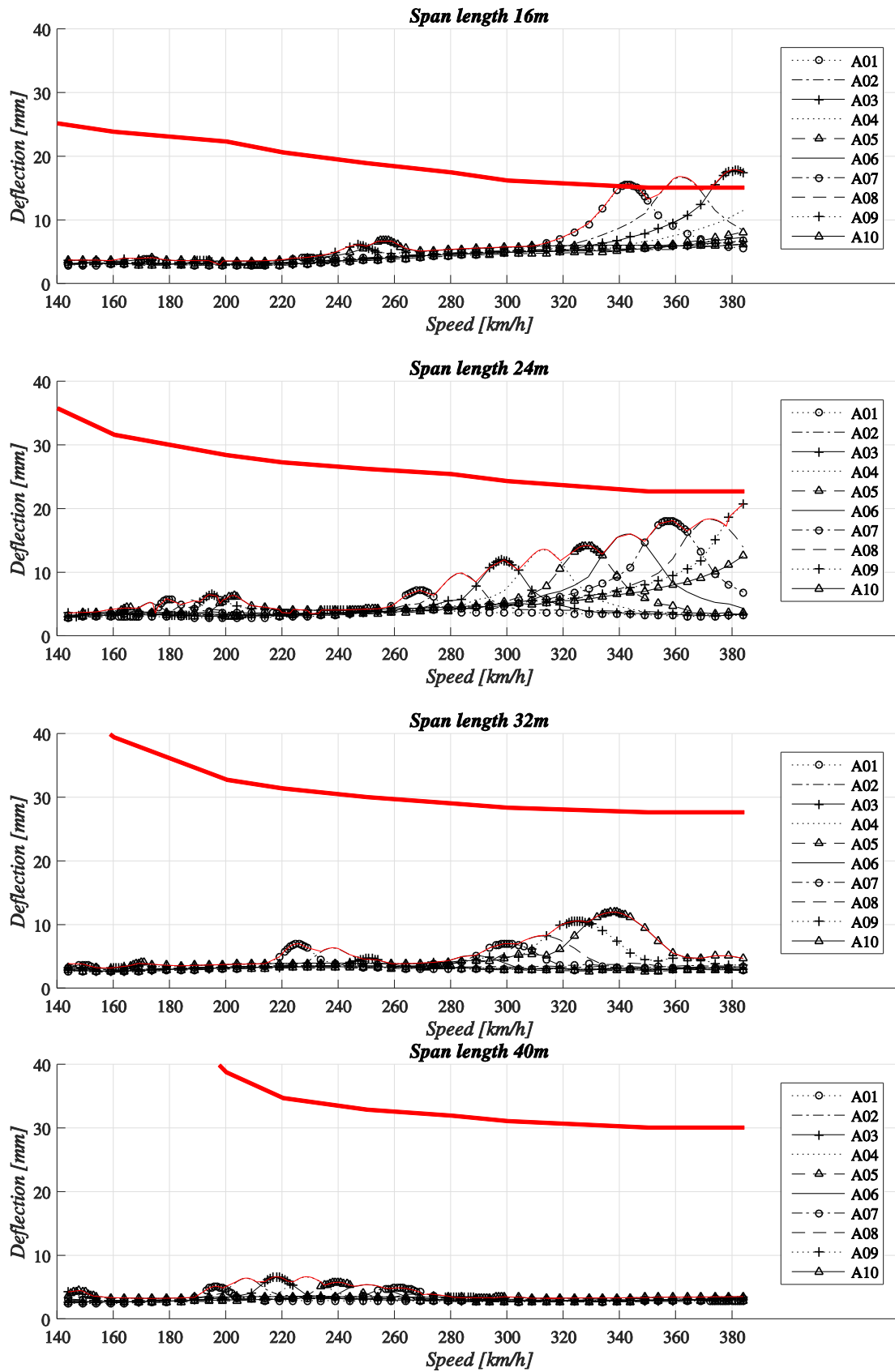
Figure 5.24   Maximum vertical deflections of the four considered span lengths for the concrete trough bridge without end shields. The horizontal line represent the maximum limit corresponding to a very good level of comfort.

5.4 Simply supported concrete trough bridge with end shields

The following section includes the result of the dynamic analysis of the simply supported concrete trough bridge when the end shields and wing walls were included in the FE-model. The applied load was the HSLM-A load model from Eurocode 1, SS-EN 1991-2 (CEN, 2003), defined in Figure 3.15 and Table 3.1.

5.4.1 Dynamic response of different span lengths

The dynamic analyses of the concrete trough bridges with end shields included the four span lengths 16, 24, 32 and 40 meters. The length of the cantilevering part with the end shields was 2.3 meters and it was the same for all four cases. The dynamic properties for each span length are given by Table 5.6 and the mode shapes of the 24 meter bridge are presented in Figure 5.25. The principal shape of the modes are similar for each span length.

Table 5.6   Dynamic properties of the four considered span lengths for the concrete trough bridge with end shields.

Span length [m]	Bending stiffness [GNm^2]	Bridge mass [ton/m]	Mass of end shields [ton]	1st bending frequency [Hz]	2nd bending frequency [Hz]	3rd bending frequency [Hz]
16	19.10	25.55	236.74	3.795	6.687	10.219
24	72.91	31.44	253.85	3.763	9.514	12.897
32	205.03	39.86	271.82	3.347	10.699	14.506
40	495.86	52.16	292.10	2.973	10.605	12.251
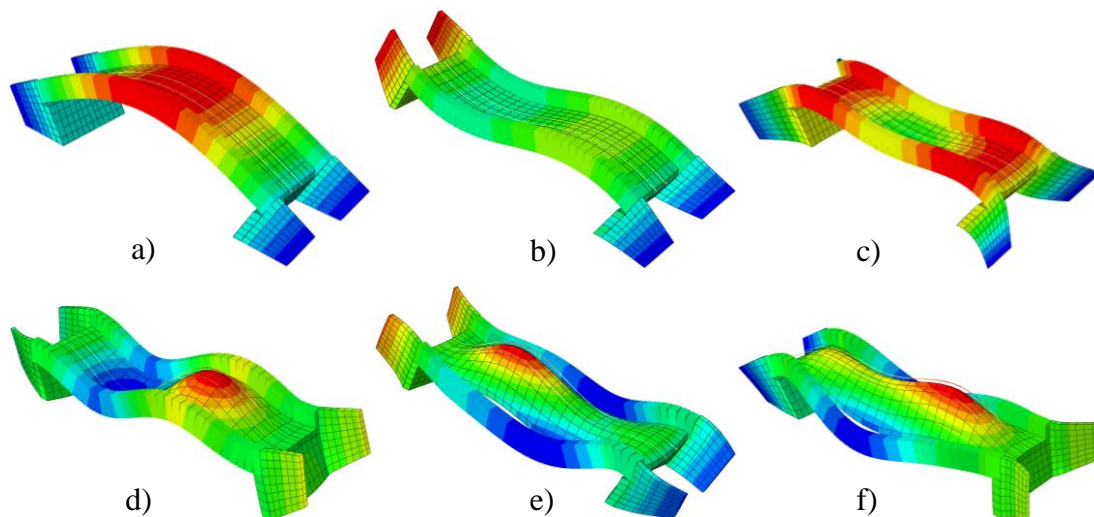
Figure 5.25   The first six vertical bending mode shapes of the 24 meter trough bridge with end shields.

By including the end shields and wing walls in the analysis, the fundamental natural frequencies were decreased because of the additional mass that the end shields provided. The difference was quite significant for the 16 meter bridge since the influence of the extra mass was more substantial for that bridge. In comparison to the

slab bridge with end shields, the natural frequencies were higher as a result of the stiffer cross-section and similar mass per meter.

By examine the mode shapes in Figure 5.25, it is clear that the end shields have provided the bridge deck with extra stiffness in the transverse direction at the short edges. Consequently, there were no longer any significant transverse movement at the regions close to the end shields, which was the case when the end shields were excluded.

The results of the dynamic analyses when subjecting the bridges with load model HSLM-A are presented in Figure 5.26 and Figure 5.27. The maximum accelerations were obtained in the middle of the span for all four bridges. For the 16 meter bridge, the peak values decreased substantially in comparison to the case without end shields. The reason being that the additional mass from the end shields were most influential for this short bridge. Furthermore, the accelerations were no longer excessive for the train speeds outside of resonance, which was the case when the end shields were disregarded. This was due to the fact that the end shields provided transverse stiffness to the edges and the mode shapes affecting the short edges were no longer present.

The 24 and 32 meter bridges showed also lower peak response but the difference to the case without end shields were not as significant as for the 16 meter bridge. For the longest bridge of 40 meters, the response was slightly increased for the case with end shields. Nonetheless, the response was still well below the permissible limit of 3.5 m/s^2. Since the same span lengths and load models were considered as before, the same behaviour of each peak response was obtained, related to the cancellation effects. This was most obvious for the 32 meter bridge where the response from HSLM-A4 and HSLM-A5 were effectively suppressed.

The deflection plots in Figure 5.27 shows a good behaviour for the three longest bridges. As a result of the decreased natural frequencies in comparison to the case without end shields, the train speeds at which resonance occurred have been decreased. Consequently, new peak values from the longer trains have been moved down to the considered speed range for the 16 and 24 meter bridges, causing higher response than before. It should be noted that the response of the trains that were present for the case without end shields were still similar for this case since the stiffness was identical.
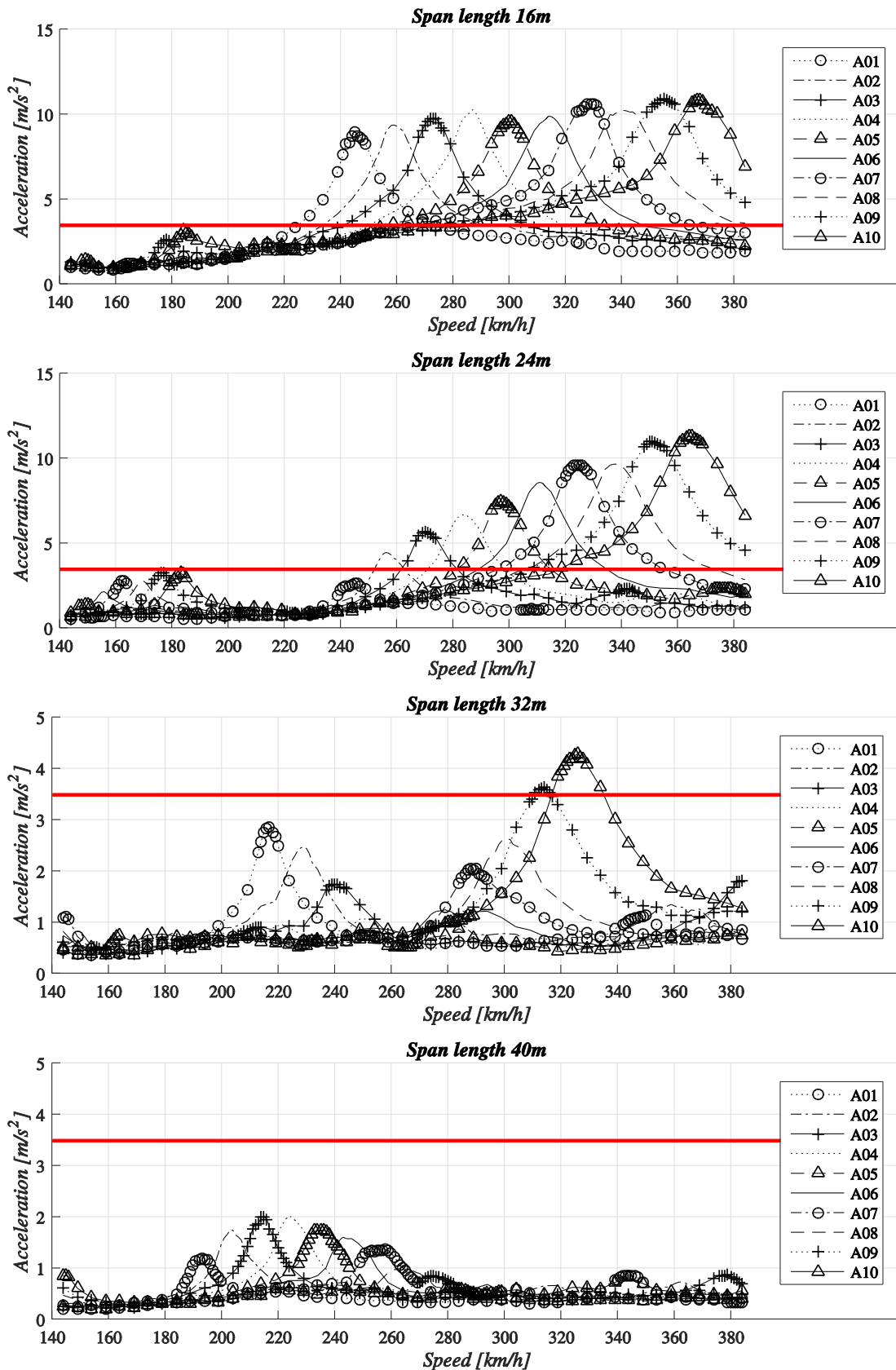
Figure 5.26   Maximum vertical accelerations of the four considered span lengths for the concrete trough bridge with end shields. Note that the scale of the y-axis differs. The horizontal line represents the maximum allowable acceleration limit according to Eurocode.
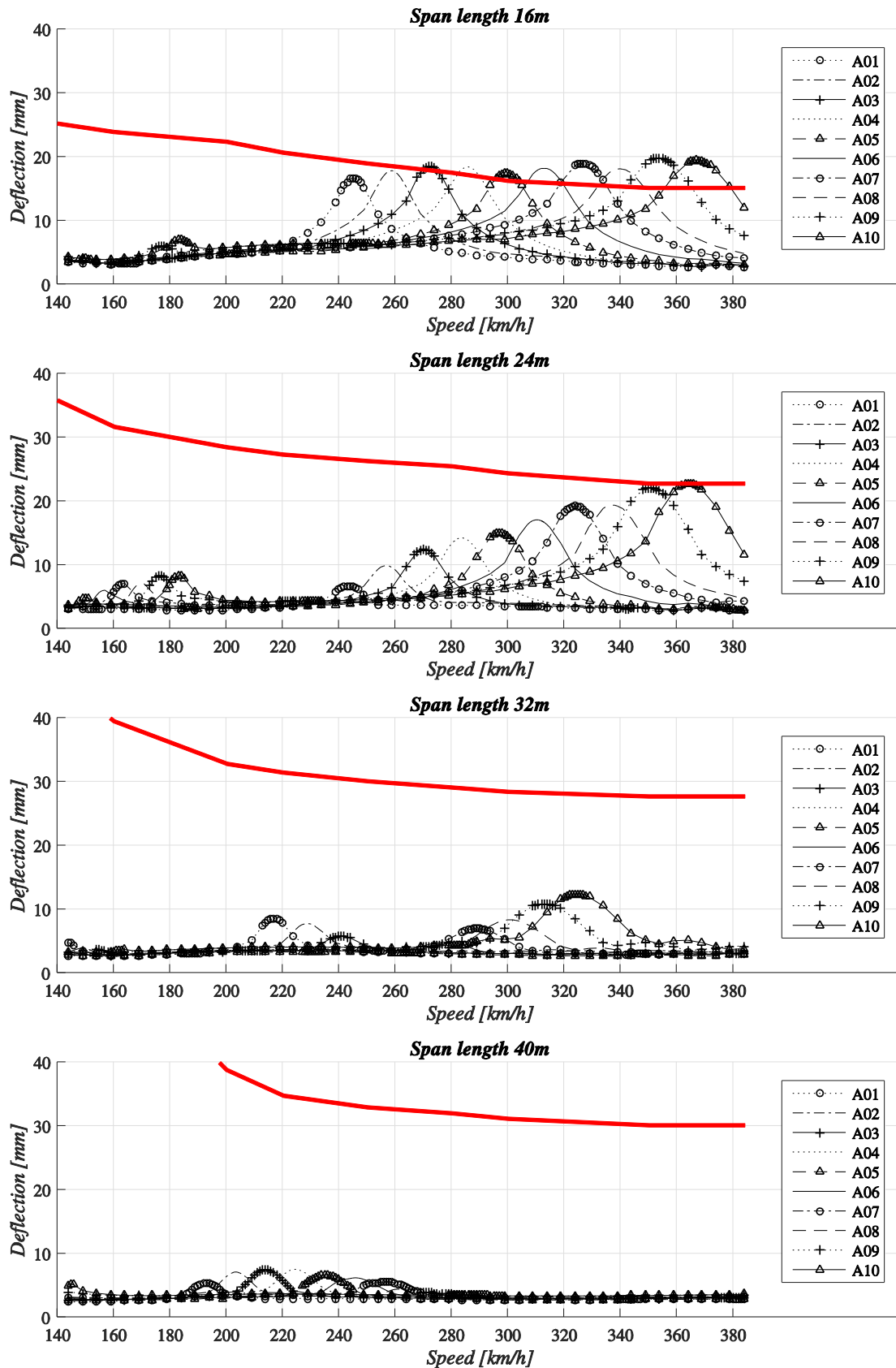
Figure 5.27   Maximum vertical deflections of the four considered span lengths for the concrete trough bridge with end shields. The horizontal line represent the maximum limit corresponding to a very good level of comfort.

5.4.2 Dynamic response of a short span trough bridge with improved cross-section

A new cross-section was considered for the 16 meter trough bridge with end shields in order to improve the dynamic performance. The new dimensions are presented in Figure 5.28 and the dynamic properties are presented in Table 5.7. The cross-section was a lot more massive than before and the natural frequencies were therefore increased significantly. The corresponding natural modes had still the same shape as the previous case in Figure 5.25.
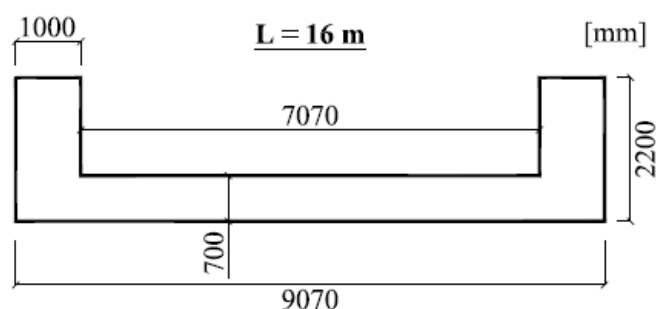
Figure 5.28   New cross-section of the 16 meter concrete trough bridge.

Table 5.7   Dynamic properties of the 16 meter trough bridge with improved cross-section.

Span length [m]	Bending stiffness [GNm²]	Bridge mass [ton/m]	Mass of end shields [ton]	1st bending frequency [Hz]	2nd bending frequency [Hz]	3rd bending frequency [Hz]
16	67.05	30.97	252.89	6.394	10.953	16.484

The maximum vertical accelerations and maximum deflections are presented in Figure 5.29 and it was clear that the new bridge design was better in terms of dynamic performance. As a result of the high fundamental frequency, the primary resonance peaks were moved outside of the considered speed range and the response was instead determined by the second resonance speed. It can be observed that the primary resonance peak of HSLM-A1 was starting to rise at train speeds above 360 km/h but it did not exceed the limit for the studied speed interval. According to the deflection diagram, the response decreased substantially in comparison to the previous 16 meter bridge.
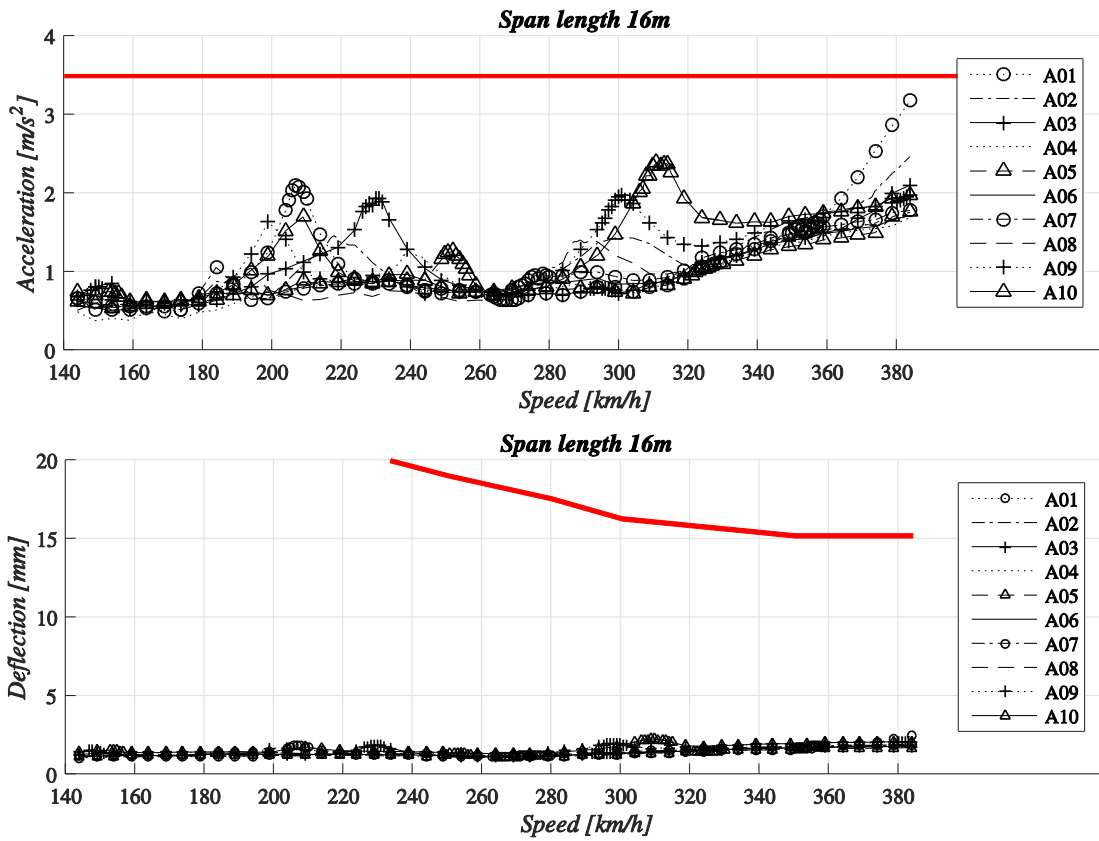
Figure 5.29 *Maximum vertical accelerations and deflections of the 16 meter trough bridge with improved cross-section. The horizontal lines represent the maximum allowable limits from Eurocode.*

5.5 Two-span continuous concrete slab bridge

This section includes the result of the dynamic analysis of the two-span continuous concrete slab bridge, based on the same cross-sections as the single span slab bridge. The applied load was the HSLM-A load model from Eurocode 1, SS-EN 1991-2 (CEN, 2003), defined in Figure 3.15 and Table 3.1.

5.5.1 Dynamic response of different span lengths

The dynamic analyses were carried out by considering two equal spans for each bridge with span lengths of 16, 24, 32 and 40 meters. The dynamic properties of each bridge are presented in Table 5.8 and since the same cross-sections were used as for the single-span simply supported case, the stiffness and mass per meter were unchanged. The fundamental frequencies have been increased in comparison the simply supported case. By providing the bridge with continuity, more mode shapes with lower frequencies emerged within the considered frequency range, which was why the higher frequencies were lower than for the simply supported case. The first six principal vertical bending mode shapes are shown in Figure 5.30.

Table 5.8   Dynamic properties of the four considered span lengths for the two-span continuous slab bridge.

Span length [m]	Bending stiffness [GNm^2]	Bridge mass [ton/m]	Mass of end shields [ton]	1st bending frequency [Hz]	2nd bending frequency [Hz]	3rd bending frequency [Hz]
16	8.92	21.45	159.55	3.379	4.684	7.566
24	34.29	30.92	175.16	2.770	4.243	9.357
32	99.07	41.35	192.36	2.316	3.607	8.381
40	233.10	52.86	211.32	2.011	3.139	7.276
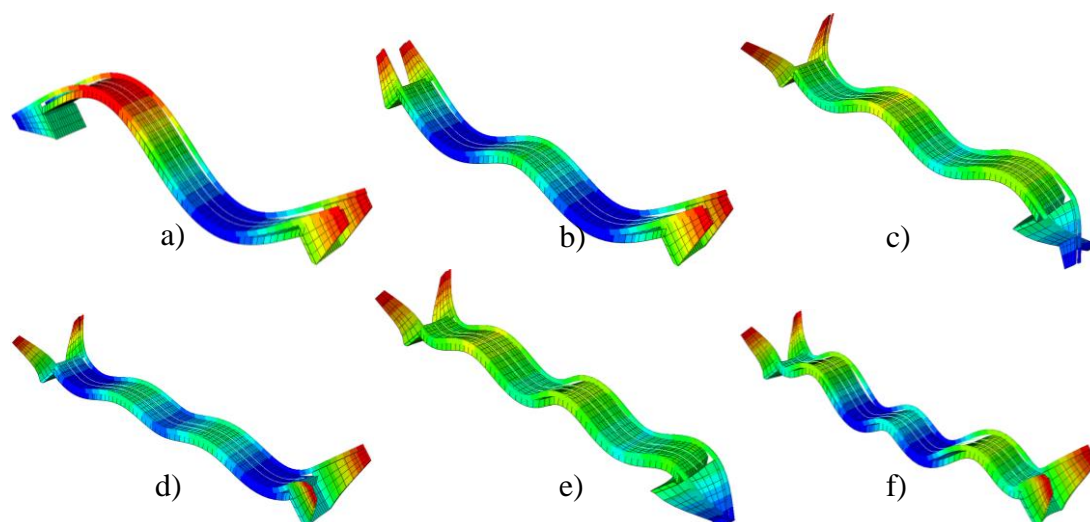
Figure 5.30   The first six principal vertical bending mode shapes of the two-span continuous slab bridge with end shields.

The resulting maximum accelerations and deflections are presented in Figure 5.31 and Figure 5.32. The two bridges with 16 and 24 meter spans showed high accelerations that exceeded the limit of 3.5 m/s^2 whereas the two longest bridges were satisfactory. The behaviour of all four cases was dominated by the first two mode shapes, i.e. a)

and b) in Figure 5.30. The resonance peaks at lower train speeds corresponded to the first mode and the peaks at higher train speeds corresponded to the second mode.

As for the simply supported case, the span length to coach length ratio highly influenced the dynamic response. For a continuous bridge there are a higher number of optimal span/coach length ratios, which was described in Section 3.1.1. A simply supported single span bridge had optimal ratios of L/d = 1.5, 2.5, 3.5 etc. whereas a continuous two-span bridge had optimal ratios of L/d = 1, 1.5, 2, 2.5 etc. This was why the response of the first mode shape for the 16 meter bridge was decreased rapidly as the trains got shorter since they approached a span to coach length ratio equal to one.

The same phenomenon occurred for the other span lengths as well whenever the span to coach length ratio was close the values mentioned above. However, this was only true for the first mode shape and the second mode shape behaved differently. When the first mode resulted in high accelerations, the second mode was cancelled out and vice versa. This may be explained by studying the shape of the two first modes in Figure 5.30. The first cancellation ratio of the first mode appeared at L/d = 1, which means that two boogie pairs were in the centre of each span at the same time. Since the first mode shape was asymmetrical, this implied that one of the boogies pushed the deck downwards whereas the other one held it back, thus reducing the response. The second mode shape on the other hand was symmetrical and both spans were pushed down simultaneously for a span to coach length ratio equal to one, hence increasing the response. This was most obvious for the 24 meter bridge where HSLM-A7 resulted in a ratio equal to one and the response was effectively suppressed for the first mode at a train speed of 239 km/h, whereas the same train resulted in the highest response for the second mode at a train speed of 366 km/h.

The dynamic response caused by the first mode shape was limited in magnitude for the longer bridges since there was always axle loads preventing the deck to move freely in one of the spans. However, by studying the shortest bridge with span length 16 meters, it can be seen that the second mode resulted in higher response for the shorter trains whereas the first mode gave higher response for the longer trains. This was due to the fact that when one boogie of the longer trains excited one of the spans, the other span could move freely since the next boogie had not yet entered the bridge.

In the deflection plots of Figure 5.32, it was only the 16 meter bridge that exceeded the allowable limit. The response of all four cases was mainly influenced by the first mode shape, except for the 24 meter bridge where the second mode provided high deflections as well. The reason being that the span to coach length ratio was equal or close to one for this bridge, which resulted in high response from the second mode. In comparison to the single span case, the deflections were lower for all four considered span lengths and the difference was more substantial for the longer bridges.
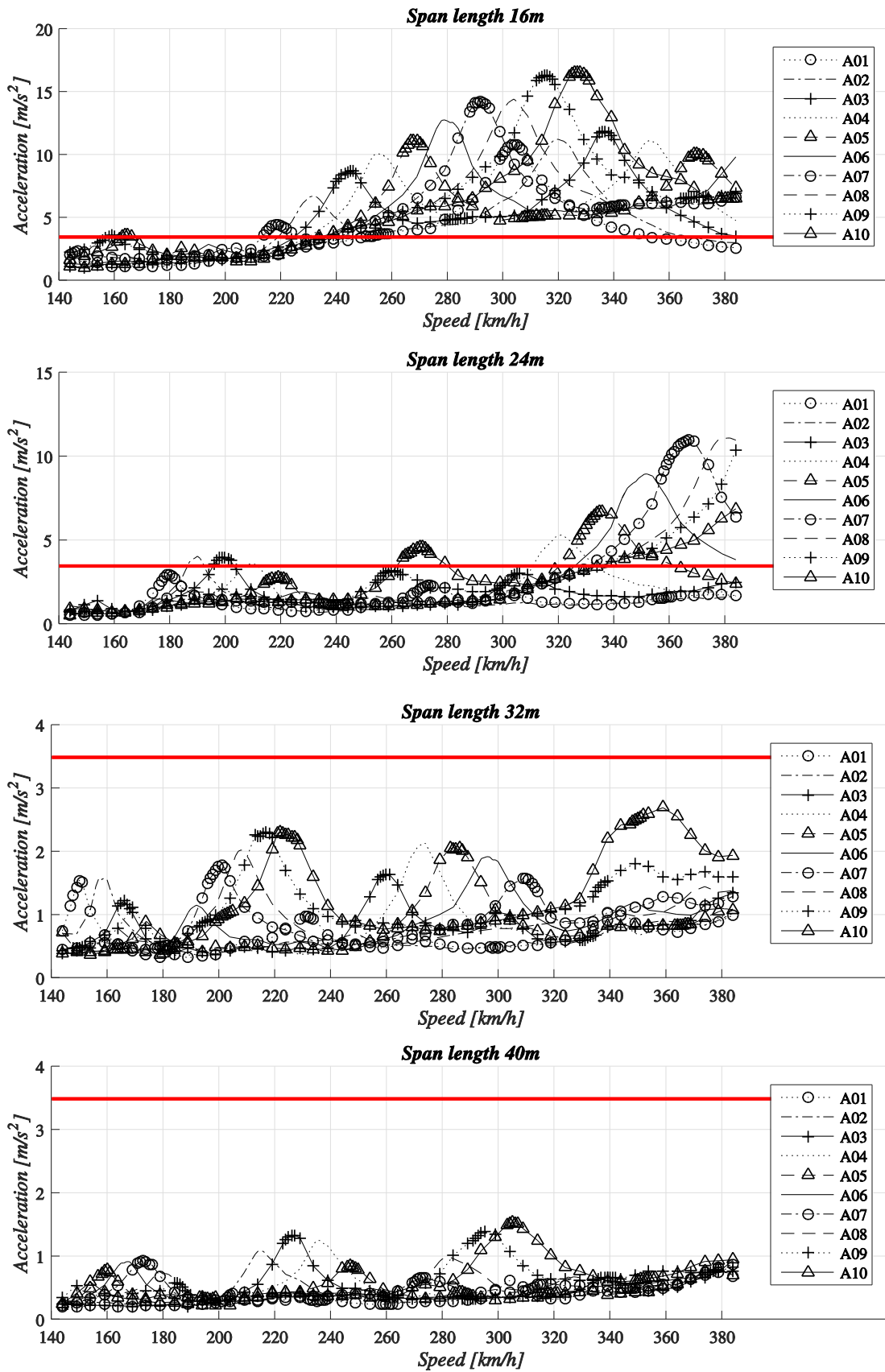
Figure 5.31   Maximum vertical accelerations of the four considered span lengths for the continuous two-span bridge. Note that the scale of the y-axis differs. The horizontal line represents the maximum allowable acceleration limit according to Eurocode.
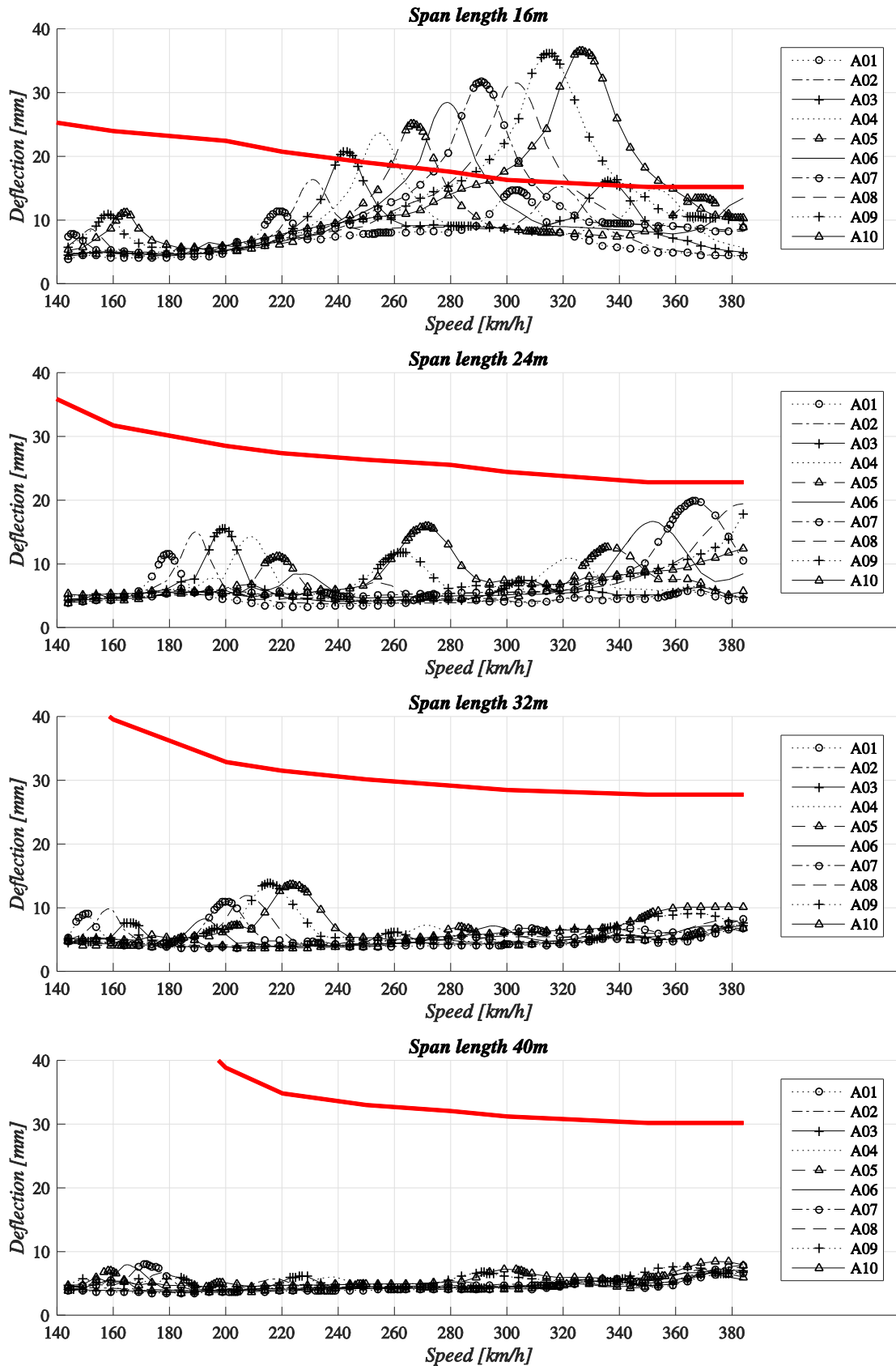
Figure 5.32   Maximum vertical deflections of the four considered span lengths for the continuous two-span bridge. The horizontal line represent the maximum limit corresponding to a very good level of comfort.

5.5.2 Dynamic response of a two-span continuous bridge with a fixed column as mid-support

In order to evaluate the effects on the dynamic response of using a fixed column as mid-support, the two-span bridge with spans of 24 meters was considered. The dynamic properties are presented in Table 5.9 and the first six vertical bending mode shapes are shown in Figure 5.33. The first frequency was slightly increased in comparison to the continuous simply supported case whereas the second frequency was basically the same. The fixed column in the centre of the bridge provided additional stiffness, thus preventing the bridge to deform as easily. Since the first mode included rotation over the mid-support, more energy was required than before in order to obtain the first mode. The second mode shape on the other hand did not include any significant movement over the mid-support, which is why the corresponding frequency had not changed. However, the third mode shape was not similar to the simply supported case. This mode was similar to the first one but without the rotation of the deck over mid-support.

Table 5.9   Dynamic properties of a two-span continuous slab bridge with a fixed column in the middle.

Span length [m]	Bending stiffness [GNm²]	Bridge mass [ton/m]	Mass of end shields [ton]	1st bending frequency [Hz]	2nd bending frequency [Hz]	3rd bending frequency [Hz]
24	34.29	30.92	175.16	2.880	4.244	5.561
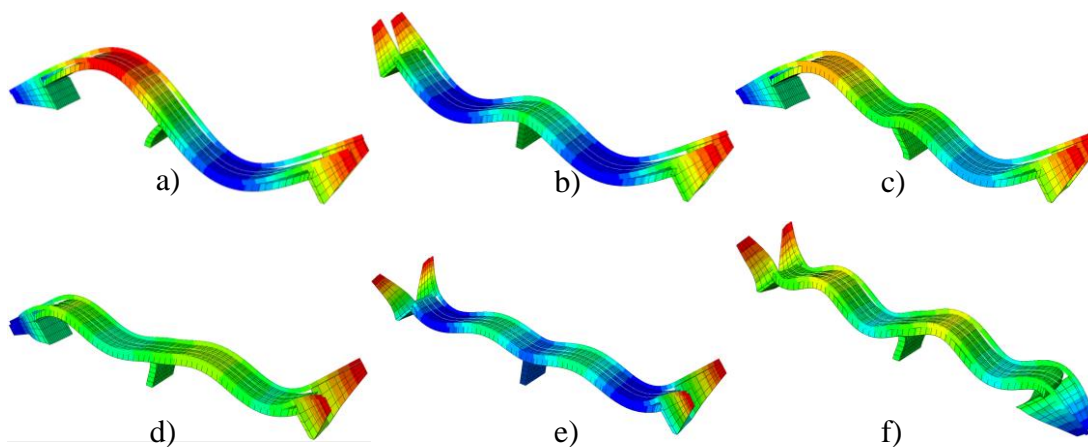
Figure 5.33   The first six vertical bending mode shapes of the two-span continuous slab bridge with a fixed column in the middle.

The dynamic response of this case is presented as maximum accelerations and deflections in Figure 5.34. The dynamic behaviour was dominated by the first two modes and since the corresponding frequencies were similar to the simply supported case, the resonance peaks occurred at similar train speeds. The response from the second mode resulted in highest accelerations once again and the maximum values were basically the same as before due to the fact that the fixation of the mid-support did not change the second mode. The response from the first mode however, was reduced and the peak accelerations were just below the limit of 3.5 m/s². The reason was that the column prevented the deck from deforming as easily as for the simply supported case, hence reducing the response. This was also true for the deflections, where the resonance peaks were decreased as well.
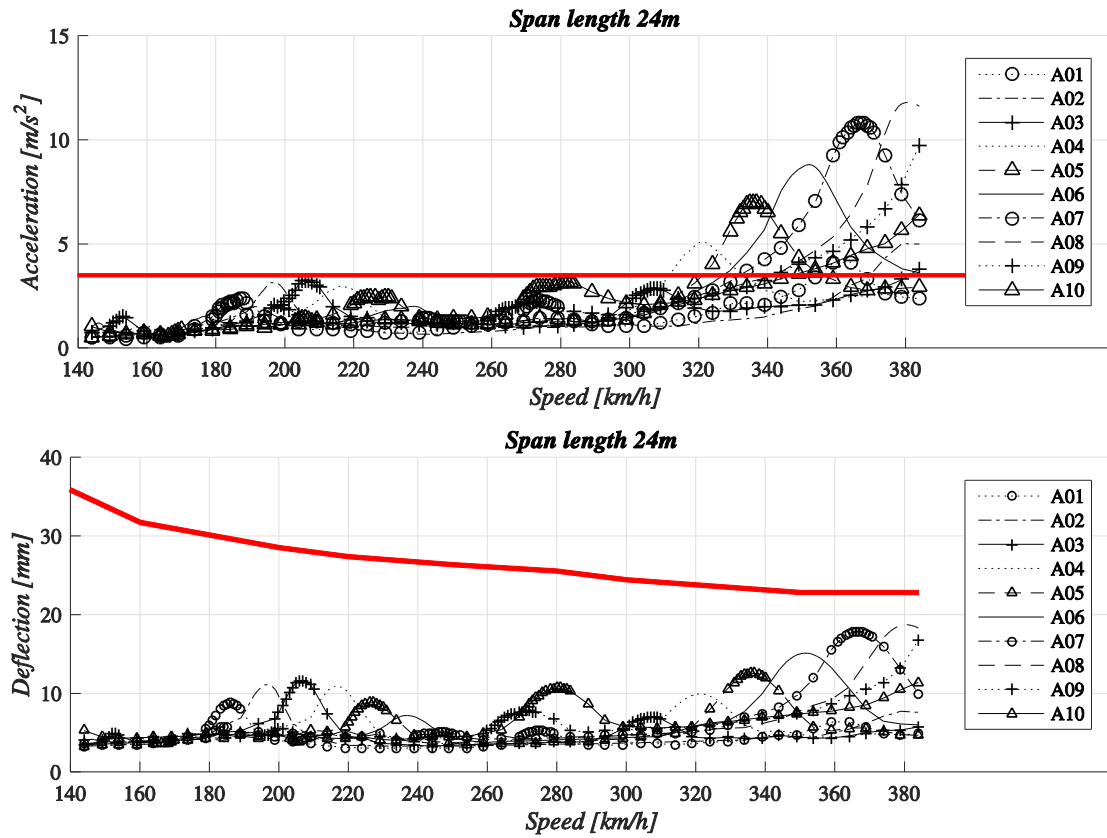
Figure 5.34   Maximum vertical accelerations and deflections of the continuous 24 meter two-span bridge with fixed column as mid-support. The horizontal lines represent the maximum allowable limits from Eurocode.

5.6 Three-span continuous concrete slab bridge

The following section includes the result of the dynamic analysis of the three-span continuous concrete slab bridge, based on the same cross-sections as the single span slab bridge. The applied load was the HSLM-A load model from Eurocode 1, SS-EN 1991-2 (CEN, 2003), defined in Figure 3.15 and Table 3.1.

5.6.1 Dynamic response of different span lengths

Equal span lengths were considered when evaluating the dynamic behaviour of three-span continuous bridges. The span lengths were the same as before, i.e. 16, 24, 32 and 40 meters and the dynamic properties for each bridge are presented in Table 5.10. The same cross-sections as the single span and two span bridges were used which means that the stiffness and mass per meter were still the same. The fundamental frequencies have been increased in comparison to the two-span case whereas the higher frequencies have decreased. The bridges with three spans have more vibration modes within the considered frequency range and consequently, the higher frequencies occurred closer to the first one. The first six vertical bending mode shapes of the bridge with 24 meter spans are illustrated in Figure 5.34.

Table 5.10   Dynamic properties of the four considered span lengths for the three-span continuous slab bridge.

Span length [m]	Bending stiffness [GNm^2]	Bridge mass [ton/m]	Mass of end shields [ton]	1st bending frequency [Hz]	2nd bending frequency [Hz]	3rd bending frequency [Hz]
16	8.92	21.45	159.55	3.534	4.109	6.122
24	34.29	30.92	175.16	2.815	3.524	5.187
32	99.07	41.35	192.36	2.335	2.968	4.335
40	233.10	52.86	211.32	2.023	2.583	3.758
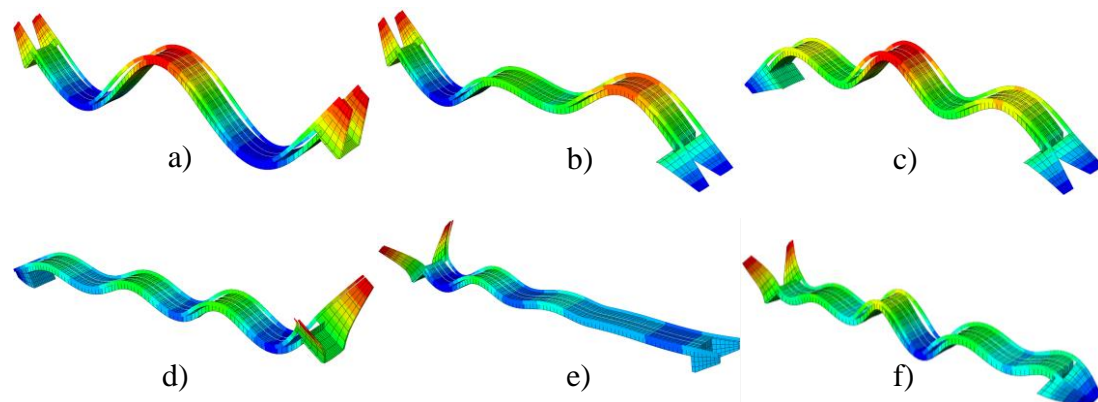
Figure 5.35   The first six principal vertical bending mode shapes of the three-span continuous slab bridge.

The maximum vertical accelerations are presented in Figure 5.36 and the maximum vertical deflections are presented in Figure 5.37. The maximum response occurred in either one of the end spans or the mid-span depending on what mode that was most influential for a certain speed. The bridge with 16 meter spans resulted in the highest accelerations and the behaviour was dominated by the first two mode shapes. For the

first seven HSLM trains, the second mode resulted in the highest accelerations whereas the three longest HSLM trains gave higher response from the first mode.

The first mode shape was less influential for the longer bridges as more axle loads excited the bridge simultaneously and thus limiting the magnitude of the resonance peaks. The two bridges with span lengths of 24 and 32 meters obtained the highest accelerations from the second mode shape for HSLM-A10. The resonance peaks of the bridge with 32 meter spans within the speed range 350-384 km/h arose from the third mode shape. The response of the longest bridge was well below the permissible limit and the peak accelerations occurred for HSLM-A3 when the loading frequency coincided with the third vertical bending frequency.

As can be observed, there were different mode shapes and trains resulting in the highest response for different span lengths. This was due to the fact that the response was cancelled out for some cases and for others the response was maximized. Since the higher frequencies were lower for a higher number of spans, the response was influenced by more mode shapes.

In the deflection diagrams of Figure 5.37, the allowable limit was exceeded for the two shortest bridges and the response was determined by the first two mode shapes. The third mode resulted in the highest peak accelerations for the 40 meter span bridge but it was not affecting the deflections since its vibrating magnitude was very low.
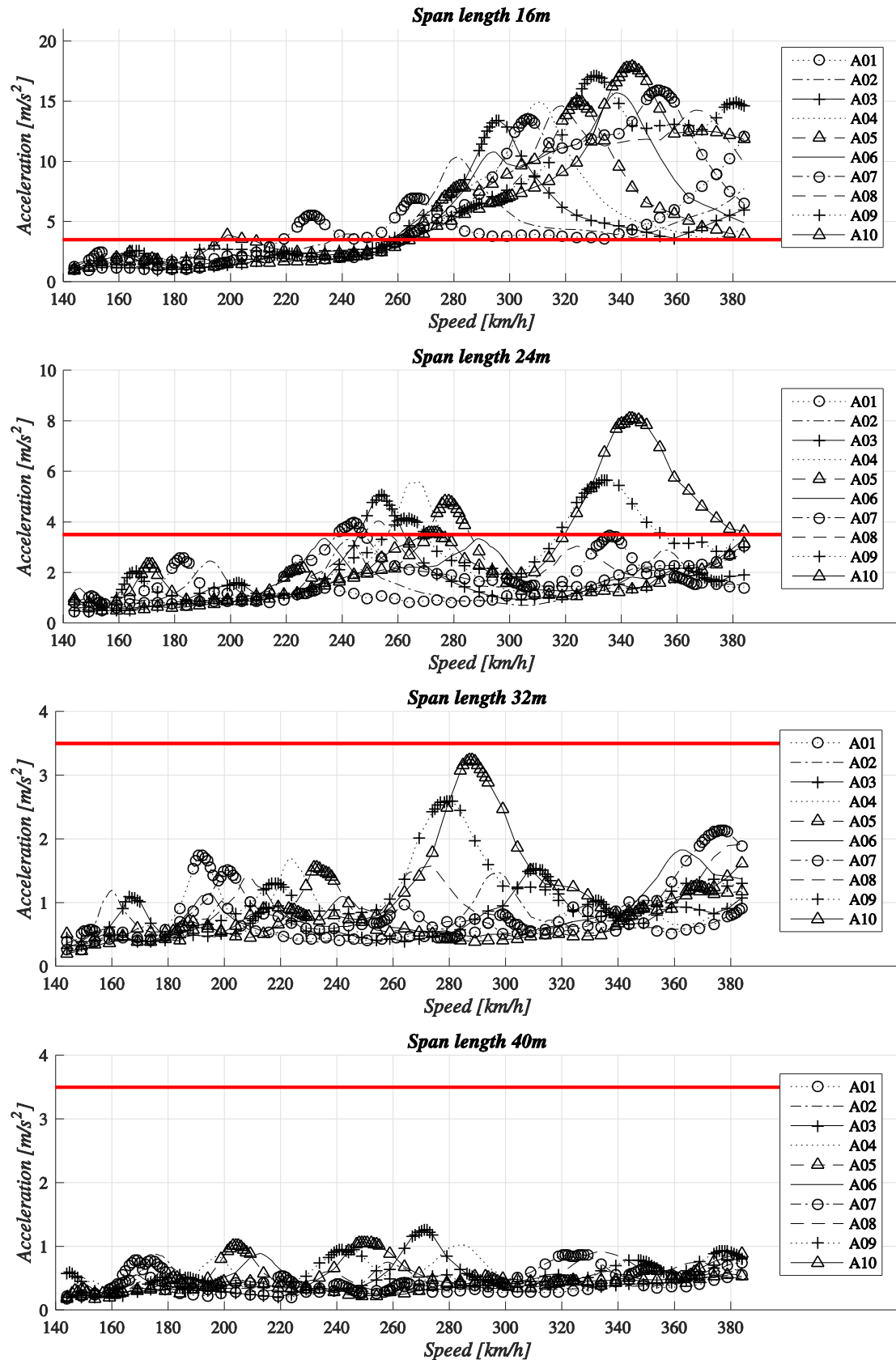
*Figure 5.36   Maximum vertical accelerations of the four considered span lengths
for the continuous three-span bridge. Note that the scale of the y-axis
differs. The horizontal line represents the maximum allowable
acceleration limit according to Eurocode.*
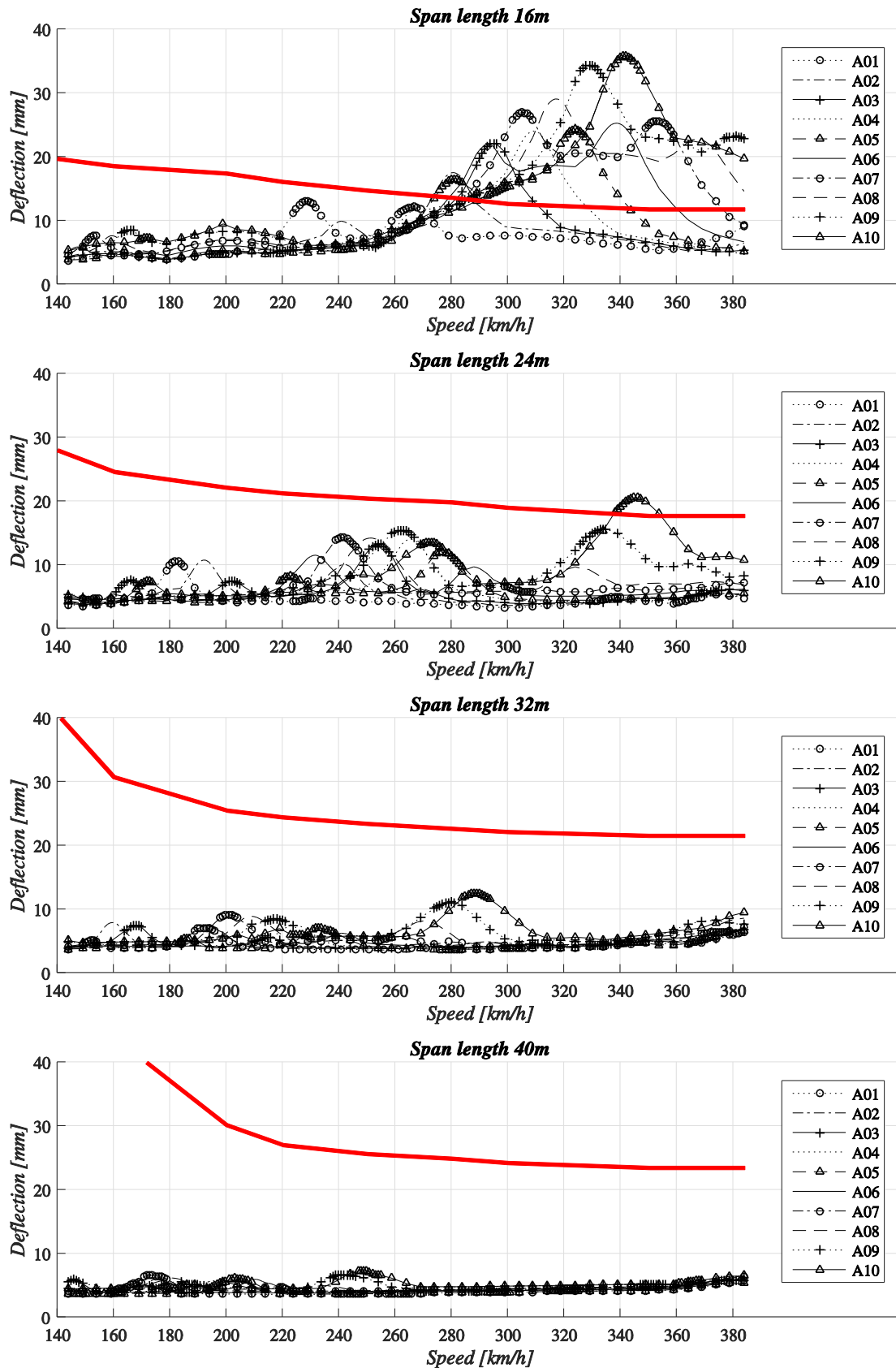
Figure 5.37   Maximum vertical deflections of the four considered span lengths for the continuous three-span bridge. The horizontal line represent the maximum limit corresponding to a very good level of comfort.

5.6.2 Dynamic response of a three-span continuous bridge with fixed columns as mid-supports

As for the two-span continuous bridge with a span length of 24 meters, the three-span case was modelled with fixed column as mid-supports in order to evaluate how the dynamic response would change. The dynamic properties of the model is presented in Table 5.11 and the first six vertical bending mode shapes are illustrated in Figure 5.38. The first natural frequency had increased in comparison with the three-span simply supported case. The first mode from the simply supported case were no longer present, instead the first mode for this bridge was similar to the second mode of the simply supported case. As a consequence, the first natural frequency for this bridge was similar to the second frequency of the simply supported case. The second and third frequencies have been increased as well and their mode shapes were quite different from the previous case.

Table 5.11   Dynamic properties of a three-span continuous slab bridge with fixed columns in the middle.

Span length [m]	Bending stiffness [GNm^2]	Bridge mass [ton/m]	Mass of end shields [ton]	1st bending frequency [Hz]	2nd bending frequency [Hz]	3rd bending frequency [Hz]
24	34.29	30.92	175.16	3.540	3.952	5.865

a)   b)   c)

d)   e)   f)
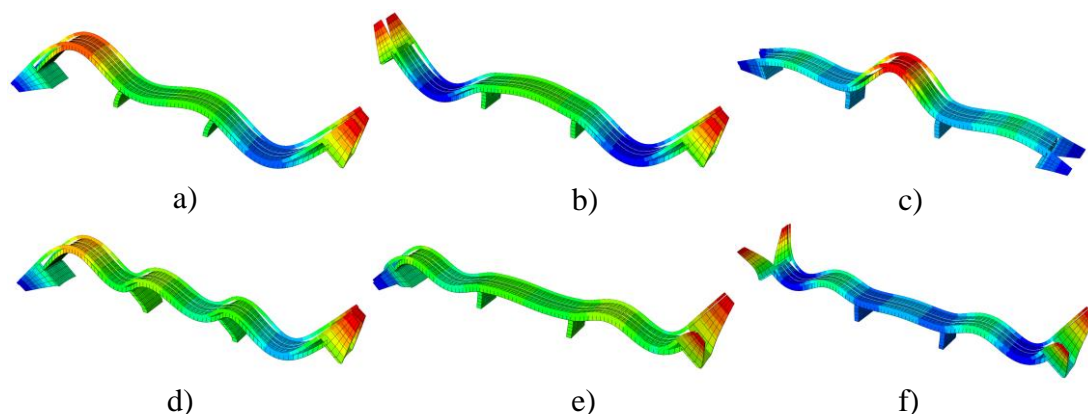
Figure 5.38   The first six vertical bending mode shapes of the three-span continuous slab bridge with fixed columns in the middle.

The dynamic response of the bridge is plotted in Figure 5.39 and the accelerations were higher than for the continuous simply supported case. Since the mode shapes were changed significantly when providing the bridge with fixed columns as mid-supports, the response was very different from the simply supported case. The deflections showed maximum peaks slightly above the allowable limit and the values were similar to the simply supported bridge.
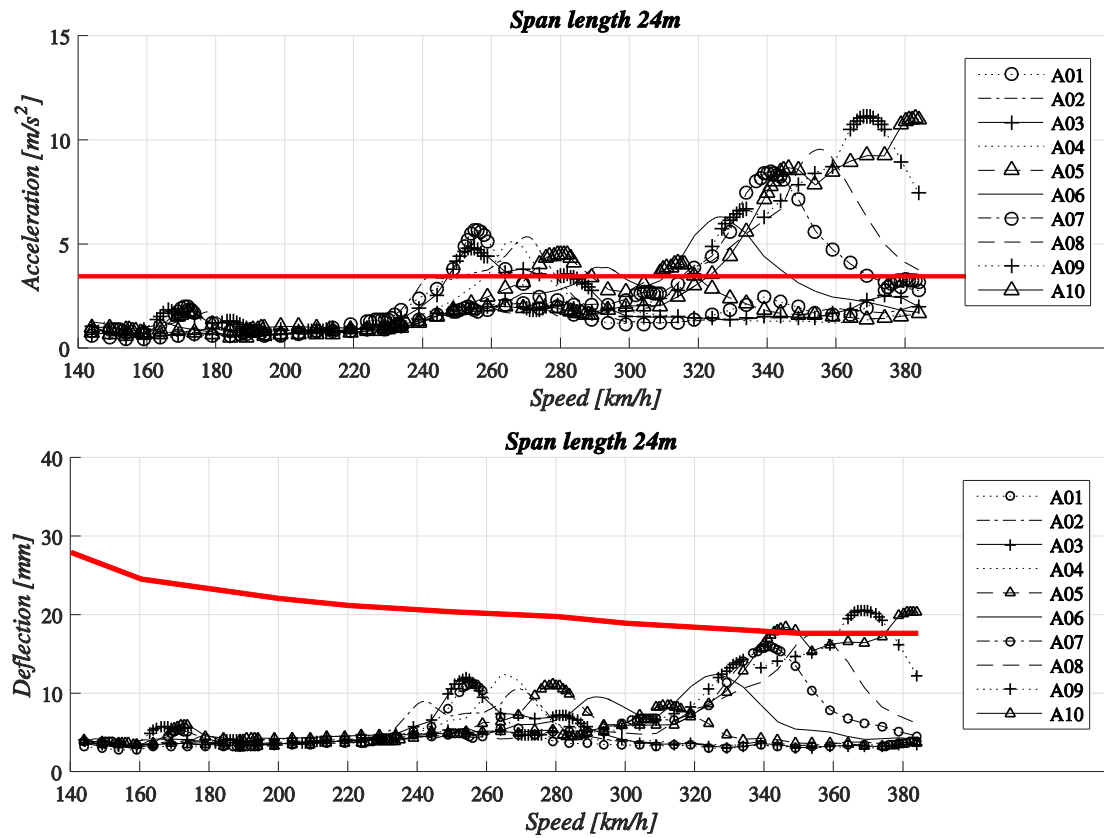
Figure 5.39   Maximum vertical accelerations and deflections of the continuous 24 meter three-span bridge with fixed columns as mid-supports. The horizontal lines represent the maximum allowable limits from Eurocode.

6   Discussion

This chapter includes a discussion with regard to the modelling choices adopted in this thesis study. Moreover, the obtained results will be reviewed and related to similar studies in order to distinguish similarities and dissimilarities. Finally, some bridge types that might be suitable for high-speed applications will be discussed.

6.1   FE-modelling

The FE-analyses in this study was carried out using the commercial software Brigade/Plus. The FE-models of the less complex studies, i.e. the simply supported cases without considering the end shields, were verified with hand calculations. Static deflections from deadweight and the first three vertical bending frequencies were compared. In addition, vertical accelerations and deflections of the bridge when subjected to a single moving point load were compared with an analytical solution. The moving point load study was performed initially in order to better understand the dynamic behaviour but also to provide a simple verification of the dynamic behaviour of the bridge. There are more complex analytical methods that includes a series of moving point loads, which would represent a moving train in a more accurate way. But due to the limited amount of time, a simple case with a single moving point load was considered to be sufficient. In order to ensure convergence of the FE-models, a convergence study was performed where the first three natural frequencies were analysed.

The analysed bridges in this study was generated from two existing reinforced concrete bridges. The real span length of the slab bridge (24 meters) was included as one of the considered lengths whereas the real span length of the trough bridge (29 meters) was not included. The cross-sections for the remaining span lengths was adjusted in order to obtain reasonable cross-sections in term of static load effects. However, one can argue that the longest bridges in this study obtained quite inefficient designs. The slab bridge with a deck thickness of 2641 mm solid concrete and the trough bridge with its large main beams of 3823 x 1684 mm. These cross-sections were required in order to obtain the same ratio between the static deflection and the span length, which was set as a requirement for the adjusted cross-sections. The use of reinforced concrete for span lengths of 40 meters are rare and a typical choice would be to utilize other bridge types instead, such as prestressed concrete and steel-composite bridges. Nonetheless, the aim of this thesis was not to assess existing bridges but rather to understand the influence of certain parameters regarding the dynamic behaviour. Even if the design of the longer bridges was questionable, they provided the study with certain dynamic properties that resulted in a certain dynamic response, which could be evaluated and reconnected to the design. The reason that the analysed cross-sections and span lengths were generated from the same two bridges, rather than choosing unique bridges, was to limit the number of parameters influencing the response. Small structural dissimilarities may influence the mode shape to a great extent, hence making it more difficult to compare the different span lengths.

The FE-models were carried out using 3D-elements, thus including the transverse behaviour of the bridges. Consequently, torsional and lateral bending mode shapes were included in the frequency analyses but these modes did not influence the results since the train loads were applied centrically. However, the transverse bending of the

deck did also affect the vertical bending modes since transverse deflections were included in addition to the longitudinal bending. This was found to have a great impact on the dynamic response of the simply supported trough bridge due to its relatively thin deck and long transvers distance between supports. The corresponding mode shapes of this bridge type included a number of modes with high frequencies where a major part of the deformations occurred in the edge of the short end of the bridge deck. As a result, high accelerations were obtained in the short end due to a transient response from the axle loads, especially for the shortest span lengths of 16 and 24 meters.

In accordance with Eurocode 1, SS-EN 1991-2 (CEN, 2003), the designer of a railway bridge for high-speed applications are encouraged to use a lower bound of the stiffness of the structure. For reinforced concrete bridges a conservative approach is to reduce the concrete stiffness with 40 % in order to account for a fully cracked section. This method have been used throughout the analyses in this thesis. However, if the designer can verify that a higher stiffness is more reasonable, that value may be used as well. The choice of stiffness will highly influence the results as have been mentioned earlier and it is important to use a realistic value. A situation which enables to account for an uncracked section is for prestressed sections.

6.2 Dynamic response

The first step of the analyses was to provide the reader with clear indications of how mass, stiffness and damping influenced the dynamic response of the bridges. This was not a unique study and many reports have covered this topic before. The outcome of the results was as expected with the mass changing the natural frequencies as well as the peak accelerations, but without affecting the deflections. The stiffness did only affect the natural frequencies and deflection peaks, but the accelerations were left unchanged. Increased damping was found to reduce the response in terms of both accelerations and deflections.

The results from the dynamic analyses with regard to different span lengths indicated that the bridges with a 16 meter span were inadequate in terms of dynamic performance. Because of their low fundamental natural frequencies, the primary resonance peaks from the HSLM trains appeared within the considered speed range. The response from these peaks caused very high accelerations and deflections with peak values well beyond the allowable limits stated in Eurocode. This was true for both the simply supported single span cases and the continuous bridges.

The bridges with span length 24 meters did also result in high accelerations for all studied cases. However, the deflection limits were only exceeded for the simply supported single span cases. The 32 meter span lengths resulted in accelerations slightly above the permissible limit for the single span cases while the continuous bridges showed satisfactory results. All bridges with a span length of 40 meters resulted in good dynamic behaviour both for accelerations and for deflections.

In general, the acceleration limit were exceeded more often than the deflection limit. The reinforced concrete trough bridge was found to be a better solution for shorter spans, mainly due to a much stiffer cross-section with higher mass. The deflection limit was only somewhat exceeded for the 16 meter bridge whereas the longer bridges were satisfactory. The differences between the slab bridges and the trough bridges were less significant for the longer spans.

The influence of providing the bridges with end shields was studied for the single span cases and the results have shown that the maximum accelerations were reduced substantially for the 16 meter span bridges, especially for the trough bridge. The main reason for the reduced response was found to be the mass contribution from the end shields, which was more significant for the shortest bridge. The additional mass gets less influential for the longer bridges and the difference in response was lower for them. In addition to the mass contribution, the end shields provided transverse stiffness to the thin bridge deck of the trough bridge. Consequently, the impact of the end shields was even higher for this bridge since the excessive vibrations in the short end of the bridge disappeared.

The evaluation of continuity in this study included two- and three-span bridges with identical span lengths. The FE-models were generated from the single span case of the slab bridge, thus the same cross-section were considered as for that case. Simply supported boundary conditions were considered and the influence of a fixed column as mid-support was evaluated for the 24 meter span bridges. The results have shown that the dynamic response got somewhat more complex due to the fact that more axle loads excited the bridge simultaneously. As a consequence, the different HSLM trains affected different mode shapes and more resonance peaks occurred within the considered speed range. The maximum accelerations were found to be increased for the 16 meter spans in comparison to the single span slab bridge whereas lower response was obtained for the longest bridges. The dynamic deflections on the other hand, were observed to be lower for all considered spans than for the single span case.

When considering fixed mid-supports for the continuous bridges with span length of 24 meters, the response became quite different. For the two-span case, the response from the first mode shape was reduced whereas the response from the second mode was pretty much unchanged. This was found to be highly associated with the mode shapes, where the first was somewhat different but the second was basically the same. The mode shapes of the three-span bridge were more affected by the fixed columns and the change in response was quite significant with higher maximum peak values than for the simply supported three-span case.

The outcome of the comparison between different span lengths was in line with results from previous studies, where it was concluded that the dynamic response was reduced for longer spans, see Section 3.2.4. The result from this study clearly indicates the same principle and the response was always found to be lower for longer spans. Moreover, the response of the continuous bridges in this study confirms what was stated in Section 3.2.4, that the accelerations of short span continuous bridges with low natural frequencies might be higher in comparison to single span bridges. However, in previous studies concerning the influence of end shields it has been concluded that the dynamic response was increased by providing the bridges with end shields. These previous studies were carried out in a simplified manner by considering 2D-models and by including the end shields as an additional mass at the ends of the bridges. According to the results in this thesis, the influence of end shields have been proven to enhance the dynamic performance and reduce the vertical accelerations. By accounting for the transverse effects in more detailed 3D-analyses, the end shields provided additional stiffness at the short ends and thus eliminating some mode shapes that caused excessive vibrations. In addition, they provided an important mass contribution for short span bridges that reduced the response significantly.

Another aspect that has been studied in this report is the influence of load distribution, meaning that the axle loads were distributed over three sleepers. According to

Eurocode 1, SS-EN 1991-2 (CEN, 2003), the influence of load distribution may be accounted for whenever loaded lengths of less than 10 meters are considered since the dynamic effects can be overestimated otherwise. The effects of load distribution was evaluated for the single span cases and due to the statement in Eurocode, which said that load distribution should be considered for loaded lengths of less than 10 meters, the difference was expected to be high for the end shield bridges. However, the response was found to be very similar for the slab bridge whether the end shields were considered or not. For the trough bridge without end shields on the other hand, the consideration of load distribution resulted in quite large differences, especially in the regions outside of resonance. The reason was found to be that the transient response, which was induced in the short edges of the thin bridge deck, increased when the axle loads were taken as single point loads. If the interpretation of the Eurocode statement would have been followed, the load distribution would not have been considered for the trough bridge since all of the loaded lengths were longer than 10 meters. Therefore, it might be appropriate to adopt load distribution models in other cases as well in order to avoid overestimations of the response.

The span to coach length ratio has proven to be a very important factor for the dynamic response. Depending on the ratio, the response may be either very high or completely suppressed. Whenever the resonance peaks have been suppressed in the diagrams from the different bridge analyses, the span to coach length ratio has corresponded very well to the values discussed in Section 3.1.1. Since the dynamic analyses included the ten HSLM trains with varying lengths from Eurocode, there were always certain trains with clear resonance peaks even though the response from some of the trains were suppressed. If it was known or decided in advance what type of high-speed train that would use the railway bridges, a very efficient structure could be obtained in terms of dynamic performance. By knowing the coach length of the train, different optimal span lengths could be chosen in order to supress the response from that certain train. However, the HSLM load model is required in the analyses whenever European interoperability is stated as a demand, which it is for the planned Swedish high-speed network.

In addition to the coach length property of the trains, the speed at which it crosses the bridges have shown to be highly influential for the dynamic response. The speed interval that has to be considered for a railway bridge with an intended speed of 320 km/h is quite wide. As a consequence, the risk of high levels of vibration at some train speeds are substantial, especially for short span bridges. The stiffness needs to be high in order to move the primary resonance peaks outside of the considered speed range. If a certain speed range could be avoided it would lead to a less redundant structure, which would be desirable in an economical point of view. Nonetheless, the railway bridges should be able to handle all possible train speeds as it is difficult to ensure that certain speeds could be completely avoided.

It should be noted that the studied dynamic effects in this report were chosen to be vertical accelerations and vertical deflection. However, as stated in Section 3.4.2.3, there are additional dynamic effects that needs to be satisfied in order to fulfil all the requirements.

6.3 Bridge types for high-speed applications

According to the obtained results from this study, short span bridges with low natural frequency have shown to be sensitive to dynamic effects in terms of vertical accelerations and deflections. An improved design of the 16 meter simply supported trough bridge with end shields was carried out and analysed. The stiffness of the cross-section was increased significantly in order to move the primary resonance peaks outside of the considered speed range. This was achieved for a fundamental frequency of 6.394 Hz and the response was instead determined by the second resonance speed, with peak values below the required limits. Short span bridges have been found to obtain high levels of vibration due to the primary resonance, which is why a sufficiently stiff cross-section is necessary in order to move these peaks to higher train speeds. Nonetheless, this requires that the maximum peaks of the second resonance speed are within the allowable limit since they will then determine the response. The continuous bridges could also benefit from a stiffer cross-section in order to enhance the dynamic performance. As described in Section 3.2.4, continuous bridges with natural frequencies within the given limits of Figure 3.15 from Eurocode, resulted generally in an adequate dynamic response.

The mass may also be modified in order to obtain a better dynamic behaviour. However, this would not be a suitable option for the short span bridges in this study since the peak values were well beyond the permissible limit and an unreasonable increase of the mass would be necessary in order reduce the response that much. For the simply supported 32 meter span bridges on the other hand, this might have been a suitable option since the acceleration limit were only slightly exceeded for this span length. The mass could be increased by using a thicker ballast layer or increasing the deck thickness for instance.

Another approach to enhance the dynamic performance of a bridge, would be to provide the bridges with dampers. These can effectively reduce the response from certain natural frequencies. By letting the dampers reduce the influence of the first vertical bending mode, which is typically causing the critical response, the dynamic behaviour of the bridge would be much more satisfying. As a result, a less redundant structure could be adequate in terms of dynamic performance if dampers are applied. However, these requires maintenance during the life time of the bridge which might be costly. Furthermore, the stiffness of the bridge is difficult to predict and thus the real natural frequencies might be different from the calculated values. In order to calibrate the dampers for the correct frequency, real tests of the bridges would be necessary. Moreover, the stiffness might change with time due to cracking and creep and hence the natural frequencies will change. Regular inspections would be necessary in order to ensure that the dampers are calibrated for the critical frequencies.

In conclusion, a stiff bridge design is desirable in order to move the primary resonance speeds outside of the considered speed range. A lot of the bridges in existing high-speed railway networks compose of prestressed concrete box girders, which was discussed in Section 3.3. The stiffness of such sections are high and the prestressing enables to account for an uncracked section, which will increase the stiffness even more in the dynamic analysis. This have proven to be a suitable solution for high-speed applications and dynamic analyses have been carried out in the design phase to verify this. The steel-concrete composite bridges that are widely used in the French high-speed network could be a suitable alternative for continuous

bridges with long span lengths since they provide an efficient structure in such situations. However, the dynamic behaviour of steel-composite bridges have indicated critical accelerations in previous studies for simply supported bridges and in such situations it might be more suitable to utilize other bridge types.

According to the technical system standard for high speed tracks (Swedish Transport Administration, 2016), bridges provided with end shields are not recommended since these might result in excessive vibrations. The result from this thesis however, have obtained a better dynamic behaviour for this bridge type in comparison to the case without end shields. This was found to be especially true for bridges with low transverse stiffness, which may obtain high accelerations in the ends of the bridge.

The substructure of high-speed railway lines are composed of either ballasted tracks or ballastless tracks. The ballastless track have been found to be a suitable choice for high-speed applications since these provide low maintenance and higher precision of the track alignment. From a structural point of view the major difference between these two alternatives is the mass contribution, which is higher for the ballasted track. The result will be reduced acceleration peaks at lower train speeds. However, the allowable acceleration limit is higher for the ballastless track which is of course an advantage. The choice to use either ballast or slabs in the substructure will be more influential for steel and steel-concrete solutions since these already have quite low mass. The effect on a concrete structure would be less significant as they are already heavy structures.

7   Conclusions

The aim of this Master's Thesis was to increase the basic understanding of the dynamic behaviour of railway bridges subjected to high-speed trains. Furthermore, the purpose was also to be able to describe for engineers and non-specialists what parameters are the most influential when designing railway bridges subjected to high-speed trains. With regard to the results from this study, the following concluding remarks can be obtained from the studied railway bridges:

- The mass had a high influence of the dynamic response. An increased mass resulted in reduced accelerations at lower train speed whereas the deflection peaks were unaffected but occurred at lower train speed.

- The stiffness had a great impact on the dynamic behaviour and a higher stiffness resulted in lower deflections at higher train speed. The acceleration peaks were unchanged but they appeared at higher train speed.

- Another very important parameter for the dynamic response was the damping. Higher damping coefficient reduced the response for both accelerations and for deflections.

- The ratio between the span length and the distance between axle loads had a high impact on the dynamic behaviour. For trains with ratios in the vicinity of 1.5 and 2.5, the response from first natural bending mode was effectively suppressed for the simply supported cases. The continuous bridges indicated similar behaviour with cancellation effects for certain ratios.

- Bridges with longer spans were found to enhance the dynamic performance, which was true for both the simply supported bridges and the continuous bridges

- The continuous bridges obtained low natural frequencies, resulting in high response from different mode shapes within the considered speed range. Hence, the response was determined by more mode shapes and when low peak values were obtained for one mode, another showed high response.

- By providing the continuous bridges with fixed columns as mid-support, the mode shapes were somewhat changed for the two-span case whereas it had even more influence on the three-span case. No general conclusion could be drawn of how the dynamic response will be affected with a rigid mid-support, more than that it may change the behaviour significantly.

- The influence of end shields was found to enhance the dynamic performance in comparison to the case when they were disregarded. The major reasons were related to the mass contribution from the end shields as well as the transverse stiffness contribution at the short ends.

- Load distribution affected the trough bridge without end shields substantially due to the influence of transversal bending and transient response in the ends. For bridges with stiffer ends, load distribution did not influence the response significantly.

8 References

Andersson, A. et al., 2011. *Höghastighetsprojekt - Bro: Inventering av järnvägsbroar för ökad hastighet på befintliga banor,* Stockholm: KTH Royale Institute of Technology.

Andersson, A. et al., 2010. *Höghastighetsprojekt - Bro - Delrapport 1: Befintliga krav och erfarenheter samt parameterstudier avseende dimensionering av järnvägsbroar för farter över 200 km/h,* Stockholm: KTH Royal Institue of Technology.

Arvidsson, T., 2014. *Train-Bridge Interaction: Literature Review and Parameter Screening,* Stockholm: KTH Royal Institue of Technology.

Arvidsson, T. & Karoumi, R., 2014. Train-bridge interaction - a review and discussion of key model parameters. *International Journal of Rail Transportation,* pp. 147-186.

Beygi, H., 2015. *Vibration Control of a High-Speed Railway Bridge Using Tuned Mass Dampers,* Stockholm: KTH Royal Institute of Technology.

Calcada, R., Delgado, R. & Compos e Matos, A., 2009. *Bridges for High-Speed Railways.* 1st ed. London: Taylor & Francis.

Calcada, R., Delgado, R., Gabaldón, F. & Goicolea, J. M., 2009. *Dynamics of High-Speed Railway Bridges.* 1st ed. London: Taylor & Francis Group.

Casal, H., Neves, M. & Proenca, J. M., 2011. *Effect of the type of track on the dynamic behaviour of high speed railway bridges,* Lisbon: ICIST/IST.

CEN, 2002. *Eurocode - Basis of structural design,* Brussels: European Committee for Standardization.

CEN, 2003. *Eurocode 1: Actions on structures - Part 2: Traffic loads on bridges,* Brussels: European Committee for Standardization.

Cho, J.-R.et al., 2016. Determination of the optimal span length to minimize resonance effects in bridges on high-speed lines. *Journal of Rail and Rapid Transit,* 230(2), pp. 334-344.

Craig Jr, R. & Kurdila, A., 2006. *Fundamentals of Structural Dynamics.* 2nd ed. Hoboken(New Jersey): John Wiley & Sons, Inc.

Dai, G.-L., Hu, N., Liu, K. & Yan, B., 2014. Recent development of design and construction of medium and long span high-speed railway bridges in China. *Engineering Structures,* Volume 74, pp. 233-241.

Dai, G.-L., Hu, N. & Yan, B., 2015. Recent development of design and construction of short span high-speed railway bridges in China. *Enginering Structures,* Volume 100, pp. 707-717.

Domínguez, J., Gabaldón, F., Goicola, J. & Navarro, J., 2009. *Dynamic loads in new engineering codes for railway bridges in europe and spain,* London: Taylor & Francis Group.

Domínguez, J., Galvín, P., Romero, A. & Solís, M., 2013. Soil-structure interaction in resonant railway bridges. *Soil Dynamics and Earthquake Engineering,* Volume 47, pp. 108-116.

ERRI, 1999. *Rail bridges for speed > 200 km/h,* Utrecht: European Rail Research Institute.

Esveld, C., 2001. *Modern Railway Track.* 2nd ed. Delft: MRT-Productions.

Europakorridoren AB, 2016. *Europakorridoren.* [Online]
Available at: http://europakorridoren.se/sv/5minuter/
[Accessed 18 May 2016].

Frýba, L., 1996. *Dynamics of Railway Bridges,* Prague: Thomas Thelford Services Ltd.

Gabaldón, F., Goicolea, J. M. & Riquelme, F., 2006. *Design issues for dynamics of high speed railway bridges,* Porto: International Association for Bridge Maintenance and Safety.

Karoumi, R. & Ülker-Kaustell, M., 2008. *Uppskattning av upplagsstyvheter och effekter av jord-bro interaktion genom dynamisk mätning - steg 1,* Stockholm: KTH Royal Institue of Technology.

Li, J. & Su, M., 1999. The resonant vibration for a simply supported girder bridge under high-speed trains. *Journal of Sound and Vibration,* 224(5), pp. 897-915.

Meng, D., Wang, P., Yi, Q. & Zhao, C., 2015. Application of polyurethane polymer and assistant rails to settling the abnormal vehicle-track dynamic effects in transition zone between ballastless and ballasted track. *Shock and Vibration,* Volume 2015, pp. 1-9.

Rådeström, S. & Tell, V., 2014. *Reduction of Vertical Acceleration in High-speed Railway Bridges Using Post-installed Viscous Dampers,* Stockholm: KTH Royal Institute of Technology.

Scanscot Technology, 2015. *Workshop 3 - Dynamic response of high-speed trains.* s.l.:Scanscot Technology.

Swedish Transport Administration, 2011. *TRVK Bro 11,* Borlänge: Swedish Transport Administration.

Swedish Transport Administration, 2016a. *BaTMan.* [Online]
Available at:
https://batman.vv.se/BaTMan/OperativFV/AF06_Objektinfo/06f_Visa_ObjInfoRitningar.aspx?Mode=Oversikt&WindowGuid=76064706-c4eb-447f-b82e-1cf5798aff76&Id=c90d26c1-405a-49f3-a3d7-e26b79075198
[Accessed 16 March 2016].

Swedish Transport Administration, 2016b. *BaTMan.* [Online]
Available at:
https://batman.vv.se/BaTMan/OperativFV/AF06_Objektinfo/06f_Visa_ObjInfoRitningar.aspx?Mode=Oversikt&WindowGuid=76064706-c4eb-447f-b82e-1cf5798aff76&Id=aea29841-e811-4ec2-bd39-dd84222ee68c
[Accessed 02 March 2016].

Swedish Transport Administration, 2016c. *BaTMan.* [Online]
Available at:
https://batman.vv.se/BaTMan/OperativFV/AF06_Objektinfo/06f_Visa_ObjInfoRitningar.aspx?Mode=Oversikt&WindowGuid=7c8fc094-d21f-4815-80ac-4cb3585bfb95&Id=9144e4d4-db16-4f0b-9567-2a4a384d28f2
[Accessed 4 April 2016].

Swedish Transport Administration, 2016. *Technical system standard for high-speed tracks,* Borlänge: Swedish Transport Administration.

UIC, 2015. *UIC.* [Online]
Available at: http://www.uic.org/High-Speed-History
[Accessed 19 May 2016].

Yang, Y., Yau, J. & Wu, Y., 2004. *Vehicle-Bridge Interaction Dynamics - With Applications to High-Speed Railways,* Singapore: World Scientific.

Yau, J.-D., 2001. Resonance of continuous bridges due to high speed trains. *Journal of Marine Science and Technology,* Volume 9, pp. 14-20.

Ülker-Kaustell, M., 2009. *Some aspects of the dynamic soil-structure interaction of portal frame bridge,* Stockholm: KTH Royal Institue of Technology.

Appendix A
Bridge over river Aspan

Bridge over the river Aspan

Input data

$h := 3600s$ $ton := 1000kg$

Material properties

$E := 21GPa$

Reduced Young's modulus of concrete C40/50 to account for a cracked section

$\rho_c := 2500 \dfrac{kg}{m^3}$

Density of concrete

$\rho_b := 2000 \dfrac{kg}{m^3}$

Density of ballast

$m_{rail} := 60 \dfrac{kg}{m}$

Mass of UIC60 rail per meter

$m_{sl} := 245kg$

Mass of a single sleeper

Geometry
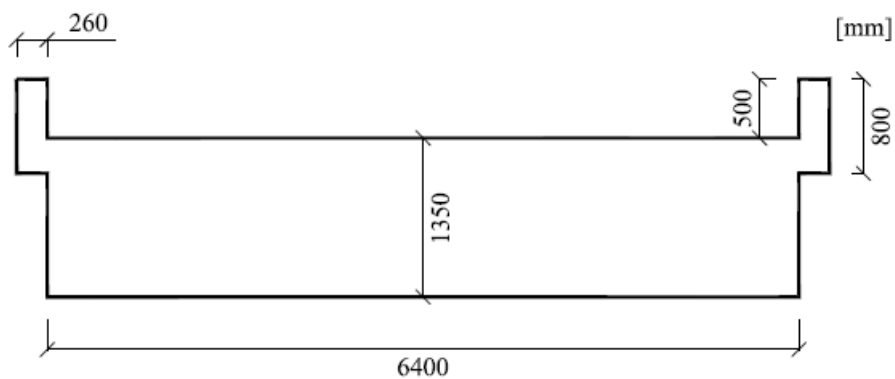
Cross-section:

$L := 24m$

Length of span

$b_{eb} := 260mm$

Width of edge beams

$h_{eb} := 800mm$

Height of edge beam

$b_{deck} := 6800mm$

Width of bridge deck

$h_{deck} := 1350mm$

Thickness of bridge deck

$A_{eb} := b_{eb} \cdot h_{eb} = 0.2\,m^2$

Cross-sectional area of edge beam

$A_{deck} := b_{deck} \cdot h_{deck} = 9.2\,m^2$

Cross-sectional area of bridge deck

$$A := 2 \cdot A_{eb} + A_{deck} = 9.6\,m^2 \qquad \text{Total area of bridge cross-section}$$

$$h_b := 0.5m \qquad \text{Height of ballast layer}$$

$$b_b := b_{deck} = 6.8\,m \qquad \text{Width of ballast layer}$$

$$s_{sl} := 0.6m \qquad \text{Spacing of sleepers}$$

Calcualting the centre of gravity z_{cog} of the cross-section:

$$z_{cog} := \frac{2A_{eb} \cdot \left(\dfrac{h_{eb}}{2} + h_{deck} - 300mm \right) + A_{deck} \cdot \dfrac{h_{deck}}{2}}{2A_{eb} + A_{deck}} = 708.6 \cdot mm$$

Moment of inertia of the cross-section:

$$I_{deck} := \frac{b_{deck} \cdot h_{deck}^3}{12} + A_{deck} \cdot \left(z_{cog} - \frac{h_{deck}}{2} \right)^2 = 1.4\,m^4$$

$$I_{eb} := 2 \cdot \left[\frac{b_{eb} \cdot h_{eb}^3}{12} + A_{eb} \cdot \left[z_{cog} - \left(\frac{h_{eb}}{2} + h_{deck} - 300mm \right) \right]^2 \right] = 0.3\,m^4$$

$$I := I_{deck} + I_{eb} = 1.655\,m^4$$

$$EI := E \cdot I = 34.76 \cdot GN \cdot m^2 \qquad \text{Bending stiffness of the bridge}$$

Permanent loads

$$g_{bridge} := A \cdot \rho_c \cdot g = 235.3 \cdot \frac{kN}{m} \qquad \text{Self-weight of the bridge}$$

$$g_b := \rho_b \cdot h_b \cdot b_b \cdot g = 66.7 \cdot \frac{kN}{m} \qquad \text{Self-weight of ballast}$$

$$g_{track} := 2m_{rail} \cdot g = 1.2 \cdot \frac{kN}{m} \qquad \text{Self-weight of track}$$

$$g_{sl} := \frac{m_{sl}}{s_{sl}} \cdot g = 4 \cdot \frac{kN}{m} \qquad \text{Self-weight of sleepers}$$

Total self-weight of the bridge:

$$g_{tot} := g_{bridge} + g_b + g_{sl} + g_{track} = 307.128 \cdot \frac{kN}{m}$$

Static deflection due to self-weight:

$$\delta_s := \frac{5 \cdot \left(g_{tot}\right) \cdot L^4}{384EI} = 38.2 \cdot mm$$

Recalculation with new span lengths

The span lengths that will be considerd is 16 m, 20 m, 24 m, 28 m and 32 m.

$$L_{new} := 32m$$

As a consequence of the new span length, the cross-section is adjusted in order to obtain a resonable bridge configuration. The width of the deck remains the same while the thickness of the bridge deck is changed in relation to the span length. The adjustment is performed so that the ratio between the static deflection and span length is kept the same for the new span length as for the original one. The considered loads are self-weight of the bridge and train load model LM71 from Eurocode. No eccentricity is considered for the train load. Furthermore, the dimensions of the edge beams will be kept constant.

The thickness of the new deck are adjusted until the ratios between the static deflection are the same for both cases:

$$h_{new.deck} := 1.964m \qquad \text{Thickness of the new deck}$$

$$A_{new.deck} := h_{new.deck} \cdot b_{deck} = 13.4\,m^2 \qquad \text{Area of the new deck}$$

$$A_{new} := A_{new.deck} + 2 \cdot A_{eb} = 13.8\,m^2 \qquad \begin{array}{l} \text{Total area of new bridge} \\ \text{cross-section} \end{array}$$

Calculating the centre of gravity $z_{new.cog}$ of the new cross-section:

$$z_{new.cog} := \frac{2A_{eb} \cdot \left[\dfrac{h_{eb}}{2} + \left(h_{new.deck} - 300mm \right) \right] + A_{new.deck} \cdot \dfrac{h_{new.deck}}{2}}{A_{new}}$$

$$z_{new.cog} = 1.015\,m$$

Moment of inertia of the cross-section:

$$I_{new.deck} := \frac{b_{deck} \cdot h_{new.deck}^3}{12} + A_{new.deck} \cdot \left(z_{new.cog} - \frac{h_{new.deck}}{2} \right)^2$$

$$I_{new.eb} := 2 \cdot \left[\frac{b_{eb} \cdot h_{eb}^3}{12} + A_{eb} \cdot \left[z_{new.cog} - \left[\frac{h_{eb}}{2} + \left(h_{new.deck} - 300mm \right) \right] \right]^2 \right]$$

$$I_{new} := I_{new.deck} + I_{new.eb} = 4.787\,m^4$$

$$EI_{new} := E \cdot I_{new} = 100.5 \cdot GN \cdot m^2 \qquad \text{Bending stiffness of the new bridg}$$

Total self-weight of the new bridge:

$$g_{new.tot} := A_{new} \cdot \rho_c \cdot g + g_{sl} + g_b + g_{track} = 409.5 \cdot \frac{kN}{m}$$

Static deflection analysis with permanent load and train load

The worst position of load model LM71 at the bridge is when one of the middle point loads are placed in the centre of the span.

$d_1 := 0.8\,\text{m}$	Distance between point loads
$d_2 := 1.6\,\text{m}$	Distance between point load and distributed load
$\alpha := 1.33$	Alpha factor according to TRVK Bro 11
$\psi_1 := 0.8$	Partial factor for SLS loads
$q_{vk} := 80\,\dfrac{\text{kN}}{\text{m}}$	Characteristic distributed load
$Q_{vk} := 250\,\text{kN}$	Characteristic point load
$q_{vd} := \alpha \cdot \psi_1 \cdot q_{vk} = 85.1 \cdot \dfrac{\text{kN}}{\text{m}}$	Distributed design load
$Q_{vd} := \alpha \cdot \psi_1 \cdot Q_{vk} = 266 \cdot \text{kN}$	Design point load

Calculating the static deflection of the original bridge design:

$a := \dfrac{L}{2} - 2 \cdot d_2 = 8.8\,\text{m}$	Distance where the left distributed load is acting
$b := \dfrac{L}{2} - d_2 = 10.4\,\text{m}$	Distance where the right distributed load is acting
$x := \dfrac{L}{2} = 12\,\text{m}$	Distance to centre of span

Deflection due to distributed train loads:

$$\delta_a := \frac{q_{vd} \cdot (a - d_1)^2}{24 \cdot EI \cdot L} \cdot (L - x)\left[-2x^2 + 4L \cdot x - (a - d_1)^2\right] = 2.6 \cdot mm$$

$$\delta_b := \frac{q_{vd} \cdot (b - d_1)^2}{24 \cdot EI \cdot L} \cdot (L - x)\left[-2x^2 + 4L \cdot x - (b - d_1)^2\right] = 3.6 \cdot mm$$

Deflection due to train point loads:

$$\delta_c := \frac{Q_{vd} \cdot L \cdot a \cdot (L - x)}{6 \cdot EI} \cdot \left(\frac{2x}{L} - \frac{a^2}{L^2} - \frac{x^2}{L^2}\right) = 2 \cdot mm$$

$$\delta_d := \frac{Q_{vd} \cdot L \cdot (a + d_2) \cdot (L - x)}{6 \cdot EI} \cdot \left[\frac{2x}{L} - \frac{(a + d_2)^2}{L^2} - \frac{x^2}{L^2}\right] = 2.1 \cdot mm$$

$$\delta_e := \frac{Q_{vd} \cdot L^3}{48EI} = 2.2 \cdot mm$$

$$\delta_f := \frac{Q_{vd} \cdot L \cdot b \cdot x}{6 \cdot EI} \cdot \left(1 - \frac{b^2}{L^2} - \frac{x^2}{L^2}\right) = 2.1 \cdot mm$$

Deflection due to permanent loads:

$$\delta_{s.g} := \frac{5 \cdot (g_{tot}) \cdot L^4}{384EI} = 38.2 \cdot mm$$

Total deflection due to permanent loads and train loads:

$$\delta_{tot} := \delta_a + \delta_b + \delta_c + \delta_d + \delta_e + \delta_f + \delta_{s.g} = 52.9 \cdot mm$$

Calculating the static deflection of the new bridge design:

$$a := \frac{L_{new}}{2} - 2 \cdot d_2 = 12.8\,m$$ Distance where the left distributed load is acting

$$b := \frac{L_{new}}{2} - d_2 = 14.4\,m$$ Distance where the right distributed load is acting

$$x := \frac{L_{new}}{2} = 16\,m$$ Distance to centre of span

Deflection due to distributed train loads:

$$\delta_{2.a} := \frac{q_{vd} \cdot (a - d_1)^2}{24 \cdot EI_{new} \cdot L_{new}} \cdot (L_{new} - x)\left[-2x^2 + 4L_{new} \cdot x - (a - d_1)^2 \right]$$

$$\delta_{2.a} = 3.5 \cdot mm$$

$$\delta_{2.b} := \frac{q_{vd} \cdot (b - d_1)^2}{24 \cdot EI_{new} \cdot L_{new}} \cdot (L_{new} - x)\left[-2x^2 + 4L_{new} \cdot x - (b - d_1)^2 \right]$$

$$\delta_{2.b} = 4.4 \cdot mm$$

Deflection due to train point loads:

$$\delta_{2.c} := \frac{Q_{vd} \cdot L_{new} \cdot a \cdot (L_{new} - x)}{6 \cdot EI_{new}} \cdot \left(\frac{2x}{L_{new}} - \frac{a^2}{L_{new}^2} - \frac{x^2}{L_{new}^2} \right)$$

$$\delta_{2.c} = 1.7 \cdot mm$$

$$\delta_{2.d} := \frac{Q_{vd} \cdot L_{new} \cdot (a + d_2) \cdot (L_{new} - x)}{6 \cdot EI_{new}} \cdot \left[\frac{2x}{L_{new}} - \frac{(a + d_2)^2}{L_{new}^2} - \frac{x^2}{L_{new}^2} \right]$$

$$\delta_{2.d} = 1.8 \cdot mm$$

$$\delta_{2.e} := \frac{Q_{vd} \cdot L_{new}^3}{48 EI_{new}} = 1.8 \cdot mm$$

$$\delta_{2.f} := \frac{Q_{vd} \cdot L_{new} \cdot b \cdot x}{6 \cdot EI_{new}} \cdot \left(1 - \frac{b^2}{L_{new}^2} - \frac{x^2}{L_{new}^2} \right) = 1.8 \cdot mm$$

Deflection due to permanent loads:

$$\delta_{s.g} := \frac{5 \cdot (g_{new.tot}) \cdot L_{new}^4}{384 EI_{new}} = 55.6 \cdot mm$$

Total deflection due to permanent loads and train loads:

$$\delta_{new.tot} := \delta_{2.a} + \delta_{2.b} + \delta_{2.c} + \delta_{2.d} + \delta_{2.e} + \delta_{2.f} + \delta_{s.g} = 70.6 \cdot mm$$

Deflection to span ratios:

Original bridge:

$$\frac{\delta_{tot}}{L} = 2.2039 \times 10^{-3}$$

New bridge:

$$\frac{\delta_{new.tot}}{L_{new}} = 2.2071 \times 10^{-3}$$

New bridge configurations:

The procedure above was performed for each span length of interest, resulting in the following deck heights:

$L_1 := 16\text{m}$ $h_{1.deck} := 792\text{mm}$

$L_3 := 24\text{m}$ $h_{3.deck} := 1350\text{mm}$

$L_5 := 32\text{m}$ $h_{5.deck} := 1964\text{mm}$

$L_6 := 40\text{m}$ $h_{6.deck} := 2641\text{mm}$

Eigenfrequencies

Calculating the natural frequencies of the bridge:

$n_{max} := 3$ Number of mode shapes

$n := 1 .. n_{max}$

$$m_{bridge} := \frac{g_{tot}}{g} = 31.3 \cdot \frac{\text{ton}}{\text{m}}$$ Total mass per meter of the bridge

$$\omega_n := \left(\frac{n \cdot \pi}{L}\right)^2 \cdot \sqrt{\frac{EI}{m_{bridge}}}$$

First three natural frequencies of the bridge:

$$\frac{\omega_n}{2 \cdot \pi} =$$

2.9	·Hz
11.5
25.9

Appendix B
Bridge over river Norrmjöleån

Bridge over the river Norrmjöleån

Input data

Material properties

$E := 20.4\,GPa$

Reduced Young's modulus of concrete C35/45 to account for a cracked section

$\rho_c := 2500\,\dfrac{kg}{m^3}$

Density of concrete

$\rho_b := 2000\,\dfrac{kg}{m^3}$

Density of ballast

$m_{rail} := 60\,\dfrac{kg}{m}$

Mass of UIC60 rail per meter

$m_{sl} := 245\,kg$

Mass of a single sleeper

Geometry
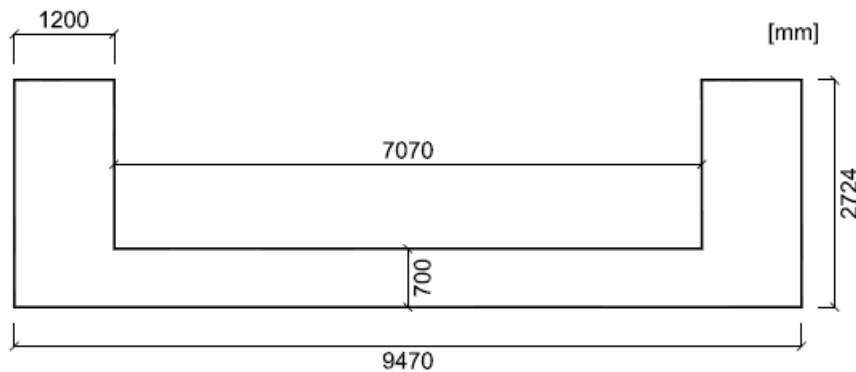
Cross-section:

$L := 29\,m$

Length of span

$b_{eb} := 1200\,mm$

Width of edge beams

$h_{eb} := 2724\,mm$

Height of edge beam

$b_{deck} := 7070\,mm$

Width of bridge deck

$h_{deck} := 700\,mm$

Thickness of bridge deck

$A_{eb} := b_{eb} \cdot h_{eb} = 3.3\,m^2$

Cross-sectional area of edge beam

$A_{deck} := b_{deck} \cdot h_{deck} = 4.9\,m^2$

Cross-sectional area of bridge deck

$A := 2 \cdot A_{eb} + A_{deck} = 11.5\,m^2$ Total area of bridge cross-section

$h_b := 0.5m$ Height of ballast layer

$b_b := b_{deck} = 7.1\,m$ Width of ballast layer

$s_{sl} := 0.6m$ Spacing of sleepers

Calcualting the centre of gravity z_{cog} of the cross-section:

$$z_{cog} := \frac{2A_{eb} \cdot \dfrac{h_{eb}}{2} + A_{deck} \cdot \dfrac{h_{deck}}{2}}{2A_{eb} + A_{deck}} = 0.926\,m$$

Moment of inertia of the cross-section:

$$I_{deck} := \frac{b_{deck} \cdot h_{deck}^3}{12} + A_{deck} \cdot \left(z_{cog} - \frac{h_{deck}}{2} \right)^2 = 1.8\,m^4$$

$$I_{eb} := 2 \cdot \left[\frac{b_{eb} \cdot h_{eb}^3}{12} + A_{eb} \cdot \left(z_{cog} - \frac{h_{eb}}{2} \right)^2 \right] = 5.3\,m^4$$

$$I := I_{deck} + I_{eb} = 7.129\,m^4$$

$EI := E \cdot I = 145.44 \cdot GN \cdot m^2$ Bending stiffness of the bridge

Permanent loads

$g_{bridge} := A \cdot \rho_c \cdot g = 281.6 \cdot \dfrac{kN}{m}$ Self-weight of the bridge

$g_b := \rho_b \cdot h_b \cdot b_b \cdot g = 69.3 \cdot \dfrac{kN}{m}$ Self-weight of ballast

$g_{track} := 2m_{rail} \cdot g = 1.2 \cdot \dfrac{kN}{m}$ Self-weight of track

$g_{sl} := \dfrac{m_{sl}}{s_{sl}} \cdot g = 4 \cdot \dfrac{kN}{m}$ Self-weight of sleepers

Total self-weight of the bridge:

$g_{tot} := g_{bridge} + g_b + g_{sl} + g_{track} = 356.1 \cdot \dfrac{kN}{m}$

Recalculation with new span length

The new span length to be considered is:

$$L_{new} := 24m$$

As a consequence of the new span length, the cross-section is adjusted in order to obtain a resonable bridge configuration. The thickness of the deck remains the same since it is already relativle thin. The width of the bridge deck is keeped the same as well.

The adjustment is performed so that the ratio between the static deflection and span length is kept the same for the new bridge as for the original one. The considered loads are self-weight of the bridge and train load model LM71 from Eurocode. No eccentricity is considered for the train load. Furthermore, the ratio between the width and height of the edge beams will remain the same for the new design.

$$r_{eb} := \frac{b_{eb}}{h_{eb}} = 0.4$$
Ratio between the width and height of the edge beams

The height of the new edge beams are adjusted until the ratios between the static deflection are the same for both cases:

$$h_{new.eb} := 2282mm$$
Height of new edge beams

$$b_{new.eb} := r_{eb} \cdot h_{new.eb} = 1.005\,m$$
Width of new edge beams

$$b_{new.eb} := 1005mm$$

$$A_{new.eb} := h_{new.eb} \cdot b_{new.eb} = 2.3\,m^2$$
Area of new edge beams

$$A_{new} := A_{deck} + 2 \cdot A_{new.eb} = 9.5\,m^2$$
Total area of new bridge cross-section

Calculating the centre of gravity $z_{new.cog}$ of the new cross-section:

$$z_{new.cog} := \frac{\left(2A_{new.eb}\right) \cdot \left(\frac{h_{new.eb}}{2}\right) + A_{deck} \cdot \frac{h_{deck}}{2}}{A_{new}} = 730 \cdot mm$$

Calculating the second moment of inertia of the new cross-section:

$$I_{new.deck} := \frac{b_{deck} \cdot h_{deck}^3}{12} + b_{deck} \cdot h_{deck} \cdot \left(z_{new.cog} - \frac{h_{deck}}{2}\right)^2$$

$$I_{new.eb} := 2 \cdot \left[\dfrac{b_{new.eb} \cdot h_{new.eb}{}^3}{12} \, ... \atop + b_{new.eb} \cdot h_{new.eb} \cdot \left(z_{new.cog} - \dfrac{h_{new.eb}}{2} \right)^2 \right] = 2.8 \, m^4$$

$$I_{new} := I_{new.deck} + I_{new.eb} = 3.7 \, m^4$$

$$EI_{new} := E \cdot I_{new} = 75.11 \cdot GN \cdot m^2 \qquad \text{Bending stiffness of the new bridge}$$

Total self-weight of the new bridge:

$$g_{new.tot} := A_{new} \cdot \rho_c \cdot g + g_{sl} + g_b + g_{track} = 308.3 \cdot \dfrac{kN}{m}$$

Static deflection analysis with permanent load and train load

The worst position of load model LM71 at the bridge is when one of the middle point loads are placed in the centre of the span.

$d_1 := 0.8m$ — Distance between point loads

$d_2 := 1.6m$ — Distance between point load and distributed load

$\alpha := 1.33$ — Alpha factor according to TRVK Bro 11

$\psi_1 := 0.8$ — Partial factor for SLS loads

$q_{vk} := 80 \dfrac{kN}{m}$ — Characteristic distributed load

$Q_{vk} := 250kN$ — Characteristic point load

$$q_{vd} := \alpha \cdot \psi_1 \cdot q_{vk} = 85.1 \cdot \frac{kN}{m}$$ Distributed design load

$$Q_{vd} := \alpha \cdot \psi_1 \cdot Q_{vk} = 266 \cdot kN$$ Design point load

Calculating the static deflection of the original bridge design:

$$a := \frac{L}{2} - 2 \cdot d_2 = 11.3\,m$$ Distance where the left distributed load is acting

$$b := \frac{L}{2} - d_2 = 12.9\,m$$ Distance where the right distributed load is acting

$$x := \frac{L}{2} = 14.5\,m$$ Distance to centre of span

Deflection due to distributed train loads:

$$\delta_a := \frac{q_{vd} \cdot (a - d_1)^2}{24 \cdot EI \cdot L} \cdot (L - x)\left[-2x^2 + 4L \cdot x - (a - d_1)^2\right] = 1.5 \cdot mm$$

$$\delta_b := \frac{q_{vd} \cdot (b - d_1)^2}{24 \cdot EI \cdot L} \cdot (L - x)\left[-2x^2 + 4L \cdot x - (b - d_1)^2\right] = 2 \cdot mm$$

Deflection due to train point loads:

$$\delta_c := \frac{Q_{vd} \cdot L \cdot a \cdot (L - x)}{6 \cdot EI} \cdot \left(\frac{2x}{L} - \frac{a^2}{L^2} - \frac{x^2}{L^2}\right) = 0.9 \cdot mm$$

$$\delta_d := \frac{Q_{vd} \cdot L \cdot (a + d_2) \cdot (L - x)}{6 \cdot EI} \cdot \left[\frac{2x}{L} - \frac{(a + d_2)^2}{L^2} - \frac{x^2}{L^2}\right] = 0.9 \cdot mm$$

$$\delta_e := \frac{Q_{vd} \cdot L^3}{48EI} = 0.9 \cdot mm$$

$$\delta_f := \frac{Q_{vd} \cdot L \cdot b \cdot x}{6 \cdot EI} \cdot \left(1 - \frac{b^2}{L^2} - \frac{x^2}{L^2}\right) = 0.9 \cdot mm$$

Deflection due to permanent loads:

$$\delta_{s.an} := \frac{5 \cdot (g_{tot}) \cdot L^4}{384EI} = 22.6 \cdot mm$$

Total deflection due to permanent loads and train loads:

$$\delta_{tot} := \delta_a + \delta_b + \delta_c + \delta_d + \delta_e + \delta_f + \delta_{s.an} = 29.7 \cdot mm$$

Calculating the static deflection of the new bridge design:

$$a := \frac{L_{new}}{2} - 2 \cdot d_2 = 8.8\,m$$
Distance where the left distributed load is acting

$$b := \frac{L_{new}}{2} - d_2 = 10.4\,m$$
Distance where the right distributed load is acting

$$x := \frac{L_{new}}{2} = 12\,m$$
Distance to centre of span

Deflection due to distributed train loads:

$$\delta_{2.a} := \frac{q_{vd} \cdot \left(a - d_1\right)^2}{24 \cdot EI_{new} \cdot L_{new}} \cdot \left(L_{new} - x\right)\left[-2x^2 + 4L_{new} \cdot x - \left(a - d_1\right)^2\right]$$

$$\delta_{2.a} = 1.2 \cdot mm$$

$$\delta_{2.b} := \frac{q_{vd} \cdot \left(b - d_1\right)^2}{24 \cdot EI_{new} \cdot L_{new}} \cdot \left(L_{new} - x\right)\left[-2x^2 + 4L_{new} \cdot x - \left(b - d_1\right)^2\right]$$

$$\delta_{2.b} = 1.7 \cdot mm$$

Deflection due to train point loads:

$$\delta_{2.c} := \frac{Q_{vd} \cdot L_{new} \cdot a \cdot \left(L_{new} - x\right)}{6 \cdot EI_{new}} \cdot \left(\frac{2x}{L_{new}} - \frac{a^2}{L_{new}^2} - \frac{x^2}{L_{new}^2}\right)$$

$$\delta_{2.c} = 0.9 \cdot mm$$

$$\delta_{2.d} := \frac{Q_{vd} \cdot L_{new} \cdot \left(a + d_2\right) \cdot \left(L_{new} - x\right)}{6 \cdot EI_{new}} \cdot \left[\frac{2x}{L_{new}} - \frac{\left(a + d_2\right)^2}{L_{new}^2} - \frac{x^2}{L_{new}^2}\right]$$

$$\delta_{2.d} = 1 \cdot mm$$

$$\delta_{2.e} := \frac{Q_{vd} \cdot L_{new}^3}{48 EI_{new}} = 1 \cdot mm$$

$$\delta_{2.f} := \frac{Q_{vd} \cdot L_{new} \cdot b \cdot x}{6 \cdot EI_{new}} \cdot \left(1 - \frac{b^2}{L_{new}^2} - \frac{x^2}{L_{new}^2}\right) = 1 \cdot mm$$

Deflection due to permanent loads:

$$\delta_{s.an} := \frac{5 \cdot \left(g_{new.tot}\right) \cdot L_{new}^{4}}{384 EI_{new}} = 17.7 \cdot mm$$

Total deflection due to permanent loads and train loads:

$$\delta_{new.tot} := \delta_{2.a} + \delta_{2.b} + \delta_{2.c} + \delta_{2.d} + \delta_{2.e} + \delta_{2.f} + \delta_{s.an} = 24.5 \cdot mm$$

Deflection to span ratios:

Original bridge: New bridge:

$$\frac{\delta_{tot}}{L} = 1.0245 \times 10^{-3} \qquad \frac{\delta_{new.tot}}{L_{new}} = 1.0228 \times 10^{-3}$$

Utilization ratios with regard to deflection:

Original bridge: New bridge:

$$u_{lim} := \frac{L}{800} = 36.3 \cdot mm \qquad u_{new.lim} := \frac{L_{new}}{800} = 30 \cdot mm$$

$$u_{defl} := \frac{\delta_{tot}}{u_{lim}} = 81.96 \cdot \% \qquad u_{new.defl} := \frac{\delta_{new.tot}}{u_{new.lim}} = 81.83 \cdot \%$$

New bridge configurations:

The procedure above was performed for each span length of interest, resulting in the following dimensions of the edge beams:

$L_1 := 16m$ $h_{1.deck} := 1592mm$ $b_{1.deck} := 701mm$

$L_2 := 24m$ $h_{2.deck} := 2282mm$ $b_{2.deck} := 1005mm$

$L_3 := 32m$ $h_{3.deck} := 3005mm$ $b_{3.deck} := 1324mm$

$L_4 := 40m$ $h_{4.deck} := 3823mm$ $b_{4.deck} := 1684mm$

Eigenfrequencies

Calculating the natural frequencies of the bridge:

$$n_{max} := 3$$

Number of mode shapes

$$n := 1 .. n_{max}$$

$$m_{bridge} := \frac{g_{new.tot}}{g} = 31.4 \cdot \frac{ton}{m}$$

Total mass per meter
of the bridge

$$EI_{new} = 75.1 \cdot GN \cdot m^2$$

$$\omega_n := \left(\frac{n \cdot \pi}{L_{new}}\right)^2 \cdot \sqrt{\frac{EI_{new}}{m_{bridge}}}$$

First three natural frequencies of the bridge:

$$\frac{\omega_n}{2\pi} =$$

4.2
16.9
37.9

$\cdot Hz$

Appendix C
Drawings of the studied bridges

CHALMERS *Civil and Structural Engineering,* Masters Thesis BOMX02-16-29

C1

PLAN 1:100

ELEVATION A-A 1:100
NORRA SIDAN UTFÖRS LIKA
LÄGE PÅ PLUSHÖJDER ENLIGT SEKTIONER

ÖVERHÖJNINGSDIAGRAM (mm)

SEKTION B-B 1:50
ÖVERGJUTNING FÖR LAGER SE RITNING 595 601-003
LYFTPUNKTER FÖR LAGERBYTE SE RITNING 595 601-003

SEKTION C-C 1:20

SEKTION D-D 1:20

FASAS 70x70 mm
FASAS 150x150 mm
ÄNDE PÅ FARBANA
ÖRNSKÖLDSVIK
UMEÅ

GÄNGAD JORDANSLUTNING (M12) TYP PFEIFER BEB 4,
ELLER LIKVÄRDIG, SOM SVETSAS TILL YTTRE "SLINGAN"
I ÖVERBYGGNADEN OCH ANSLUTS TILL S-RÄLEN MINST
VAR 300E m

GÄNGAD JORDANSLUTNING (M12) TYP PFEIFER
BEB 4 ELLER LIKVÄRDIG, PLACERAS I VARJE
HÖRN.

MÄTPUNKT FÖR ELEKTROKEMISK
POTENTIALMÄTNING
FÖRBINDELSE TYP PFEIFER
BEB 20 EL LIKVÄRDIG
ISOLERING 100 mm TYP
PAROC GRS 30

DROPPNÄSA
YTAVLOPP

KOORDINATER

PKT	X	Y
31	7044824,234	4527753,706
32	7044795,738	4527727,668
33	7044791,150	4527732,687
34	7044819,645	4527758,724

HÄNVISNINGAR:
FÖRESKRIFTER ENLIGT RITNING NR 595 601-003
FÖRKLARINGAR
⊠ BETECKNAR AVVÄGNINGSDUBB
⊕ BETECKNAR MÄTPUNKT FÖR ELEKTROKEMISK POTENTIALMÄTNING

FASTSTÄLLD ENLIGT BV SKRIVELSE DATERAD 2003-12-0

WSP SAMHÄLLSBYGGNAD

RELATIONSHANDLING
ÄNDRING ENL PM NR 2

A V A
JVG-BRO ÖVER ASPAN
ÖRNSKÖLDSVIK – UMEÅ
km 53+250
MÄTT II (ÖB)

RELATIONSRITNING

BB-6576-520 595 601 004 B

SKALA 1:100

CHALMERS *Civil and Structural Engineering, Master's Thesis BOMX02-16-29*

C2

BRO ÖVER NORRMJÖLEÅN
ÖRNSKÖLDSVIK – UMEÅ
KM 100+795

RELATIONSRITNING

SAMMANSTÄLLNING

PLAN 1200

VY A-001 1200

SEKTION B-001 1:100

SEKTION C-001 1:100

SITUATIONSPLAN 1:10000

PROFIL JÄRNVÄG

PLANDATA JÄRNVÄG

AVVÄGDA HÖJDER FÖR DUBBAR

LAGERINSTÄLLNINGAR

ALLMÄNNA ANVISNINGAR

FÖRESKRIFTER

RITNINGSFÖRTECKNING

TILLSATSMEDEL BETONG

Denna ritning är Botniabanans egendom. Allt obehörigt
begagnande av ritningen beivras enligt lag.
BOTNIABANAN

ÅSA LÖVBLOM
KEN RYBERG
JÖRGEN MOSESSON

2006-01-20

BB_7421-501

XREF: ..\modell\md6541001.dwg 2009-09-28 08.03
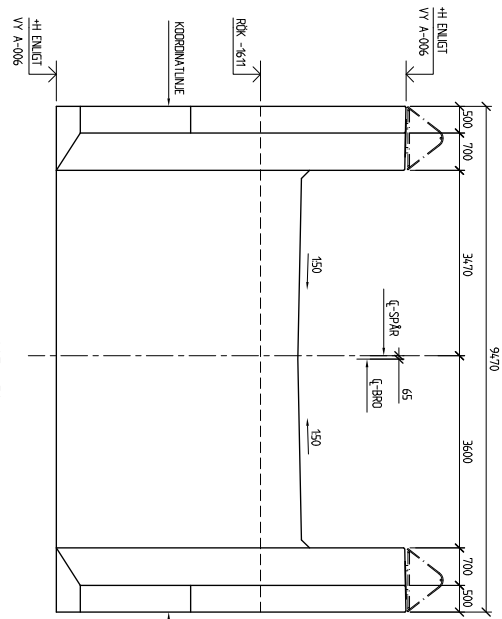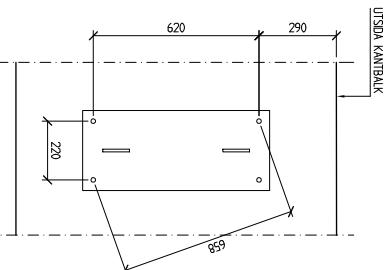
1:100

0
1
2
3
4
5
10 m

FÖRESKRIFTER
SE RITNING NR BB 7421-501 BLAD 006.

DETALJ C-007 1:10
PLACERING GRUNDSKRUVAR
TILLGÄNGLIGHETSSKYDD ALT. A
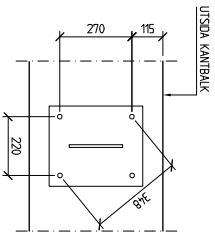
620   290
220
859
UTSIDA KANTBALK

DETALJ D-007 1:10
PLACERING GRUNDSKRUVAR
TILLGÄNGLIGHETSSKYDD ALT. B

270   115
220
87°E
UTSIDA KANTBALK
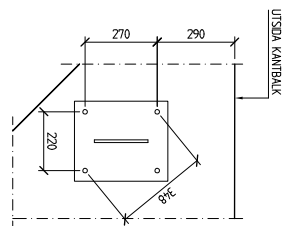
DETALJ E-007 1:10
PLACERING GRUNDSKRUVAR
TILLGÄNGLIGHETSSKYDD ALT. B
I ANSLUTNING TILL ALT. A MOT BRO

270   290
220
87°E
UTSIDA KANTBALK

VY A-007 1:50
ÄNDSKÄRM STÖD 1 GÄLLER ÄVEN STÖD 2

+H ENLIGT
VY A-006

KOORDINATLINJE
RÖK -1611
+H ENLIGT
VY A-006

500 700
3470
150
€-SPÅR
€-BRO
65
150
9470
3600
700 500
KOORDINATLINJE
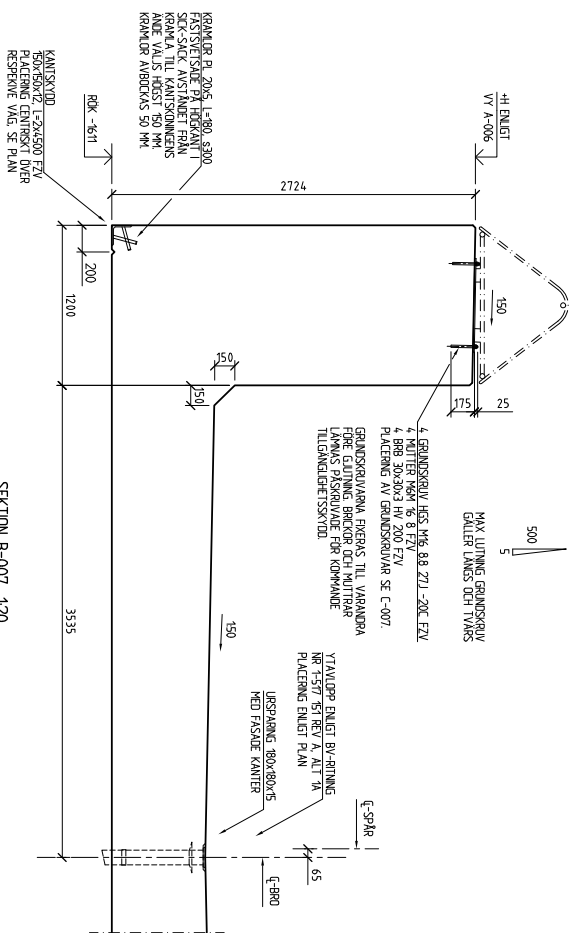
SEKTION B-007 1:20
GÄLLER I PRINCIP ÄVEN SÖDRA SIDAN

KANTSKYDD
150x150x12 L=2x4500 FZV
PLACERING CENTRISKT ÖVER
RESPEKTVE VÄG, SE PLAN

KRAMLOR PL. 200, L=180, s300
FASTSVETSADE PÅ HÖGKANT
SACK-SACK, AVSTÅNDET FRÅN
KRAMLA TILL KANTSKONINGENS
ÄNDE VALS HÖGST 150 MM
KRAMLOR AVBÖCKAS 50 MM

RÖK -1611
+H ENLIGT
VY A-006

2724
200
1200
150
150
150
3535

4 GRUNDSKRUV HCS M16 8.8 Z71-20C FZV
4 MUTTER M&M 16 8 FZV
4 BRB 30x30x3 HV 200 FZV
PLACERING AV GRUNDSKRUVAR SE C-007.

GRUNDSKRUVARNA FIXERAS TILL VARANDRA
FÖRE GJUTNING BRICKOR OCH MUTTRAR
LÄMNAS PÅSKRUVADE FÖR KOMMANDE
TILLGÄNGLIGHETSSKYDD

YTAVLOPP ENLIGT BV-RITNING
NR F-517 151 REV A, ALT 1A
PLACERING ENLIGT PLAN

URSPARING 180x180x15
MED FASADE KANTER

MAX LUTNING GRUNDSKRUV
GÄLLER LÄNGS OCH TVÄRS

500
5

€-SPÅR
€-BRO
65

175   25

CHALMERS *Civil and Structural Engineering,* Masters Thesis BOMX02-16-29

C3

2009-09-28 08:24 tobiasw   D:\63\6382\Arbetshandlingar_new\HandlingarE\Relation\K\RitDef\BB_7421-501-007.dwg